A study on mechanical behavior and thrust restraint design of buried pipe bends

太田, 遥子

(Degree)
博士（学術）

(Date of Degree)
2023-03-25

(Date of Publication)
2024-03-01

(Resource Type)
doctoral thesis

(Report Number)
甲第8663号

(URL)
https://hdl.handle.net/20.500.14094/0100482411

Doctoral Dissertation

A Study on Mechanical Behavior and Thrust Restraint Design of Buried Pipe Bends

埋設管路屈曲部の力学挙動と スラスト対策工法の設計に関する研究

January 2023

Graduate School of Agricultural Science,

Kobe University

Yoko OHTA

太田　遥子

The research reported in this dissertation was conducted at the Laboratory of Geotechnical Engineering for Agriculture, Graduate School of Agricultural Science, Kobe University, Japan.

Acknowledgments

First, I would like to express my sincere gratitude and appreciation to Dr. Toshinori Kawabata and Dr. Yutaka Sawada from the Graduate School of Agricultural Science, Kobe University, for their patience and expert guidance on my study and research since I was an undergraduate. Dr. Kawabata, who encouraged me to move on to a Ph.D. course, taught me fundamental attitudes toward research, sometimes gently and sometimes strictly. Dr. Sawada, my closest adviser, gave me specific advice during our discussions about experimental methods and results. Both professors offered me many opportunities to try new things, helping me grow as a person.

I am also profoundly grateful to Dr. Haruya Tanakamaru and Dr. Kazuya Inoue from the Graduate School of Agricultural Science, Kobe University. Their explicit comments and perceptive advice on my annual presentation brought me new perspectives on my research. In addition, their review comments as a dissertation committee make my dissertation clear and more understandable.

My appreciation is extended to Dr. Yoshiyuki Mohri from Ibaraki University and Dr. Mitsuru Ariyoshi from the National Agriculture and Food Research Organization for their sincere and valuable guidance and support extended to me. I also appreciate Dr. Takashi Kimata and Dr. Yosuke Kudo from Osaka Metropolitan University for their helpful comments on my research at the seminars held three times a year. I would like to thank Dr. Hoe I. Ling from Columbia University for his warm suggestion for my papers.

I owe a debt of gratitude to Dr. Kenichi Soga from the University of California, Berkeley, who accepted me as a visiting student in his research group. He provided opportunities to study abroad and to experience research on pipelines from different aspects. I thank the group members for their kind support during my stay.

I appreciate Dr. Mariko Suzuki from Kobe University, Dr. Kohei Ono from Ehime University, and Dr. Naoki Takegawa from the National Institute of Advanced Industrial Science and Technology for their friendly advice not only in my research but also in my life as a Ph.D. student at the Laboratory of Geotechnical Engineering for Agriculture. I also appreciate Ms. Emi Fujimoto for her warm support in my daily research life. I would like to thank Mr. Yusuke Sonoda, a Ph.D. student in the same laboratory, for encouraging

and helping my research. I am also thankful for the laboratory members who spent the same time during my Ph.D. course: Mr. Mitsuaki Tokiyoshi, Mr. Makoto Hirokawa, Ms. Mayu Toda, Ms. Mina Kawamura, Mr. Haruki Abe, Ms. Megumi Kitada, Ms. Mizuki Tokumasu, Mr. Taishi Nagatani, Mr. Takeru Matsumoto, Mr. Tatsuya Aoki, Mr. Naoki Morino, Ms. Chihaya Ikawa, Ms. Hina Yamashita, Ms. Ruka Ikebata, Mr. Yusuke Inoue, Ms. Kotone Tsujimoto, Ms. Hina Nagatomo and Mr. Yuki Konishi. I am also grateful to all people involved with me during my student life at Kobe University.

Finally, I would like to dedicate this thesis, with appreciation, to the special people in my life, especially my family, who always trust and encourage me. I wasn't able to accomplish my research work without their support.

January 2023
Yoko Ohta

Contents

Figures

Chapter 1

Chapter 3

Chapter 4

Chapter 5

Tables

Notations

A	Cross-sectional area
B_{bend}	Projected width of a pipe bend
b	Width of a block
C_u	Coefficient of uniformity
C_c	Coefficient of curvature
D	Pipe diameter
D_{out}	Outer diameter of a pipe
D_m	Diameter of a model pipe
D_p	Diameter of a prototype pipe
d_{10}	Grain size corresponding to 10% finer in the particle-size distribution
d_{50}	Grain size corresponding to 50% finer in the particle-size distribution
E_m	Tensile stiffness of model geogrid
E_p	Tensile stiffness of prototype geogrid
g	Acceleration due to gravity
H	Depth of earth cover or depth to the top of a buried structure
H'	Depth to the center of a buried structure
h	Height of a block
K_0	Coefficient of earth pressure at rest
K_a	Coefficient of active earth pressure
K_p	Coefficient of passive earth pressure
k_1, k_2	Coefficients for hyperbolic curves
k_3, k_4	Coefficients for the 3D effect factor

$L_{straight}$	Length of a straight pipe
l	Length of a block
l'	Length of a thrust restraint
M	3D effect factor
N_h	Bearing capacity factor
P_a	Active resistance force
P_p	Passive resistance force
P_b	Frictional resistance force at the bottom of a buried structure
P_s	Frictional resistance force at the side of a buried structure
P_t	Frictional resistance force on the top of a buried structure
p	Internal water pressure
R	Lateral resistance force
R_u, R_{u1}, R_{u2}	Ultimate lateral resistance force
R'	Normalized lateral resistance force
T	Thrust force
t	Time
$v(t)$	Velocity at time t
V	Rate of pipe displacement
W_{block}	Weight of a block
W_{soil}	Weight of soil above a block
Y	Lateral displacement
Y_{bend}	Displacement of a pipe bend
Y_u, Y_{u1}, Y_{u2}	Ultimate lateral displacement
Y'	Normalized lateral displacement

α	joint separation at the pipe center
γ_{sat}	Unit weight of saturated sand
γ_{soil}	Unit weight of soil
γ_{w}	Unit weight of water
θ	Bending angle of a pipe bend
δ_{allow}	Allowable joint separation
δ_{j}	Total joint separation
δ_{ja}	Axial joint separation
δ_{jb}	Joint separation with angular movement
$\phi_{g\text{-}s}$	Friction angle between geogrid and surrounding soil
λ	Scaling factors for the geometry
λ_{ts}	Scaling factors for the tensile stiffness
ρ_{s}	Density of soil particles
ψ	Angular deflection
ψ_{allow}	Allowable angular deflection

Chapter 1

Chapter 1

Introduction

1.1 Background

Water is essential for sustaining life on earth, including for humans' societal and technological development in both developed and developing countries. Notably, two-thirds of the total water consumption in Japan is used for agricultural purposes. Two of the most crucial uses are for irrigation of crops and vegetables and drainage systems of many farms. The channels and pipes used in these systems span more than 400,000 km, linked in a nationwide network. Additionally, many agricultural water facilities are used as public infrastructure, accommodating emergency purposes, such as firefighting and backup drainage systems during heavy rainfall.

In recent years, Japan's irrigation facilities have faced two main challenges: resiliency against natural disasters and structural aging. Several large earthquakes have severely damaged many agricultural facilities in the past decades. For example, as shown in **Fig. 1-1**, water leakage that occurred around the bends of a pipeline during the 2018 Hokkaido Eastern Iburi Earthquake caused subsequent soil erosions, which disturbed the

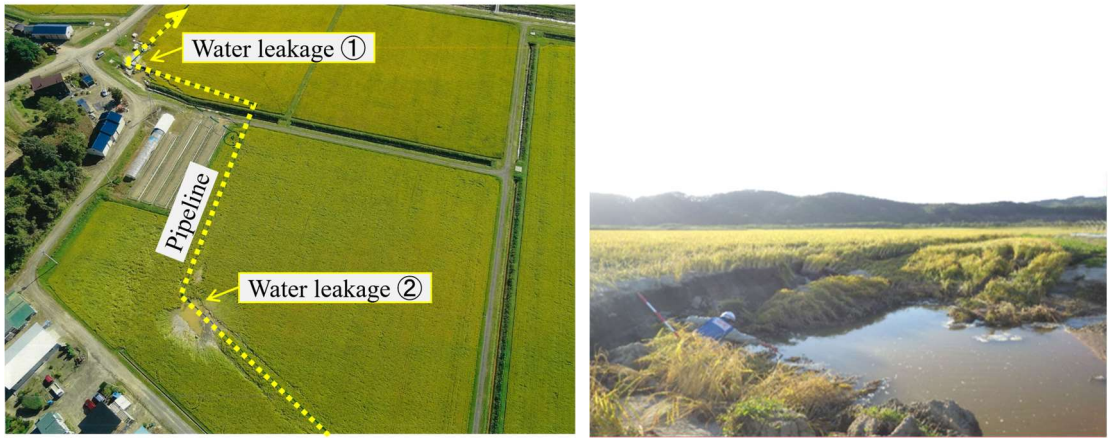

(a) Damage of pipeline (b) Soil erosion at water leakage

Fig. 1-1 Water leakage caused by the 2018 Hokkaido Eastern Iburi Earthquake (The Hokkaido branch of JSIDRE, 2019; modified by the author)

surrounding agricultural activities and required repair. Damage to water facilities not only affects the surrounding environment and the water supply but also costs a substantial amount of money and takes time to repair. Efforts to alleviate such damages are indeed in high economic demand. This has become substantial in Japan since the probability of future Nankai megathrust earthquakes has been predicted to increase to about 80% within the next 30 years.

Therefore, disaster mitigation measurements must focus on strengthening weak points in the pipeline systems. In particular, since pipelines are usually arranged linearly, damages occurring in these weak points might cause the system to fault and malfunction. From the structural viewpoint, one of the weakest parts of pipelines is located at pipe bends. They are structurally weaker due to unbalanced forces, referred to as *thrust forces*, produced depending on the magnitude of internal water pressure acting on the pipe wall; this is schematically illustrated in **Fig. 1-2**. During an earthquake, the surrounding soils often liquefy, thus, reducing the resistance force supporting the pipe structure. Several case history studies have recently indicated that pipeline damage mainly occurred near pipe bends. Harumoto et al. (2015) reported that about 25% of the pipeline damage occurred at bends during the 2011 off the Pacific Coast of Tohoku Earthquake, and Ono et al. (2019) observed that 70% of pipe bends within the survey area were damaged during the

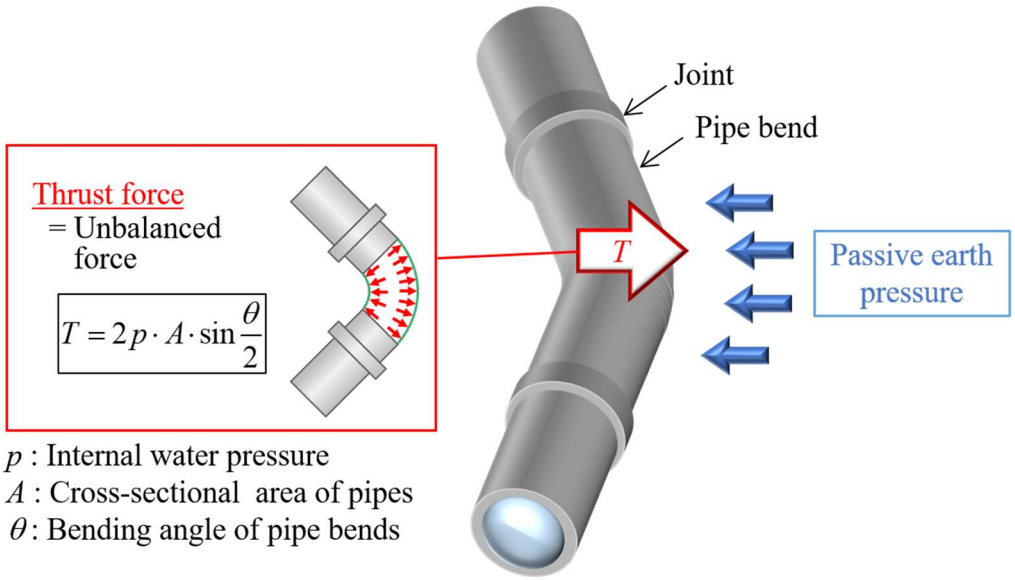

Fig. 1-2 Thrust force acting on a pipe bend

2018 Hokkaido Eastern Iburi Earthquake. Their studies further indicate the importance of reinforcing pipe bends to maintain function and improve the resiliency of pipelines during and after earthquakes.

There are several proposed methods in the literature to reinforce the pipe bends. The simplest approach is to use a *thrust block*, a support structure usually made from concrete, to transfer the load from the pipe to a wider load-bearing surface, such as the surrounding soil. While the thrust block has been widely used for general and practical purposes, subsequent problems have occurred during earthquakes. Since the thrust block is comparably heavier than the pipe structure, it exerts more significant inertial force and is often displaced farther relative to the surrounding pipes. This displacement may damage pipe joints and generate leakage. Furthermore, if the surrounding soil liquefies, the heavier thrust block often sinks due to the sudden loss of support, whereas the underground pipes, which are relatively lighter, are generally lifted due to buoyant forces. As shown in **Fig. 1-3,** this relative deformation often damages pipe joints and induces leakage (Mohri et al., 1995; Mohri et al., 2014). The literature proposes other methods to replace the use of thrust blocks, such as by using geosynthetics (Kawabata et al., 2003;

Fig. 1-3 Joint separation due to the 1993 Hokkaido-Nansei-Oki Earthquake (Mohri et al., 1995)

Sawada et al., 2009), shown in **Fig. 1-4**. However, a standardized procedure to accommodate different pipeline sizes or shapes is currently unavailable. Another possible approach is to replace the surrounding liquefiable soils with non- or hardly liquefiable mediums, such as gravel (Ono et al. 2022), in the hope of retaining reaction force at pipe bends during earthquakes. However, comprehensive studies using gravels to support thrust forces during an earthquake have not been conducted so far.

Along with providing additional support around pipe bends during an earthquake, selecting the appropriate design and material for pipe joints around the bends is also essential. Several designs of improved pipe joints to accommodate large relative deformation have been proposed in the literature (e.g., Itani et al., 2016; Wham and O'Rourke, 2016). However, it is worth noting that such considerations of special or deformable joints are currently not incorporated in pipeline design codes, which are traditionally based on comparing thrust forces with resistant forces, such as Rankine passive earth pressure. In this regard, force-displacement-based approaches, which consider both force and displacement coupling of pipes and the surrounding soil, may be beneficial to create a more effective performance-based design.

In addition to natural disaster mitigation and resiliency, aging must also be considered to avoid structural degradation-induced damages. Many facilities in Japan were built during

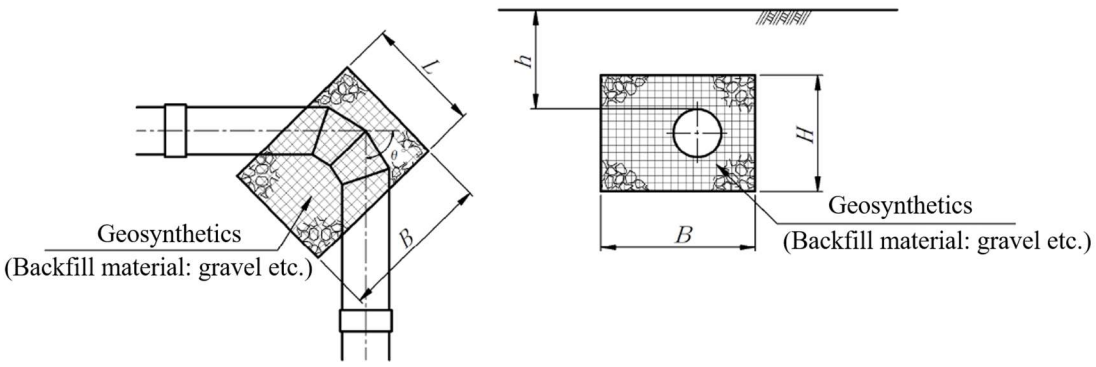

Fig. 1-4 Thrust restraint using geosynthetics
(Ministry of Agriculture, Forestry and Fisheries, 2021; modified by the author)

the period of high economic growth around the 1960s, which means that many are currently over a service life of 50 years. As illustrated in **Fig. 1-5**, more than 40% of irrigation and drainage facilities have been denoted as over-service life, and another 20% of them will exceed their service life within the next decade. These aging facilities require maintenance and repair to prevent unprecedented accidents from occurring, which may cause further damage to civil and infrastructure systems.

According to the data published by the Ministry of Agriculture, Forestry and Fisheries, 2019), pipeline systems take up around 30% of Japan's irrigation and drainage facilities. The rest are primarily open channels, which convey water as free-surface flows. While many benefits are associated with transporting water through open channels, there are some significant disadvantages to using them as the main irrigation and drainage systems. First, open channels exhibit several safety issues, as unwanted objects may fall into these channels and cause further damage or blockage to the systems. Second, open channels are proven less efficient than pipelines since the water flowing in open channels is subject to evapotranspiration. Thus the amount of transported water may change. Furthermore, open channels are unable to transport water under high pressure, and the maximum flow rate is generally much lower than pipelines. Lastly, open channels often require regular maintenance and cleaning and, thus, might demand additional costs and efforts. In

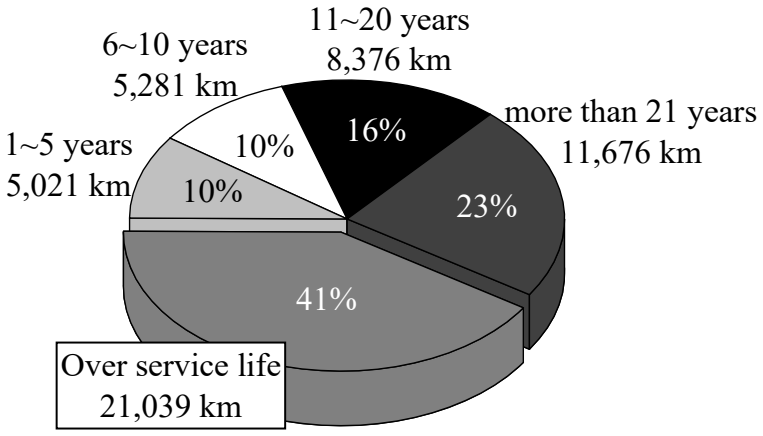

Fig. 1-5 Residual service life of the main irrigation and drainage systems in 2018 (Ministry of Agriculture, Forestry and Fisheries, 2019)

addition to this, these open channels are subjected to aging, and due to a few considerations, there are recent movements to convert old open channels to pipelines to improve safety and efficiency.

1.2 Aims of the study

This study aims to investigate the challenges facing irrigation pipelines, especially in the vicinity of pipe bends, through model experiments. Here four scopes of research were decided to make the design procedure of pipe bends more practical and rational.

1 **Consideration of displacement of pipe bends to improve the current design**
Since the resistance force against the thrust force changes depending on the amount of pipe displacement, considering pipe displacement is vital for understanding the behavior of buried pipe bends. If the pipe displacement can be predicted from the thrust force, the joint separation that substantially reduces the function of pipelines can be calculated using the geometrically derived relationships from previous studies (Itani et al., 2016; Shumaker et al., 2017). Then the stability of pipe bends can be evaluated by comparing the estimated and the allowable joint separation, leading to a rational design procedure.

2 **Proposed design of thrust restraint methods with geosynthetics as an alternative to thrust blocks**
Several studies on geosynthetic thrust protection, especially geogrid-based methods, began in 2003. While it is expected to be an effective alternative countermeasure to solve problems occurring during earthquakes, the use of geosynthetics in actual construction projects is uncommon. The primary reason for this is that, currently, there is no proposed calculation method to predict resistance against thrust forces. Additionally, only a few studies have indicated that it is sufficiently effective compared to conventional methods. The current work is expected to provide a systematic calculation procedure for the geogrid-based thrust restraint method by comparing its effectiveness with the traditional block method.

3 **Improvement of seismic resistance at pipe bends using gravel**
Gravel is often used to improve the seismic resistance of pipelines, primarily to mitigate the flotation of pipes due to buoyancy forces during earthquakes. Some studies reported that gravel backfills moderated pipe displacement at pipe bends

during earthquakes (Kawabata et al., 2008; Ono et al., 2022), whereas others did not find the effectiveness of gravel as thrust restraints (Itani et al., 2016). Therefore, it is essential to determine the proper placement of the gravel layers around pipe bends to use gravel for seismic protection in pipe bends.

4 **Investigating the effect of existing open channels to support pipe bends from thrust forces**
When open channels are converted to pipelines, pipes are sometimes buried without withdrawing the existing channel walls to reduce construction costs by shortening the construction period. Although this is frequently done in practice, only a few studies show how the remaining walls will affect the behavior of buried pipe bends. If the remaining walls provide reaction forces against the thrust force, the walls can be effectively used as a thrust restraint method.

1.3 Overview of thesis

This thesis details the experimental studies to improve the design of irrigation pipelines in line with Japan's current situation. The organization of this thesis is briefly described as follows.

Chapter 2 reviews previous studies focusing on the lateral behavior of buried pipes and thrust restraint methods. First, experimental and numerical studies on the lateral behavior of buried pipelines are provided, particularly studies that evaluated the pipe behaviors through F–D relationships represented by hyperbolic curves. Then, the research on new thrust restraint methods is summarized.

Chapter 3 investigates the seismic resiliency of pipe bends buried with gravel. The shaking table tests were conducted under centrifugal acceleration, simulating the behavior of large-diameter pipes buried with various layouts of gravel layers. From the comparison of experimental results, the effectiveness and practical layout of gravel layers as thrust restraints during earthquakes are evaluated.

Chapter 4 considers the performance of pipe bends buried in existing open channels. First, case studies are summarized to understand the overview of this construction technique. Then, the effect of existing open channels on the behavior of pipe bends is discussed based on the lateral loading experiments conducted on pipes buried with four different

wall shapes. Finally, the effect of walls on the pipe behavior and geogrid's effectiveness for reinforcing existing walls are discussed.

Chapter 5 details the two kinds of lateral loading experiments on thrust restraint using geogrids and gravel to investigate the resistance mechanism of this restraint method. An experiment was conducted on the thrust restraint with various dimensions to examine the effect of the dimensions of wrapped areas by geogrids on the lateral resistance and the failure mechanism of the surrounding ground. Another was carried out on the geogrid-based thrust restraint and thrust blocks to evaluate the effectiveness of the thrust restraints by comparing the results of both methods.

Chapter 6 provides a proposed design of pipe bends considering pipe displacement. As explained in previous sections, the prediction of pipe displacement is required to include joint performance as a design parameter. Therefore, F–D relationships were proposed, particularly for the thrust restraint method using geogrids described in Chapter 5 to calculate the pipe displacement from the thrust forces. Finally, after formulating F–D relationships based on the experimental results, a calculation example is provided following a proposed design chart using F–D relationships.

Chapter 7 concludes and summarizes this thesis as well as discusses the directions for future works.

Chapter 2

Chapter 2

Literature review

2.1 Lateral behavior of buried pipe

2.1.1 Experimental and numerical studies on the behavior of buried pipelines

Some studies have been conducted to understand the reaction force offered by surrounding soil against the movement of buried pipelines during earthquakes and ground movements. As the earliest work on lateral behavior of buried pipes, Audibert and Nyman (1977) performed pipe displacement-controlled tests in dry sand to investigate the influence of soil densities, pipe diameters D from 25 to 114 mm, and embedment depth ratio H/D from 1 to 24 on the behavior of buried pipes. Based on the experimental results, the failure mechanism was divided into three classes according to H/D. They also performed an in-situ test to confirm that the results of the laboratory tests could apply to in-situ conditions and compared the results of field tests and the predicted results based on the laboratory experiments. Trautmann and O'Rourke (1985) carried out 30 cases of lateral loading experiments with various pipe diameters, soil densities, burial depths, and pipe surface frictions. They found that F–D relationships could be estimated using a rectangular hyperbola and a bilinear representation. Hsu (1993) conducted a total of 120 tests which varied the pipe diameter from 38.1 to 228.6 mm, H/D from 1 to 10.5, soil densities, and the loading rate to discuss the effect of the loading rate for the lateral behavior of buried pipes. Ansari et al. (2021) noticed that although the lateral behavior of pipelines had been studied experimentally under various conditions, there are significant differences among the different data sets. The authors conducted 13 lateral loading test cases and compared the test results with the published date to examine the effect of test conditions, including loading systems and boundary conditions, on the behavior of buried pipes.

In recent years, numerical studies have often been performed to understand pipe-soil interaction deeply. Yimsiri et al. (2004) conducted FE analysis with two different soil models to compute the peak resistance for deep embedment conditions. The results were compared with the results of Trautmann and O'Rourke (1985) to examine the accuracy

of the analysis. Further FE analysis was conducted to evaluate the transition of the peak force from shallow to deep embedment conditions. Guo and Stoll (2005) investigated the effects of the model scale, stress level, burial depth ratio, and soil properties on the lateral behavior of buried pipes through FE analyses. To incorporate the scale effect into the pipeline design guideline, the authors proposed the equation for the maximum dimensionless lateral forces N_h with the scaling effect. Kouretzis et al. (2013) applied a large-deformation numerical methodology to FE analysis, simulating the pipe-soil interaction buried in a trench with loose to medium-dry sand. The authors suggested that the critical state parameters were adequate to describe the deformation mode of a backfill inside a trench based on the comparison of the numerical results and the experimental results conducted by Trautmann and O'Rourke (1985). Roy et al. (2018) performed an FE analysis to investigate the similarities and differences in lateral behaviors of buried pipes and vertical strip anchors. The results showed that the proposed modified Mohr-Coulomb model could explain the variation of peak and post-peak resistances for anchors and pipes observed in the published experimental results.

All the above studies were conducted under conditions where the ground was made of uniform dry sand. In contrast, the following studies considered the ground conditions, such as the degree of saturation and the influence of the native grounds. Robert et al. (2016) investigated the lateral load-displacement behavior of pipelines buried in unsaturated sands through large physical model experiments and FE analysis. The results showed that the effect of unsaturation on peak resistance force was more obvious in the finer sand than in the coarse sand. Ono et al. (2018) conducted lateral loading experiments on pipes buried in saturated sand with various effective stress controlled by the upward seepage to consider the degree of liquefaction into pipe-soil interactions. Chaloulos et al. (2017) conducted FE analysis on buried pipelines with lateral displacement to find size and shape effects for trenches excavated in stiff soils and rocks and then proposed analytic relationships between trench dimensions and the soil pressure on pipelines.

2.1.2 Prediction of F–D relationships

The lateral displacement behavior of underground structures such as pipes and anchors has often been examined as Force–Displacement relationships. Analytical studies for representing F–D curves using the hyperbolic approximation have been conducted since Das and Seely (1975) conducted experiments on shallow vertical anchors. Das and Seely (1975) normalized reaction forces and displacements by the peak force and the corresponding displacement, respectively, and then approximated the normalized F–D

relationships by a hyperbolic curve. A similar approach has been attempted to formulate the lateral displacement behavior of buried pipelines as follows.

Audibert and Nyman (1977)

The authors provided the normalized F–D relationship based on the results of the dense sand test.

$$\frac{P}{P_u} = \frac{Y/Y_u}{0.145 + 0.855\,Y/Y_u} \tag{2.1}$$

In this study, the authors described that the ultimate resistance force of buried pipes could be calculated using the bearing capacity factor proposed by Hansen (1966).

$$P_u = N_h \gamma_t H' \tag{2.2}$$

Trautmann and O'Rourke (1985)

The relationship, as shown in Eq.(2.3), was developed using the test results with three different soil densities. The authors found that the ultimate displacement changes depending on the embedded depths and soil densities and proposed the prediction equations for each ground density.

$$\frac{P}{P_u} = \frac{Y/Y_u}{0.17 + 0.83\,Y/Y_u} \tag{2.3}$$

$$Y_u = 0.13H' \quad \text{(for loose sand)} \tag{2.4}$$

$$Y_u = 0.08H' \quad \text{(for medium sand)} \tag{2.5}$$

$$Y_u = 0.03H' \quad \text{(for dense sand)} \tag{2.6}$$

Hsu (1993)

The authors proposed the normalized F–D relationships considering the rate of pipe displacement V as follows:

$$\frac{P}{P_u} = \frac{Y/Y_u}{0.29\left(V/D\right)^{-0.052} + 0.71\left(V/D\right)^{0.025}} \tag{2.7}$$

Yimsiri et al. (2004)

The normalized F–D relationships, as shown in Eq.(2.8), were obtained from the results of FE analysis with deep embedment conditions.

$$\frac{P}{P_u} = \frac{Y/Y_u}{0.1 + 0.9Y/Y_u} \tag{2.8}$$

Jung et al. (2016)

The authors proposed Eq.(2.9) based on the numerical results of the lateral behavior of buried pipes in dry sand.

$$\frac{P}{P_u} = \frac{Y/Y_u}{0.20 + 0.82Y/Y_u} \tag{2.9}$$

Ono et al. (2017)

To consider the effect of liquefaction, the authors introduced γ' into normalized F-D relationships and the bearing capacity factor N, as shown in Eq. (2.10). Note that γ' is the submerged unit weight of the soil, taking into account the excess pore water pressure ratio.

$$\frac{P}{P_u} = \frac{Y/Y_u}{\left[1-\gamma'/\left(2.36+1.25\gamma'\right)\right]+\gamma'/\left(2.68+1.22\gamma'\right)} \tag{2.10}$$

$$N_h = \frac{P_u}{\gamma' DH'L} \tag{2.11}$$

2.2 Thrust restraint method

As described in Chapter 1, thrust blocks, commonly used as thrust restraints, become a weak point in pipelines during earthquakes. Since the weakness of thrust blocks became apparent, thrust restraint methods that are effective even during earthquakes have been studied.

Some methods have been developed to ensure the stability of bend sections from pipeline structures. One of the methods is laying straight pipes in curved alignment to distribute thrust force. Fujita et al. (2007a) conducted laboratory tests using a model pipe with internal pressure and numerical analysis to compare the behavior of pipe bends and straight pipes with curved alignment. The results indicated that the displacement of the pipes with curved alignment was smaller than that of the pipe bends because the thrust force acting on the pipes with curved alignment was distributed wider than that working

on the pipe bends. In addition, Fujita et al. (2007b) investigated seismic damage of large-diameter pipes based on the results of the shaking table tests. The author concluded that the displacement of straight pipes with curved alignment was smaller than that of a pipe bend with a thrust block, indicating the seismic resistance of this method.

The other way is using a chain structure pipeline which has special joints allowing expansion and contraction. In pipelines with special joints, if one joint fully extends, the joint pulls on the neighboring pipe, and then the entire pipeline behaves like a chain. Itani et al. (2015) conducted lateral loading tests in the liquefied ground and numerical analysis to investigate the mechanical behavior of a chain structure pipeline with a bend. The results showed that no joint detachment occurred on the pipeline because the entire pipe followed the displacement of the bend. Itani et al. (2016) performed shaking table tests for the chain structure pipeline, confirming the chain structure's effectiveness against the displacement of the pipe bends during earthquakes.

Our research group has developed a thrust restraint method using geogrids as a thrust countermeasure and has studied the installation method and effectiveness of the method through model experiments. In this method, geogrids integrate a pipe bend and the surrounding ground, increasing the thrust resistance without using heavy structures such as concrete blocks. Kawabata et al. (2003, 2004) devised a thrust restraint method that unified a pipe bend and the active side of the ground using geogrid and an anchor plate. They began experimental and numerical studies on the resistance mechanism against thrust force. Kawabata et al. (2011) performed shaking table tests and verified that the displacement of a pipe bend with geogrid-based thrust restraint was smaller than that of a pipe bend with a thrust block in liquefied ground. Sawada et al. (2009, 2010) proposed the equation for calculating additional resistance of the geogrid-based method considering the tensile characteristics of geogrid. In addition, the authors provide a calculation procedure for the thrust restraint that geogrid wrapped the active side of ground and pipe bends. Kawabata et al. (2008) conducted lateral loading tests to investigate the effects of reinforcement of passive ground using geogrid. The results showed that using gravel and geogrid was effective for increasing lateral resistance against pipe displacement since gravel backfill increased the degree of unification in the wrapped area by geogrid. Kawabata et al. (2010) performed a field test for nine months using a pipe bend with an outer diameter of 800 mm and a bending angle of 56^{o} to confirm the workability and safety of the thrust restraint method. Ono et al. (2016) conducted lateral loading experiments under different hydraulic gradients to clarify the mechanical characteristics

of pipes reinforced with gravel and geogrids in liquefied grounds. The results indicated that unification with a pipe and gravel by geogrid generated the resistance force even in the liquefied ground because the tensile force of geogrid contributed to the resistance against pipe displacement.

Chapter 3

The contents of this chapter are based on:

Ohta, Y., Sawada, Y., Ariyoshi, M., Mohri, Y., and Kawabata, T. (2022), "Effects of gravel layer as thrust restraint for pipe bends subjected to earthquake loading", *Int. J. Phys. Model. Geotech.*, 22(2), pp. 99-110.

Chapter 3

Effective location of gravel layer as thrust restraint during earthquake loading

3.1 General

Backfilling with gravel is a commonly used seismic mitigating method for buried pipes. Although previous studies have discussed the effectiveness of gravel layers for mitigating pipe displacement during earthquakes, there has yet to be any discussion on where the gravel layer needs to be placed to maintain the stability of pipe bends. In addition, the previous experimental study remains a limitation for large-diameter pipes, such as agricultural pipes, which can reach 1000 mm in diameter.

In this study, centrifugal shaking table tests were conducted on buried pipes to investigate the practical layout of gravel backfill to stabilize the bends of large-diameter pipes under earthquake loading.

3.2 Outline of experiments

A series of model tests were performed under 30*g* at a corresponding length scale factor of 1:30 using a geotechnical beam centrifuge equipped with a seismic shaker at the National Agricultural and Food Research Organization in Japan, as shown in **Fig. 3-1**. The specifications of the centrifuge are summarized in **Table 3-1**. These tests facilitated observing the seismic behavior of a pipe representing a prototype diameter of 1800 mm. The centrifuge scaling laws for these tests are summarized in **Table 3-2**.

Fig. 3-2 shows a rigid test container with dimensions of 1350×400×450 mm: The front face of the container was transparent glass, while the side walls and the back wall were made of steel. Valves were installed on the bottom of the container to allow fluid to be supplied to the model ground. The loading system as shown in **Fig. 3-3** was inside of the container: it consisted of a wire, a weight, and pulleys to apply a lateral load which simulated thrust force to the model pipe during experiments. The mass of the weights was

Fig. 3-1 Geotechnical beam centrifuge at the National Agricultural and Food Research Organization in Japan

Table 3-1 Specifications of the centrifuge

Radius of rotation	4800 mm
Maxi centrifugal acceleration during dynamic tests	75*g*
Maximum carrying mass	3000 kg
Dimensions of seismic shaker	1000 mm×1500 mm
Maximum shaking acceleration	55*g*
Available shaking frequencies range	10 to 400 Hz

Table 3-2 Scaling laws

Quantities	**Model / Prototype**
Acceleration	n
Length	$1/n$
Force	$1/n^2$
Time (inertia)	$1/n$
Time (permeability)	$1/n$

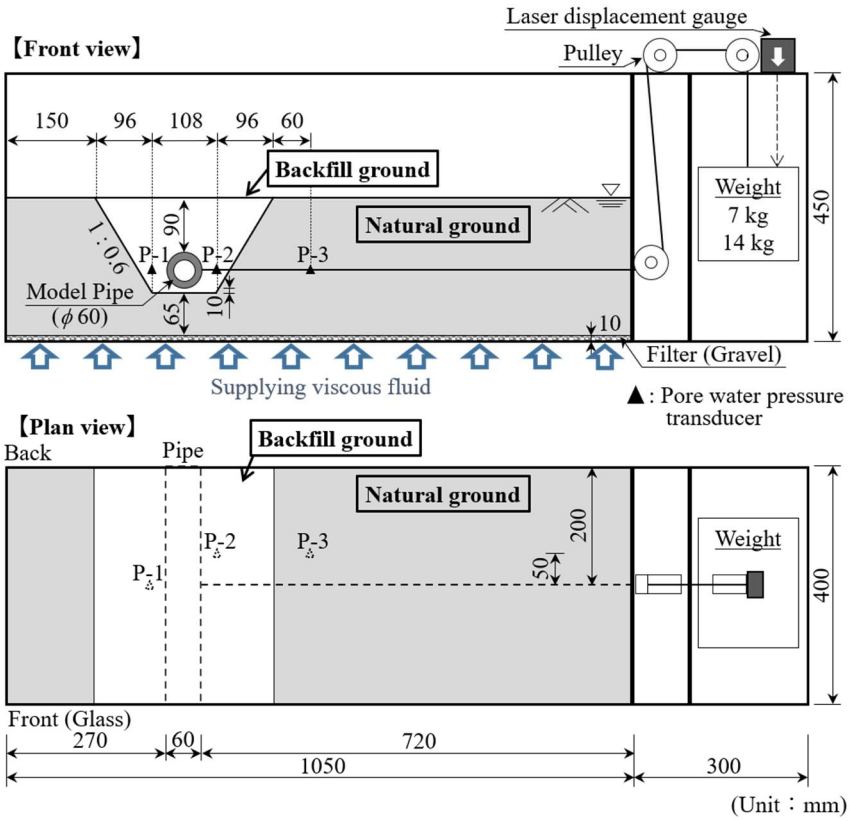

Fig. 3-2 Test container of centrifugal shaking table test

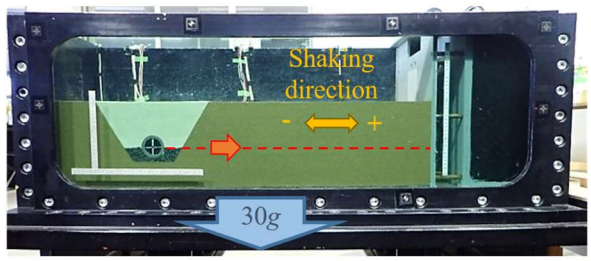

(a) Test container

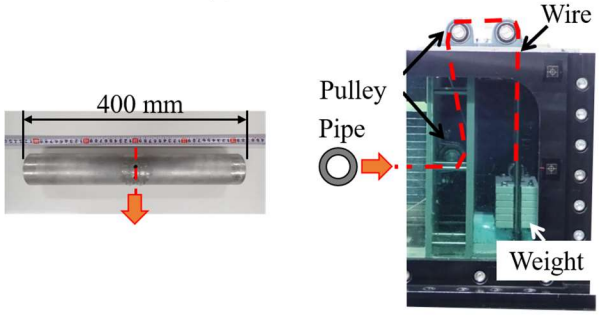

(b) Model pipe (c) Loading system

Fig. 3-3 Test equipment: (a) test container; (b) model pipe; (c) loading system

7 kg and 14 kg: these weights on the prototype scale corresponded to the thrust forces acting on a pipe bend, with a diameter of 1800 mm and a bending angle of 45º, under internal pressure of 150 or 300 kPa.

An aluminum straight pipe shown in **Fig. 3-3**(b) was used in the present experiments, although the thrust force is actually generated at the pipe bend. Ohta et al. (2018a) conducted lateral loading experiments for three model pipes with different bending angles but the same projected length, showing that the bending angle of the pipes hardly affected the lateral resistance. Additionally, the centrifugal tests had limitations on the choice of the test container. Therefore, the authors decided to conduct the experiments under two-dimensional conditions. The outer diameter, length, and mass of the model pipe were 60 mm, 396 mm, and 2.3 kg, respectively. Both ends of the pipe were closed. A sponge was put on the two ends of the pipe along the edges to prevent soil from flowing into gaps between the pipe ends and the container walls. The friction between the sponge and the container wall was reduced by fluorine coating. The unit weight of the model pipe approached that of the model ground to avoid the uplifting and sinking of the model pipe during experiments. The unit weights of the model pipe and the saturated silica sand were 20.5 and 19.5 kN/m^3, respectively. The model pipe was pulled laterally by the wire through the center of the model pipe. The wire (ϕ 4) passed through an aluminum tube (ϕ 6) buried in the model ground to decrease the friction between the wire and the soil.

The model grounds were prepared using three kinds of soil to simulate the natural ground and the backfill ground, respectively. In most practical fields, the backfill ground is easier to liquefy than the natural ground. Therefore, in this study, the backfilled ground and the natural ground were simulated separately using soils with different liquefied strengths.

Well-graded sand, called Kasama sand classified as SF, was used to reproduce the natural ground to reduce the saturation time. The natural ground made from Kasama sand did not liquefy during experiments, as described later. The dry unit weight of the well-graded sand was 13.8 kN/m^3, which was 93% of the maximum dry weight based on a standard Proctor compaction test. The initial void ratio of the sand was 0.84. Silica sand and gravel were used to reproduce the backfill ground. The dry unit weights of silica sand and gravel were 15.6 and 16.2 kN/m^3, respectively. The initial void ratio of silica sand and gravel were both 0.66. The unit weight of silica sand corresponded to a relative density of 60%. Note that the maximum and minimum dry densities of silica sand were 17.2 and 13.7 kN/m^3, respectively. Densities of silica sand and gravel were determined based on the

results of cyclic undrained triaxial tests described later. The particle sizes and physical properties of the ground materials are shown in **Fig. 3-4**.

Klinkvort et al. (2018) summarized the results of previous studies and reported that no scale effect on the lateral load of a model pile was observed when the ratio of pile diameter and d_{50} (the average grain size) was greater than 40, 60 or 88. Gravel in experiments of this study was too large to avoid the scale effect because the ratio of the pipe diameter and d_{50} of gravel is 18. To ignore the scale effect, d_{50} of a backfill material have to be less than 1.5 mm. Ono et al. (2019) showed that the layers made of the soil with d_{50} of about 1.5 mm were liquefied during shaking (i.e. excess pore-water pressure= 1.0). The result does not correspond to the well-known fact that the layer made with gravel (maximum particle size of 25–40 mm) hardly liquefied in the real field. Selection of the material which meets both requirements of the bearing capacity and the permeability is impossible. Gravel with d_{50} of 3.29 mm was chosen for the experiments to ensure the dissipation of the excess pore-water pressure, which was the important characteristic of gravel.

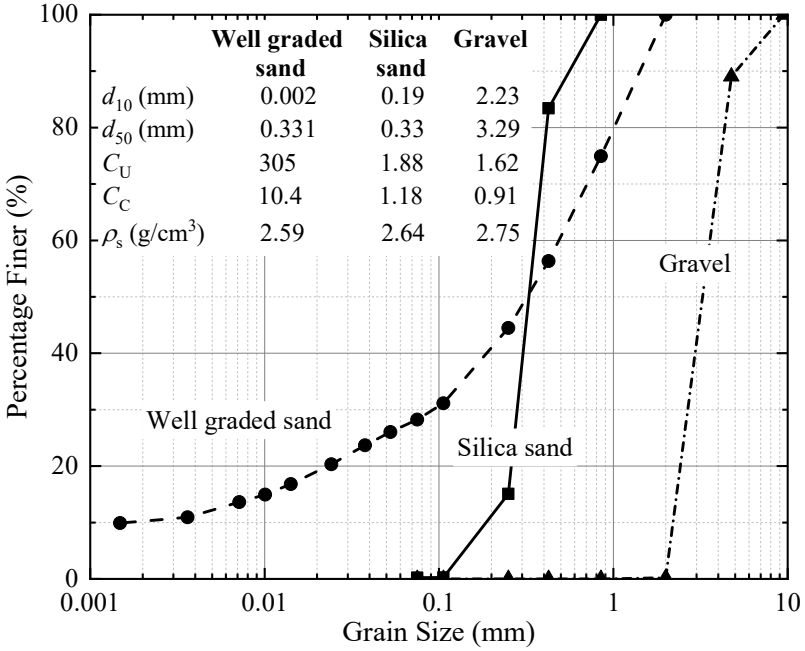

Fig. 3-4 Grain size distribution of Kasama sand, silica sand, and gravel

The cyclic undrained triaxial tests were performed on silica sand and gravel. In the triaxial tests, specimen densities were the same as in the centrifugal tests. A confining pressure of 35 kN/m^2 was applied to each specimen. This confining pressure was nearly equal to the effective confining pressure at the spring line of the pipe. The results of the cyclic undrained triaxial tests are shown in **Fig. 3-5**. Based on the results in **Fig. 3-5**(a), the liquefied strength ratios of silica sand and gravel were 0.42 and 1.12, respectively. Although the liquefied strength of silica sand was slightly high for reproducing a liquefied ground, this density was adopted in the experiments as a means of considering the

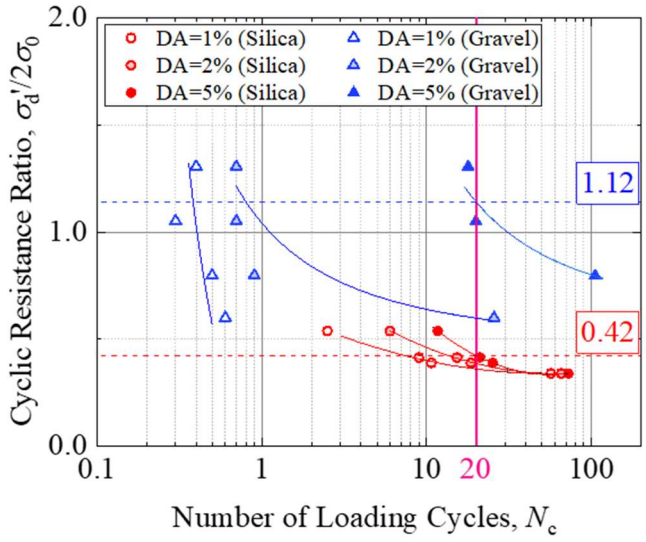

(a) Relationship between cyclic stress ratio and number of loading

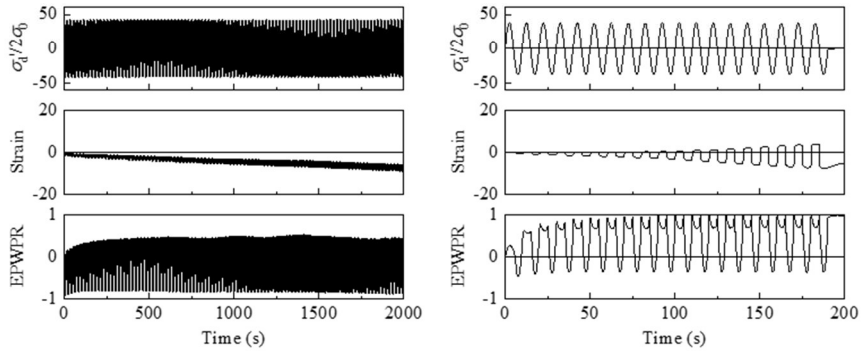

(b) Gravel (c) Silica sand

Fig. 3-5 Results of the cyclic undrained triaxial tests: (a) relationship between cyclic stress ratio and number of loading; (b) time histories of stress ratio, strain and excess pore water pressure

condition of sand ground in situ. Note that the liquefied strength was determined by the cyclic stress ratio at a cycle number of 20 and a double-amplitude axial strain of 5%.

The following describes the preparing procedure of the model ground. Before preparing the ground, a filter of 10 mm thickness was set on the bottom of the test container. The filter was made of gravel with an average grain size of 3.29 mm. A non-woven fabric covered the surface of the filter in order to protect the soil from running out into the filter layer. The natural ground was prepared on the filter. The well-graded soil was compacted in 13 layers (10–20 mm/layer). The water content of the well-graded soil was adjusted to 24%, which is the optimum moisture content for easing compaction. After the natural ground was compacted, a trench was excavated, and the model pipe was buried with gravel and silica sand as shown in **Fig. 3-6**. The backfill ground was compacted in ten layers (10–20 mm/layer). The water content of the silica sand was adjusted to 5%. When the model ground was completed, the test container was mounted on the centrifuge shaker. The saturation process was conducted under the centrifugal field of 30*g*.

Four different types of backfilling conditions were investigated in this study, as shown in **Fig. 3-6**. The dimensions of the trench were determined on the basis of the design guidelines in Japan (MAFF, 2021). The depth of the trench was 160 mm (H/D=1.5), where H is the depth to the top of the pipe and D is the outer diameter of the pipe. H/D=1.5 is

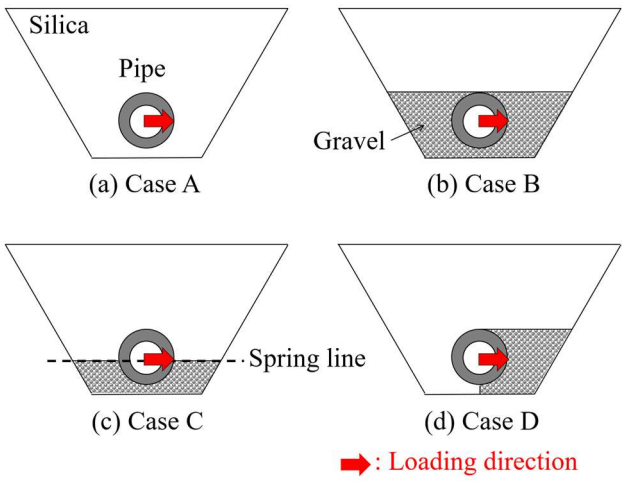

Fig. 3-6 Arrangements of gravel layers in the experiments

the typical ratio for large-diameter pipes. The gradients of both slopes were 1:0.6. The width of the trench at the bottom of the pipe was 120 mm. The thickness of the bedding under the pipe was 10 mm.

In Case A, the pipe was backfilled only with silica sand. In Case B, a gravel layer extended upwards from the bottom of the trench to the top of the pipe. The amounts of gravel used in Cases C and D were approximately half that of Case B in order to assess the effects of the amount and arrangement of gravel in thrust restraint. In Case C, gravel was placed up to the height of the spring line as shown in **Fig. 3-6**. The resistance acting on the lower half of the pipe was important in resisting pipe displacement. Kawabata et al. (2002) pointed out that the passive horizontal earth pressure distribution acting on the pipe experiences a peak at about 45º below the spring line for a laterally loaded pipe. Therefore, if the ground on the lower half of the pipe is not liquefied, the lateral resistance might be maintained sufficiently. On the other hand, Palmer et al. (2009) mentioned that the vertical force at the lower leading quarter of the pipe causes the uplifting of the pipe. Reinforcing only the ground on the bottom half of the pipe might therefore risk uplifting of the pipe. In Case D, only the passive side of the pipe was backfilled with gravel. Needless to say, passive resistance is important in thrust restraint. The pipe in Case D was expected to experience the same resistance force as in Case B because Cases B and D had the same amount of gravel on the passive side of the pipe. On the other hand, if the soil on the active side of the pipe were to liquefy, then the pipe could move substantially to the active side under seismic conditions. In other words, the displacement amplitude of the pipe could become large and affect the stability of the buried pipe.

Shaking tests in all cases were carried out with a loading mass of 7 kg initially to assess the effectiveness of the gravel layer as the thrust restraint. After preparing the model ground, the testing container was placed on the centrifuge, and a mass of 7 kg was installed. The saturation process was performed under a centrifugal field of 30*g*. In the saturation process, a viscous liquid made of Metolose was used. The viscosity of the fluid was adjusted to 30 times that of water to reduce the permeability of the sand, thereby reproducing the desired pore-pressure response of water under the centrifugal field. The centrifuge was equipped with a rotary joint so that the liquid was provided from the outside during each run. Pressurized fluid was introduced to the model ground slowly from the bottom of the model ground under a centrifugal field of 30*g*. Each saturation process was performed gradually over the course of more than 12 h to avoid the occurrence of air bubbles in the model ground.

After shaking under a loading mass of 7 kg, the centrifuge was stopped, and the loading mass was increased to 14 kg. In Cases C and D, the shaking process was then conducted again. The mass was increased to 14 kg because a loading mass of 7 kg produced no displacement difference between Cases C and D. A difference in results between Cases C and D under a loading of 14 kg was observed, and the gravel layer's effects on pipe behavior were investigated. Note that displacement of the pipe due to the change of lateral load from 7 to 14 kg was rarely observed.

In the shaking process, four shaking regimes with prototype accelerations of 2, 4, 6 and 8 m/s^2 were applied to the models. The prototype frequency and duration of the shaking were 5 Hz and 60 s, respectively. Acceleration responses of the shaking table are shown in **Fig. 3-7**. The shaking interval had sufficient time to dissipate excess pore-water pressure in the model ground. To judge the level of shaking applied to the test models, the power spectral intensity (PSI) was calculated. The PSI value, proposed by Nozu and Iai (2001), indicates the intensity of an earthquake. Nozu and Iai (2001) pointed out that the PSI value has a higher correlation with seismic damage to structures than does the maximum acceleration. The PSI value was calculated using the following equation:

$$\mathrm{PSI} = \left(\int_0^{\infty} \left(v(t)^2 \right) dt \right)^{0.5} \tag{3.1}$$

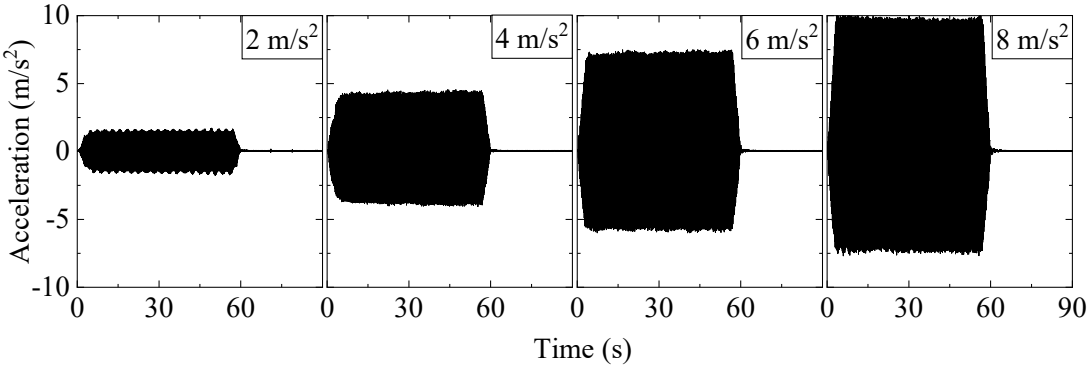

Fig. 3-7 Acceleration responses of the shaking table

Table 3-3 Calculated PSI values

	Maximum acceleration m/s^2	PSI values $cm/s^{0.5}$
Shaking table tests	2.0	24
	4.0	66
	6.0	103
	8.0	133
The 2011 off the Pacific coast of Tohoku Earthquake*	NS: 3.8	NS: 130
	EW: 4.0	EW: 161
	UD: 3.5	UD: 37

*Observation point: Shinmachi, Oketani cho, Miyagi prefecture, Japan

where $v(t)$ (m/s) is the velocity at time t. The calculated PSI values for the prototypes are shown in **Table 3-3**. PSI values for the 2011 off the Pacific coast of Tohoku Earthquake are also calculated for comparison. The calculated results imply that the level of shaking at 8 m/s^2 (PSI of 133) was almost the same as that of the 2011 Tohoku earthquake (PSI of 130). The shaking condition of this experiment was therefore quite severe.

3.3 Experimental results

All experimental results are presented at the prototype scale

3.3.1 Response of excess pore water pressure ratio

Fig. 3-8 shows the response of the excess pore-water pressure ratio (EPWPR) in Cases A and B. The EPWPR is defined as the measured excess pore-water pressure divided by the initial effective overburden pressure at the depth of the pore-pressure transducers, as shown in Eq.(3.2). The actual initial effective stress in the model ground was different from the simple overburden pressure due to the effects of the trench and the pipe. Therefore, the value of EPWPR calculated from Eq.(3.2) is used only as a guide.

$$\mathrm{EPWPR} = \frac{\Delta u}{(\gamma_{\mathrm{sat}} - \gamma_{\mathrm{w}}) \cdot H} \tag{3.2}$$

where, Δu is the excess pore water pressure; γ_{w} is the unit weight of water; γ_{sat} is the unit weight of the saturated sand; H is the depth of the earth cover. In Case A, in which the pipe was backfilled with only silica sand, the EPWPR in the backfill ground rose to around 0.6, while the EPWPR in the natural ground barely increased. The difference in liquefaction properties between the backfill ground and the natural ground manifested clearly. In Case B, in which the pipe was backfilled with gravel and silica sand, the pore-water pressure accumulated less than in case A because gravel was able to dissipate the excess pore pressure rapidly. The large amplitude of the pore-water pressure in gravel as shown in **Fig. 3-8** is the typical shear behavior of gravel under undrained conditions. A similar behavior is confirmed for gravel in **Fig. 3-6**, which shows the responses of gravel and silica sand during the cyclic loading tests described in **Fig. 3-5**.

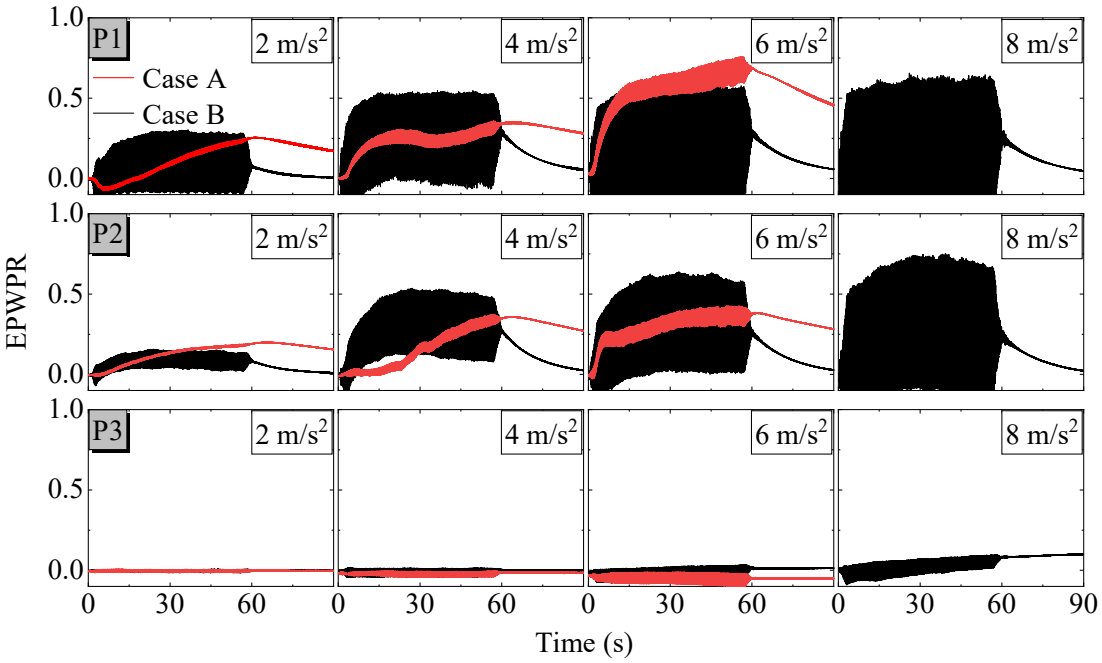

Fig. 3-8 Response of excess pore water pressure ration at model ground

3.3.2 Pipes after experiments

Fig. 3-9 (a) and (b) show images of the test models after shaking at a maximum acceleration of 8 m/s^2. Yellow crosses in the images denote the positions of the pipe centers after each shaking. As shown in **Fig. 3-9** (a), the pipe without gravel (Case A) moved substantially, whereas the pipes with gravel (Cases B, C and D) moved only slightly.

Focusing on pipe behavior, the pipe in case A displaced drastically not only laterally but also upwards. Ono et al. (2016) reported pipe uplift associated with lateral displacement in liquefied ground when the pipe moved along the slope of the failure surface as suggested by Audibert and Nyman (1977). Note that the unit weight of the model pipe in this study was adjusted to that of the saturated silica sand to avoid buoyancy-related uplift

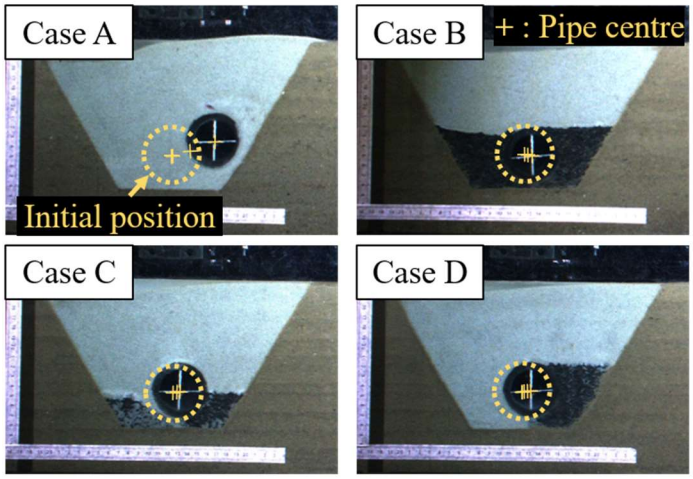

(a) Loading mass of 7 kg

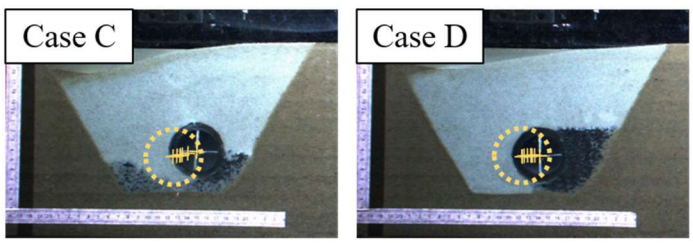

(b) Loading mass of 14 kg

Fig. 3-9 Images of test models after shaking at the amplitude of 8.0 m/s^2: (a) loading mass of 7 kg; (b) loading mass of 14 kg

of the pipe. As for the cases with gravel, the pipe in Case C uplifted at a loading mass of 14 kg, whereas the pipe in Case D seemed to move only laterally during shaking. The relationship between the gravel layer layout and the uplift of the pipe is further discussed in Section 3.4.4.

Focusing on the behavior of the gravel layer, the gravel layer on the passive side seemed to be compressed by the pipe. However, the shape of the layer did not deform drastically, except in Case C at a loading mass of 14 kg.

3.3.3 Lateral displacement of pipes

Fig. 3-10 (a) and (b) show the lateral displacement of the pipe as measured by a laser displacement transducer. The lateral displacement values for the pipe in **Fig. 3-10** are normalized by the outer diameter of the model pipe. The dotted line in **Fig. 3-10** represents the normalized displacement limit at which a pipe with ϕ1800 is able to maintain function. The displacement limit is determined by the displacement of the pipe bend when an angular displacement ψ or a sum of δ_{ja} and δ_{jb} (see **Fig. 3-11**) reaches its allowable value. The allowable values of ψ and $\delta_{ja}+\delta_{jb}$ were set to 5º and 168 mm, respectively, referring to FRP pipe standards. ψ, δ_{ja} and δ_{jb} were calculated using Eq. (3.3)-(3.6), quoted from Itani et al. (2016).

$$\delta_{ja} = \frac{\alpha}{2} - \frac{D}{2}\sin\psi \tag{3.3}$$

$$\delta_{jb} = D\sin\psi \tag{3.4}$$

$$\alpha = \sqrt{\left(L_{straight} + Y_{bend}\sin\frac{\theta}{2}\right)^2 + \left(Y_{bend}\cos\frac{\theta}{2}\right)^2} - L_{straight} \tag{3.5}$$

$$\psi = \cos^{-1}\left[\frac{L_{straight} + Y_{bend}\times\sin(\theta/2)}{L_{straight} + \alpha}\right] \tag{3.6}$$

where $L_{straight}$ is the length of the straight pipe; Y_{bend} is the displacement of the pipe bend; θ is the bending angle of the pipe bend. The displacement limit was calculated based on the following assumptions: D=1800 mm, θ=45º and $L_{straight}$=4000 mm. When the displacement of the pipe bend Y_{bend} was 393 mm, the corresponding values of ψ and δ_{ja}

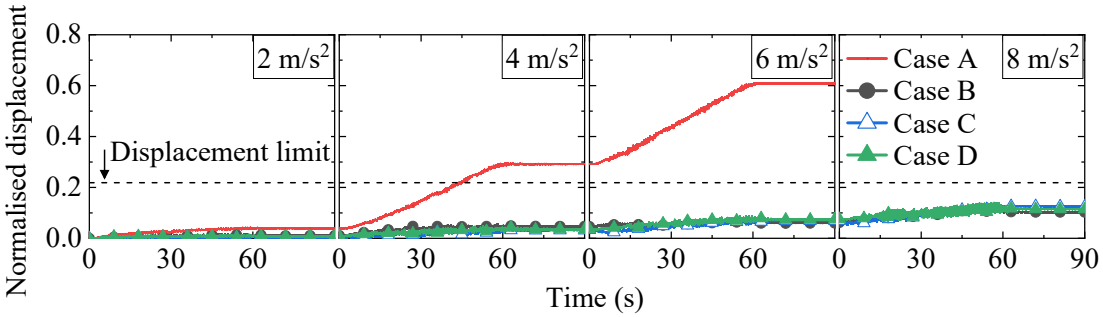

(a) Loading mass of 7 kg

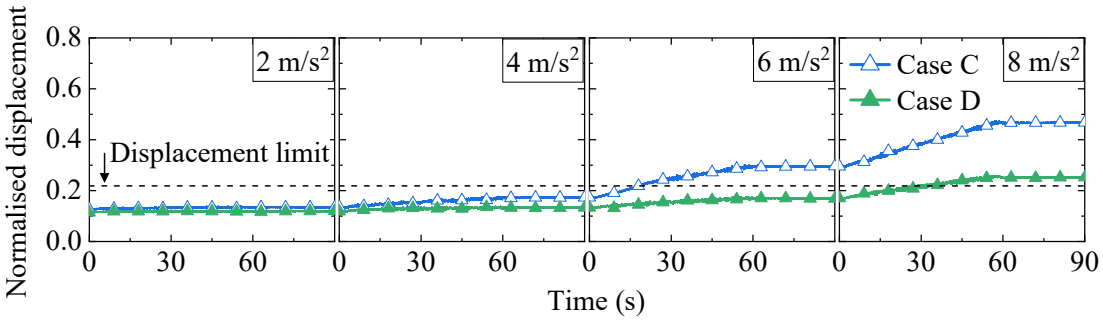

(b) Loading mass of 14 kg

Fig. 3-10 Normalized lateral displacement of the pipe: (a) loading mass of 7 kg; (b) loading mass of 14 kg

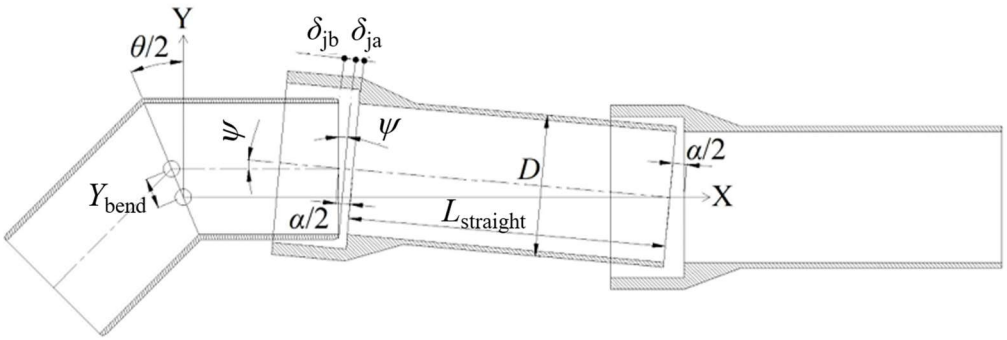

Fig. 3-11 Flexible joint (Itani et al, 2016; modified by the author)

$+\delta_{jb}$ were 5º and 162 mm, respectively. Therefore, the displacement limit of the pipe bend was determined to be 393 mm, representing a normalized value of 0.22.

3.4 Discussion

3.4.1 Effectiveness of gravel backfill as thrust restraint

The effectiveness of a gravel layer as a thrust restraint (**Fig. 3-10**(a)) was examined. In case A without gravel, the pipe displaced far beyond the displacement limit at a shaking acceleration of 4 m/s^2 (PSI of 66), while in the cases with gravel, the pipe displaced within the displacement limit even at a shaking acceleration of 8 m/s^2 (PSI of 133). These results show that backfilling the pipe with gravel is effective in preventing the displacement of large-diameter pipes subjected to thrust force during large earthquakes.

3.4.2 Effectiveness of gravel layer for mitigating lateral pipe displacement

Regarding the layout of gravel backfill, there was little difference among the lateral displacement responses in Cases B, C and D during shaking (loading mass=7 kg), as shown in **Fig. 3-10** (a). These results imply that a small amount of gravel, as used in Case C or D, is sufficient for thrust restraint to counter typical thrust forces generated on pipes during large earthquakes. However, the results for a loading mass of 14 kg **(Fig. 3-10** (b)) show that the displacement of the pipe in Case C increased during shaking at an amplitude of 6 m/s^2. **Fig. 3-9**(b) shows images of test models after shaking (amplitude= 8 m/s^2, loading mass= 14 kg). As for the gravel layer on the passive side, the shape of that gravel layer deformed more in Case C than in Case D. The thickness of the gravel layer apparently affected this deformation. Increasing the thickness of this gravel layer may reduce the compressive stress on the gravel layer. Therefore, the layout of the gravel layer on the passive side of a pipe is important for pipeline stability.

3.4.3 Effectiveness of gravel on the active side of a pipe

Gravel on the active side of the pipe is expected to reduce the movement of the pipe in the trench. The role of gravel on the active side is confirmed by the results of Cases B, C and D. **Fig. 3-12**(a) shows the acceleration of the pipe and the model ground during shaking (amplitude=8 m/s^2, loading mass=7 kg). Note that the acceleration shows a negative value if the acceleration generates towards the active side. Case C shows no data due to a measurement fault. The responses in Case B with gravel on the active side showed no phase difference between the pipe and the ground, whereas the responses in

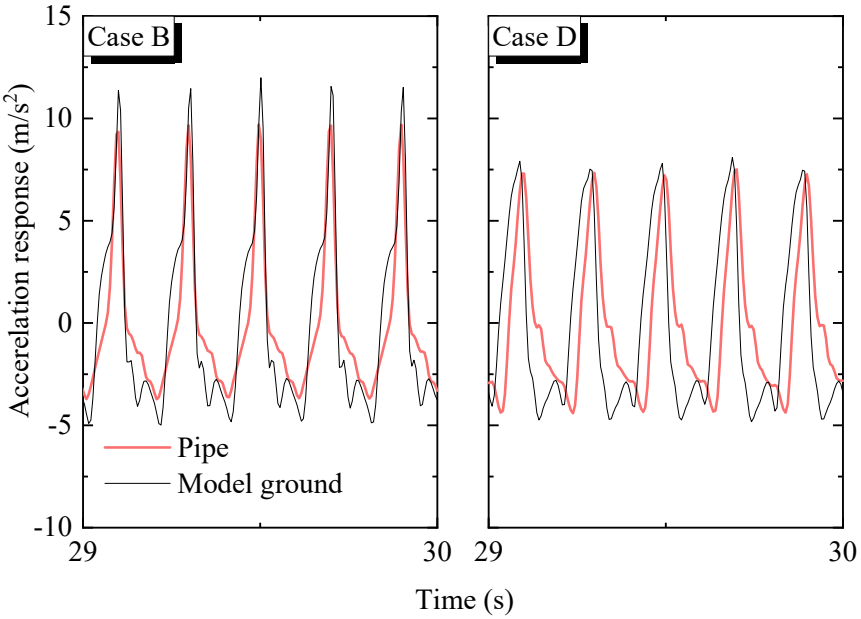

(a) Acceleration response at 8 m/s^2 shaking (Loading weight with 7 kg)

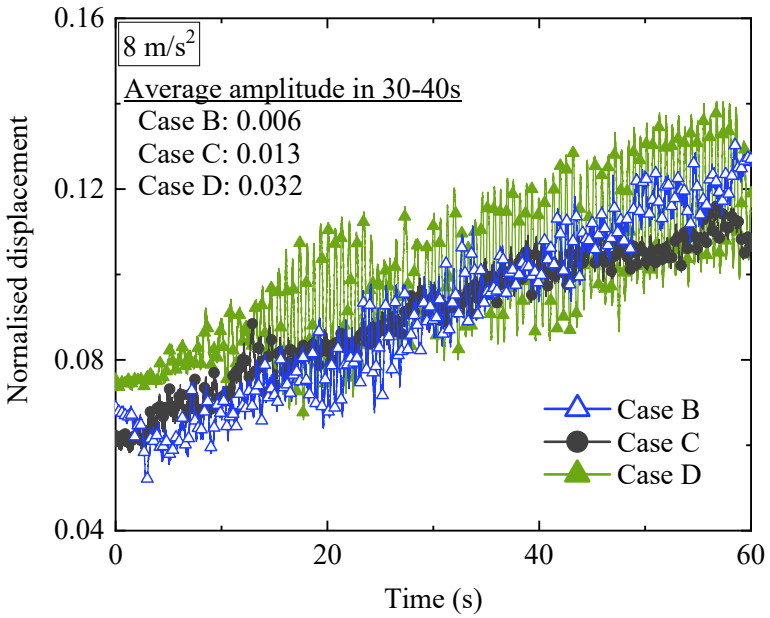

(b) Displacement of the pipe at 8 m/s^2 shaking (Loading weight with 7 kg)

Fig. 3-12 Responses of pipes buried with gravel: (a) acceleration response at 8 m/s^2 shaking; (b) displacement of the pipe at 8 m/s^2 shaking

Case D without gravel on the active side showed a slight phase lag between the pipe and the model ground. **Fig. 3-12**(b) shows an enlarged view of pipe displacement during shaking (amplitude =8 m/s^2, loading mass= 7 kg). The average amplitude of displacement between 30 and 40 s was 0.03 in Case D but 0.01 in Cases B and C. Although the amplitude of pipe displacement in Case D was the largest, the total lateral displacement in Case D after shaking was the same as in Cases B and C, as shown in **Fig. 3-10**(a). These test results indicate that gravel on the active side provides no thrust-restraint effect.

3.4.4 Effectiveness of gravel backfill in uplift mitigation

As mentioned in Section 3.3.2, the pipe without gravel (Case A) moved obliquely. Mitigating the uplift is important for the stability of the pipe because uplift also causes pipe damage (e.g. joint separation). The effect of gravel in mitigating pipe uplift was confirmed by the test results.

Fig. 3-13 shows the relationships between the lateral and upward components of pipe displacement. Pipe displacement measurements were obtained from photos and

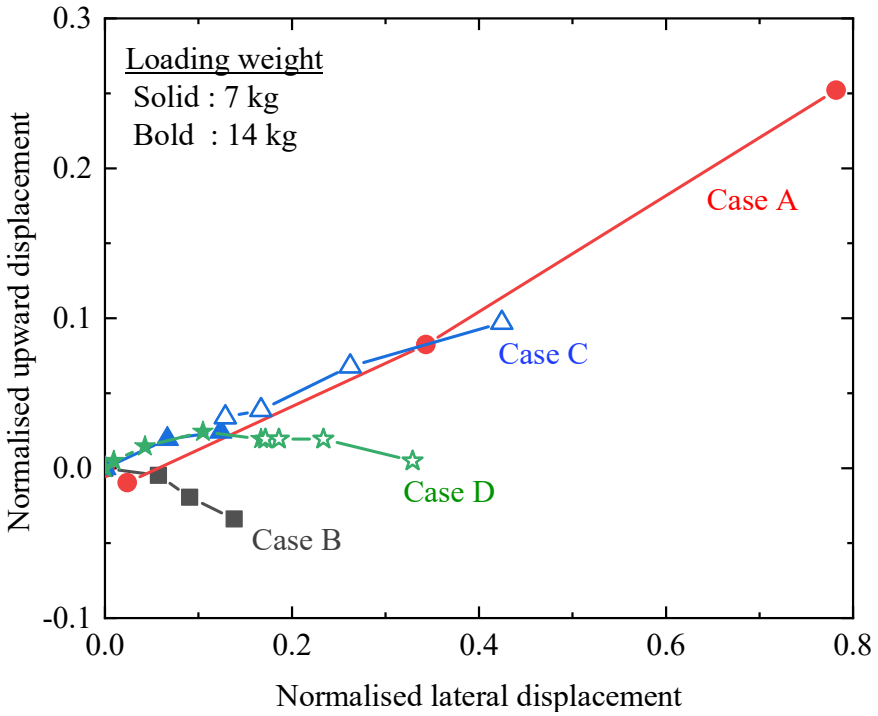

Fig. 3-13 Relationship between lateral and upward displacement of the pipe

normalized by the outer diameter of the pipe. The upward displacement in Cases A and C increased drastically with increasing lateral displacement. Furthermore, the relationship between lateral and upward displacement in Case C was similar to that in Case A. On the other hand, the pipes in Cases B and D moved laterally while hardly uplifting. These differences in pipe behavior were caused by the differences in gravel layout; gravel in Cases B and D covered the upper quarter of the pipe on the passive side, while gravel in Cases A and C did not. Some studies have assessed the effectiveness of gravel above a pipe in mitigating uplift. Ling et al. (2003) proposed a design procedure for mitigating pipe uplift based on test results and pointed out that the deadweight and stiffness of the gravel unit above a pipe, confined by geosynthetics, were important in mitigating pipe uplift in the liquefied ground. The test results indicate that gravel above the pipe might suppress pipe uplift associated with lateral displacement.

3.5 Conclusions

In this study, four shaking table tests were conducted on the buried pipes under a 30*g* simulated gravitation field for the purpose of evaluating effective layouts of gravel backfill as a thrust restraint under earthquake conditions. The main conclusions are as follows.

1 Under the typical thrust force magnitudes, the displacement of a pipe backfilled without gravel increased drastically beyond the allowable value during shaking, whereas that of a pipe with gravel remained within the allowable value even under large earthquake conditions. These results revealed that gravel backfill works effectively as a thrust restraint against typical thrust force generated on pipes during earthquakes.

2 Under large thrust force magnitudes, the pipe moved substantially when the gravel layer extended only to the spring line of the pipe. On the other hand, the pipe remained within the allowable displacement when the gravel layer on the passive side extended to the top of the pipe, even if there was no gravel layer on the active side of the pipe.

3 The amplitude of pipe displacement during shaking increased when no gravel was placed on the active side of the pipe. However, the amplitude of the pipe displacement barely affected the total lateral displacement of the pipe. Therefore, gravel on the

active side produced no meaningful thrust-restraint effect.

4 Gravel on the upper half of the passive side of the pipe suppressed pipe displacement not only laterally but also upwards.

5 The above conclusions indicate that gravel is required on the passive side from the bottom to the top of the pipe. Therefore, a gravel layer on the passive side from the bottom to the top of the pipe (Case D) is the best layout for thrust restraint among the four test conditions. The layout of gravel on the passive side of the pipe is crucial in mitigating lateral displacement at pipe bends.

Chapter 4

The contents of this chapter are based on:

Ohta, Y., Nagatani, T., Sawada, Y., and Kawabata, T. (2022), “Effectiveness of existing channel wall on thrust restraint for pipe bends and effect of geogrid on reinforcement of channel walls”, *Geosynth. Eng. J.*, 37, pp. 1–8.

Chapter 4

Effectiveness of existing channel wall on thrust restraint for pipe bends

4.1 General

In this chapter, the stability of pipe bends buried in open channels is examined based on the results of the model experiments. As introduced in Chapter 1, a pipe is sometimes buried without removing an existing channel wall when an aging open channel is converted to a pipeline. Although the number of construction experiences is increasing, only some previous studies focus on the behavior of pipes buried in old open channels. At a bend of pipelines, while channel walls are expected to act as reaction walls, the effectiveness of channel walls as reaction walls can vary depending on the types and conditions of existing channel walls. In this study, model experiments were conducted to investigate relationships between channel walls and pipe bends, especially the effect of channel geometry on the lateral resistance force against thrust force. In addition, the possibility of using geogrids for reinforcing channel walls was also examined.

4.2 Construction experience

Examples of past constructions are summarized in this section to provide a general idea of conversion from open channels to pipelines without removing existing channel walls. Harada (1998) and Harima et al. (2015) reported on the Ryoso irrigation project, which aimed to update aging irrigation facilities. In this project, aging open channels were converted to 2000 mm class pipelines, as shown in **Fig. 4-1**. Shiraeda et al. (2008) reported the design and construction methods of a project in the basin area of the Shin-Yahagigawa river. The authors described a series of steps, from a selection of the design method to actual construction management, to convert flume channels to 1200 mm pipes, as shown in **Fig. 4-2**. Zaitsu et al. (2016) show an example of the conversion of pipelines in the basin area of the Kuzuryugawa river. In this project, a part of the existing open channels was converted to pipelines, as shown in **Fig. 4-3**(a). In the same basin area, pipes were buried in channels whose bottom slabs were removed to ensure the burial depth, as shown in **Fig. 4-3**(b).

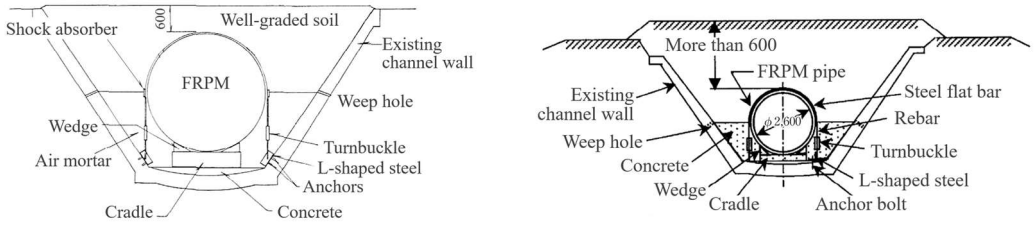

(a)Harada (1998) (b)Harima et al. (2015)

Fig. 4-1 Cross-sectional view of pipes in open channels reported by Harada (1998) and Harima et al. (2015) (modified by the author)

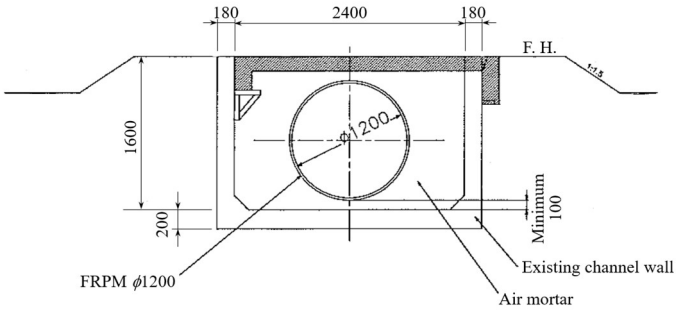

Fig. 4-2 Cross-sectional view of pipes in open channels reported by Shiraeda et al. (2008) (modified by the author)

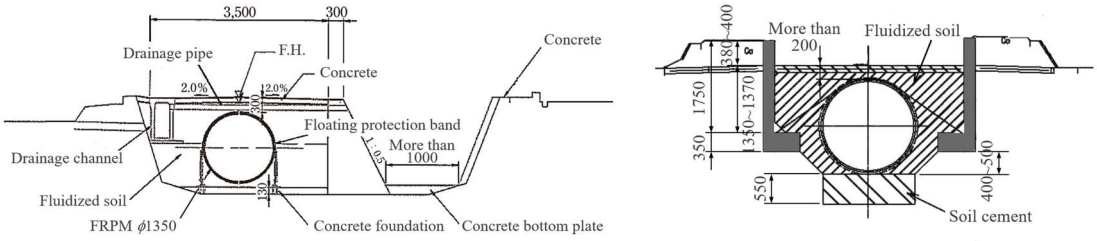

(a)Zaitsu et al. (2016) (b) Hokuriku Regional Agricultural Administration Office (2012)

Fig. 4-3 Cross-sectional view of pipes in open channels reported by Zaitsu et al. (2016) and Hokuriku Regional Agricultural Administration Office (2012) (modified by the author)

4.3 Outline of the experiments

As shown in Section 4.2, construction conditions, such as channel and pipe sizes, vary from site to site, making it difficult to define general conditions. In this study, a simple test model was built to focus on the effect of channel walls on the passive side of pipes as a primary investigation. Dimensions of the model were set at approximately 1/18 scale, assuming a large-diameter pipe with ϕ2000.

4.3.1 Test setup

Fig. 4-4 illustrates the schematic diagram of model experiments. The steel soil box has an inner dimension of 1500 mm in length, 500 mm in height, and 600 mm in width. The side walls of the soil box are transparent acrylic panels reinforced with steel bars to obtain the behavior of the model pipe and ground. The loading equipment, as shown in **Fig. 4-4**, consists of a motor, a jack, and loading shafts. A load cell and a displacement transducer were installed between the loading shafts and the jack to obtain the displacement and the resistance force of the model pipe. A rigid polyvinyl chloride (PVC) pipe with an outer diameter of 114 mm and length of 600 mm was used. A straight pipe was used to simulate the behavior of pipe bend under plane strain conditions. The apparent density of the model pipe was adjusted to 1.0 g/cm^3, which is the apparent density of the FRPM pipe with full water. The ends of the buried pipes were covered with aluminum plates and sponge tape to prevent sand from going between the pipe ends and the test box. A spherical seat was placed between the loading rods and the model pipe to prevent the pipe from floating or sinking during loading.

Four types of Aluminum plates were used to simulate channel walls, as shown in **Fig. 4-5**. Each plate is referred to as Type A-D. In Type A, a vertical plate has 12 mm in thickness, 186 mm in height, and 600 mm in length. In Type B, a bottom plate was attached to Type A, with dimensions of 12 mm in thickness, 171 mm in height, and 600 mm in length. In Type C and D, Type A was divided into two and three parts, respectively. A geogrid used to reinforce Type D was made of high-density polyethylene with a square opening of 10 × 10 mm and tensile strength of 77 kN/m. The tensile property of the geogrid is shown in **Fig. 4-6**. Sponge tape was also attached to both ends of the plates and the geogrid. The model ground was made from dry silica sand with a unit weight of 14.9 kN/m^3, corresponding to a relative density of 79 %. The properties of silica sand are described in **Fig. 4-7**.

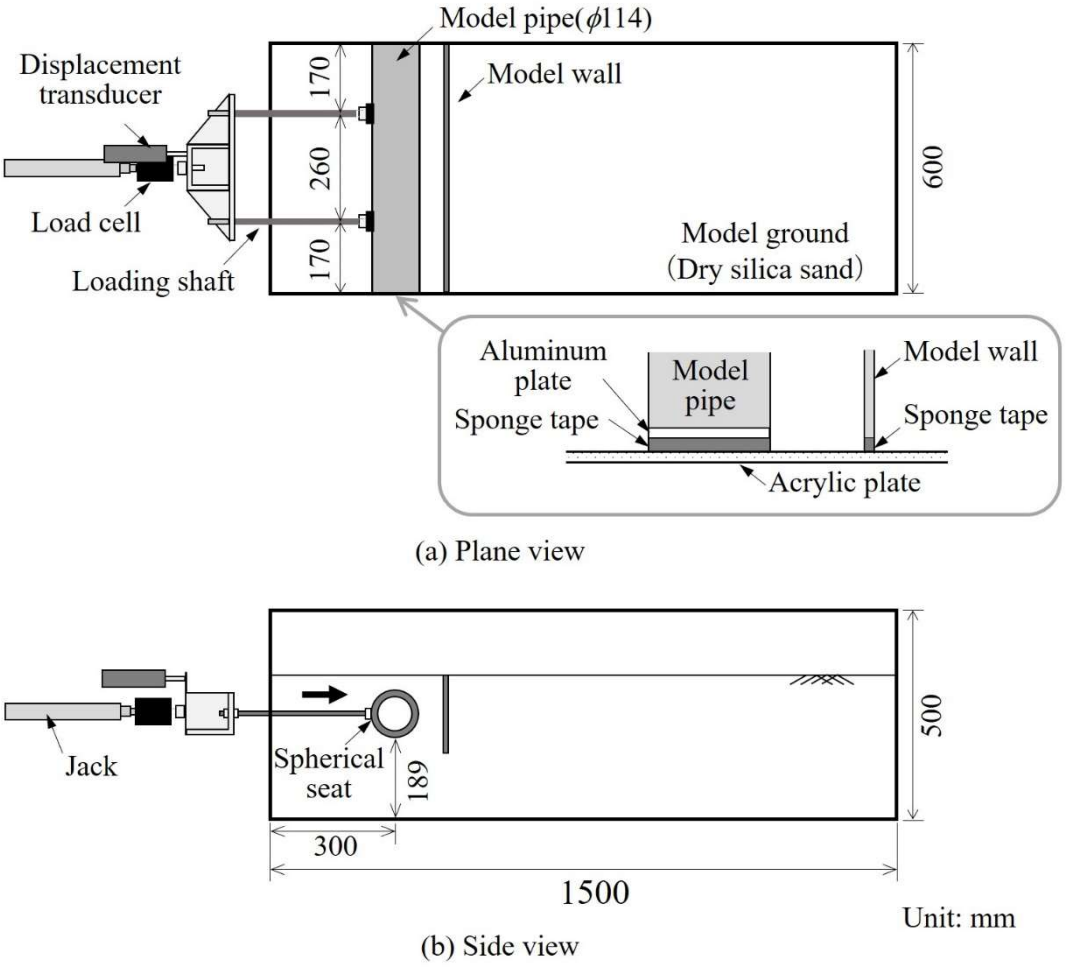

Fig. 4-4 Setup of the model experiments on pipes buried with channel walls

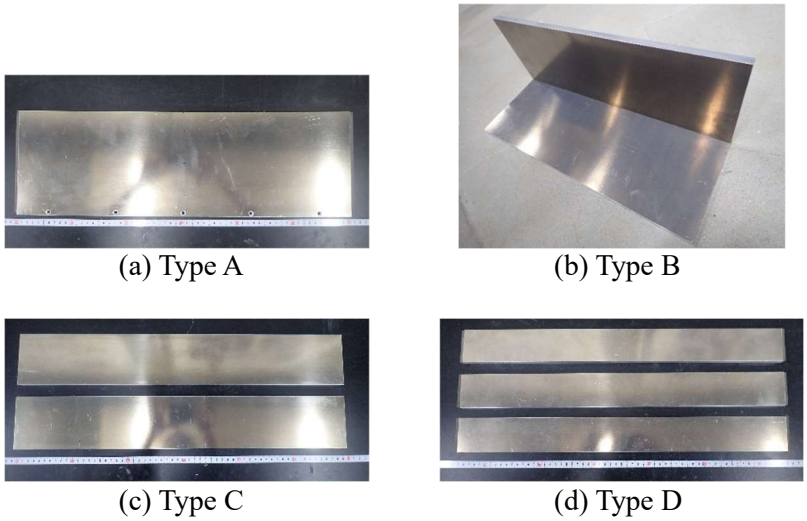

Fig. 4-5 Model channel walls

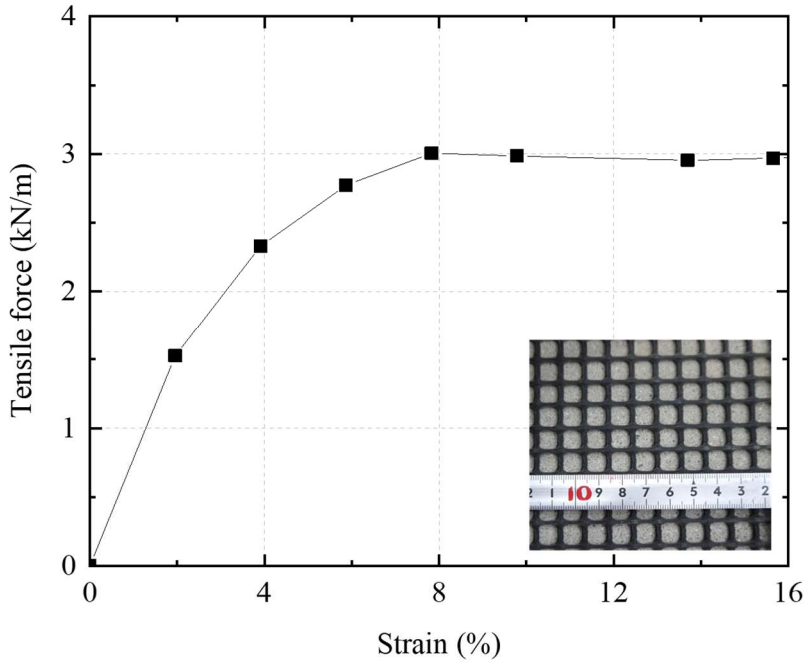

Fig. 4-6 Result of the tensile test of the geogrid

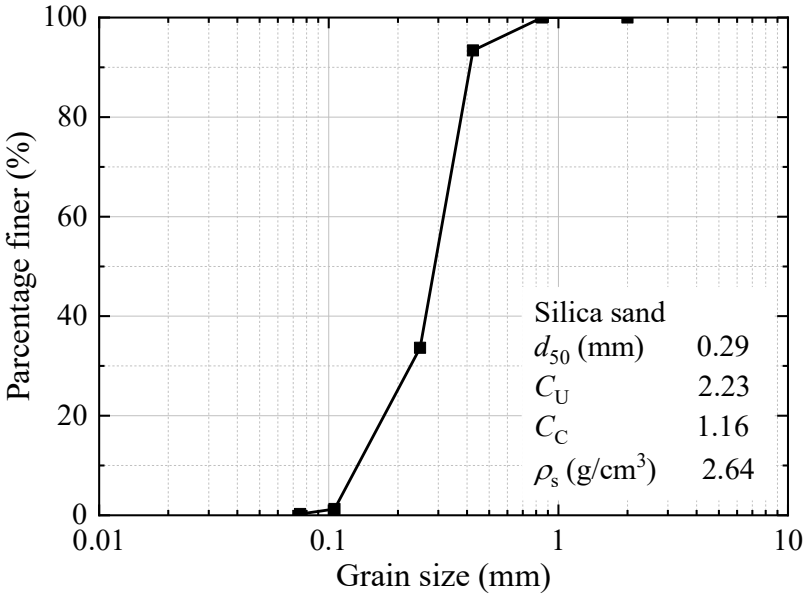

Fig. 4-7 Particle size distribution of silica sand

4.3.2 Test condition

A total of 8 test cases were conducted, varying shapes of walls and with or without the geogrid. The experimental conditions are summarized in **Fig. 4-8** and **Table 4-1**. In Case A, the Type A plate was placed in front of the pipe to simulate the vertical wall of open channel. In Case B, the bottom plate of Type B was expected to prevent the vertical plates from rotating and to increase the resistance force. The horizontal wall was fixed to the vertical wall. In Case B-separated, the horizontal plate was detached from the vertical plate to clarify the effectiveness of the bottom plate. Cases C and D assumed channel walls which cannot be considered as a single unit, such as a block wall. In Case D-gridI and D-gridL, the geogrid was installed along the Type D plate to reinforce the vertical plate and to increase the resistance force. Two types of geogrids, I-shaped and L-shaped, were attached to the vertical walls but not bonded to them.

In all cases, the model pipe was buried 35 mm below the ground surface. According to the current Japanese guideline of MAFF (2021), the soil cover must be at least 60 mm, corresponding to 30% of the diameter of 2000 mm. Therefore, the soil cover was set to 35 mm, approximately 30% of the model pipe diameter. The vertical walls were penetrated to a depth of 186 mm, and the horizontal walls were installed 25 mm (=0.2D) below the bottom of the pipe. The depth of 25 mm was also determined based on MAFF (2021): the bed thickness should be at least 0.2D from the bottom of the pipe. Note that the bed thickness is the depth from the bottom of a pipe to a trench surface.

4.3.3 Test procedure

After the model ground was completed, the buried pipe was displaced horizontally by 25 mm at a rate of 0.5 mm/min. The resistance force and the lateral displacement were measured during loading. A digital camera was used to capture images of the ground at an interval of 2 shots/min.

4.4 Experimental results

Fig. 4-9 shows the relationships between the displacement and the resistance force. All force–displacement relationships have peak values regardless of with or without channel walls. The peak resisting forces with walls were 1.1 to 2.5 times larger than that of Case Pipe, indicating that a channel wall effectively increases the lateral resistance force. In addition, the resistance force in some cases did not decrease rapidly after the peak. The ability to maintain resistance force during large displacement is important for the safety

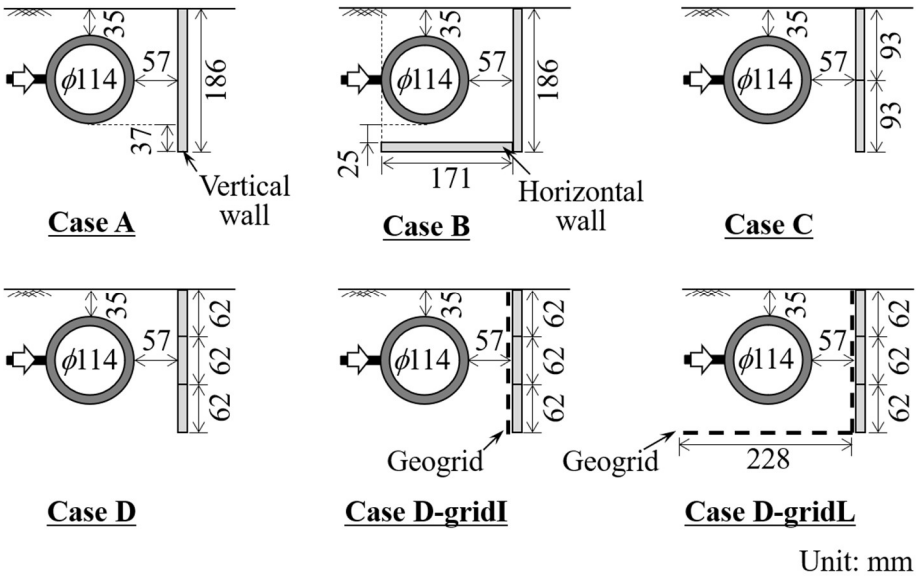

Fig. 4-8 Pipes and channel walls

Table 4-1 Test conditions

Case	Types of channel wall
A	Vertical wall (Type A)
B	Vertical+Horizontal walls (Type B) Both were fixed.
B-separated	Vertical+Horizontal walls (Type B) Both were not fixed.
C	Vertical wall with two parts (Type C)
D	Vertical wall with three parts (Type D)
D-gridI	Vertical wall with three parts (Type D) + I-shaped geogrid
D-gridL	Vertical wall with three parts (Type D) + L-shaped geogrid
Pipe	Without walls

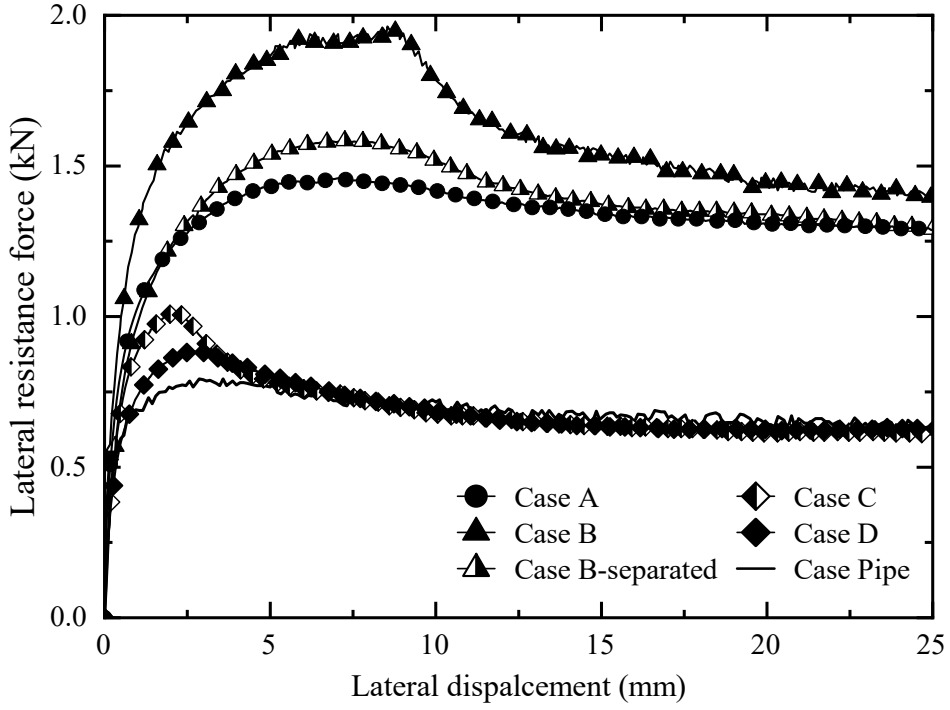

(a) various shape of walls

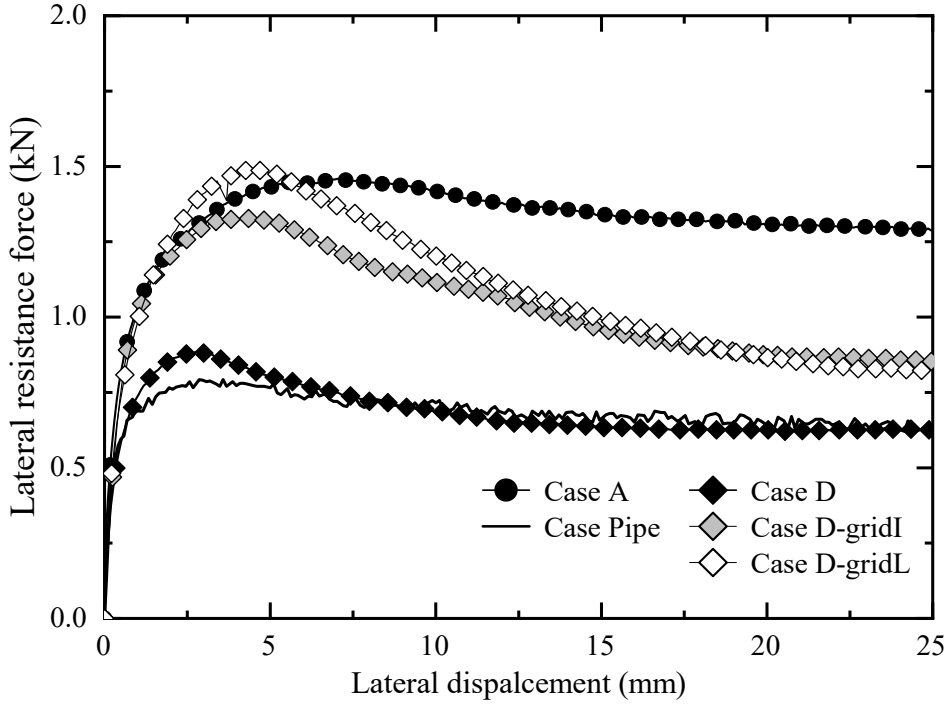

(b) walls with geogrids

Fig. 4-9 F–D relationships of pipe with walls: (a) various shape of walls; (b) walls with geogrids

of structures. Therefore, it was found that the remaining channel wall has a positive effect on the stability of the pipe bend.

Fig. 4-10 is images of the experimental models after loading. The black dot and solid line in **Fig. 4-10** denote the location of the pipes, walls, and geogrids before and after loading, respectively. The location of the shear bands are also described in **Fig. 4-10**. There was no significant difference in pipe behavior among the test cases, whereas the behavior of the walls, such as rotation and uplift, differed greatly depending on the wall geometry.

The shear strain of the model ground was calculated using *Strain-mp*, a software that measures strains from images. **Fig. 4-11** shows the distribution of the maximum shear strain between 0.0 to 2.5 mm of lateral pipe displacement. Values in **Fig. 4-11** are the accumulated values. In Case Pipe, the large shear strain is concentrated on the ground at the spring line of the pipe. Palmer et al. (2009) measured the normal stress acting on the buried pipe using tactile pressure sensors during lateral loading. The results showed that the distribution of normal stress was biased in the lower quarter of the pipe as the displacement of the buried pipe increased. The strain distribution in this study is consistent with the results of Palmer et al. (2009). In cases with channel walls, the shear strain is distributed to the passive side of the channel wall (outside of the channel). This result indicates that the resistance force increased due to the expansion of the strain area generated in the ground.

4.5 Discussion

4.5.1 Effects of geometry of channel wall to lateral resistance

Firstly, the results of Cases A and B are compared to investigate the effect of the bottom plate. **Fig. 4-9** shows that the peak resistance force of Case B was 1.3 times higher than that of Case A, which indicates that the vertical walls can increase the lateral resistance. According to **Fig. 4-10**, the vertical wall in Case A rotated due to the pipe displacement, resulting in the shear failure in the ground between the pipe and the sidewall. On the other hand, in Case B, the vertical and horizontal walls displaced accordance with the displacement of the pipe but hardly rotated. The strain distribution in the ground shown in **Fig. 4-11** indicates that the area of strain generation in Case B is larger than in Case A. In particular, strain in Case B was distributed downward from the bottom of the vertical wall. The suppression of rotation of the vertical plate led to expanding the shear failure zone on the surrounding ground, contributing to the increased resistance in Case B.

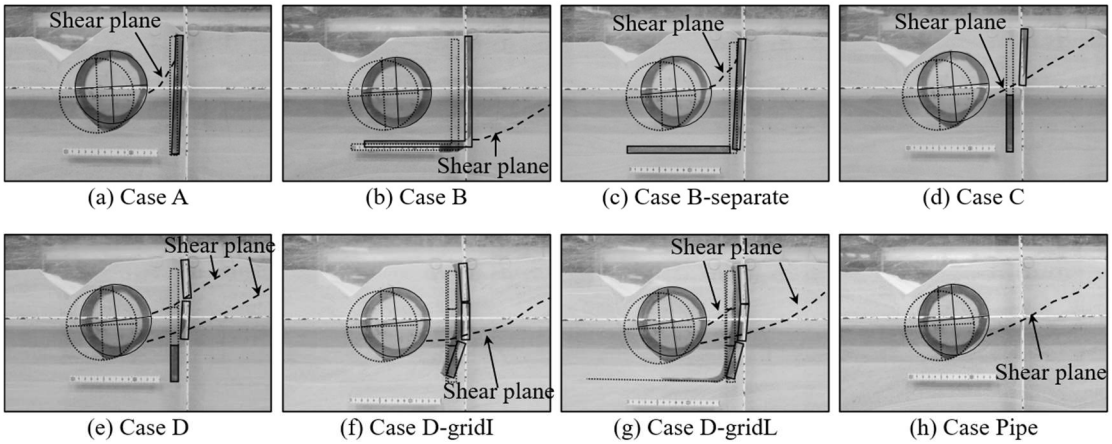

Fig. 4-10 Images of pipes and walls after loading

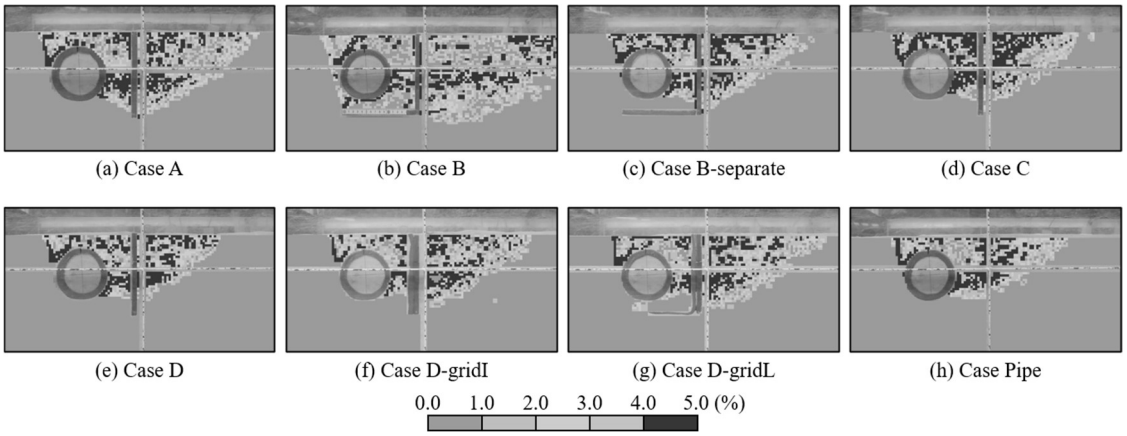

Fig. 4-11 Distribution of the maximum shear strains when the pipes was displaced from 0.0 to 2.5 mm

To clarify the effect of the bottom plate, the results of Case B-separated are added to the discussion. From **Fig. 4-9**, the peak resistance of Case B-separated is slightly higher than that of Case A but significantly lower than that of Case B. In **Fig. 4-10** and **Fig. 4-11**, the bottom plate of Case B-separated rarely changed before and after the experiment, while the rotation of the vertical wall and the deformation of the ground were almost the same as those of Case A. This result indicates that the bottom plate helps to increase the resistance force when the bottom wall is completely fixed to the vertical wall.

Next, the effect of the condition of the vertical walls is examined based on the test results of cases C and D. From **Fig. 4-9**, the resistant forces in Cases C and D were much lower than those in Case A and almost the same as in Case Pipe. From **Fig. 4-10**, the upper one or two pieces of walls in Case C and D displaced following the deformation of the model ground. **Fig. 4-11** shows that, especially in Case C, a large strain was concentrated between pieces of walls. Sawwaf et al. (2006) investigated the increment of lateral resistance force due to the installation of piles on the passive side of the anchor plate. The authors suggested that the interruption of piles to failure planes on the anchor plate's passive side led to the increased lateral resistance force. It was also noted that the resistance of the soil increased with the depth of penetration of piles. In Cases C and D, the channel wall did not intercept the shear plane of the ground. In addition, no reaction forces seem not to be obtained from the lowest piece because the shear planes were generated above it. Therefore, it is considered that vertical walls with several parts, such as Cases C and D, do not provide as much resistance as vertical walls composed of a single piece like Case A.

4.5.2 Effectiveness of reinforcement using geogrid

In this section, the effectiveness of geogrids for the reinforcement of vertical walls with several parts is evaluated from the results of Case D-gridI and D-gridL. **Fig. 4-9** shows that the peak resisting forces in Case D-gridI and gridL were higher than those in Case D, approximately the same as those in Case A. This result indicates that the geogrid reinforced the divided vertical walls, increasing the horizontal resistance force. The L-shaped geogrid increased the peak resistance force more than the I-shaped geogrid, whereas there was almost no difference in the resistance force at large displacements. **Fig. 4-10** shows that the bottom piece of the wall in Case D-gridI and gridL rotate, which is the major difference from Case D. **Fig. 4-11** shows that in Case D, there is almost no strain in the ground around the bottom piece of the wall, while in Cases D-gridI and D-gridL, the strain was also generated in the ground around the bottom piece of wall. These results indicate that geogrids lead to attaining the reaction force from the bottom piece of the wall.

To visualize the velocity and direction of the geogrid and the model ground during loading, PIV analysis with *Flow-PIV* was conducted. **Fig. 4-12** shows the distribution of the displacement vectors of the soil at 5 mm and 20 mm loading. As shown in **Fig. 4-9**(b), the displacement of 5 mm is near the peak resistance force, and the displacement of 20 mm is the large drop after the peak resistance force. Note that there is a possibility that

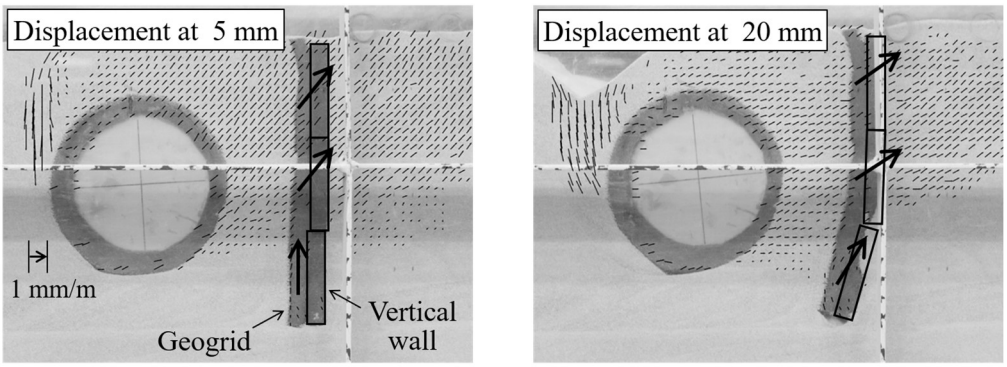

(a) Case D-gridI

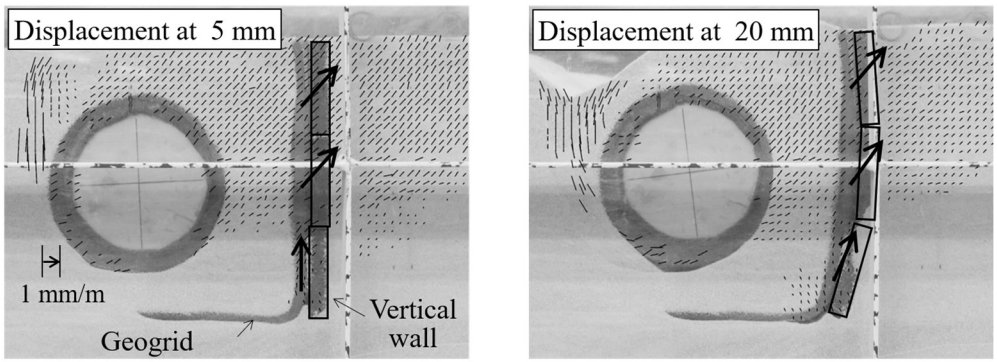

(b) Case D-gridL

Fig. 4-12 Displacement vectors of soil during loading

PIV analysis does not accurately capture the behavior of the ground around the geogrid because the sponge tapes between the geogrid and the acrylic plate were thicker than the geogrid. It should also be noted that the image analysis may not fully capture the behavior of the ground around the channel wall, especially at the 20 mm displacement, because of the inflow of sand between the bottom piece of the wall and the acrylic plate.

In Case D-gridI, the upper part of the geogrid displaced following the movement of the soil mass when the pipe displaced 5 mm. The lower part of the geogrid was pulled out in the vertically upward direction under the influence of the upper part of the geogrid, which had to cause the pullout resistance force and contributed to the increase in the lateral resistance force against the pipe displacement. At 20 mm displacement, the upper part of

the geogrid followed the movement of the soil mass as in 5 mm displacement, while the lower part of the geogrid was pushed the bottom piece of the wall at the same time as it followed the behavior of the upper part of geogrid.

The reason for tilting of the bottom piece of the wall is discussed below. In Case D-grodI, the relative displacement increased between the middle and bottom pieces of the wall during loading because the shear plane in the model ground was generated between them. Although the geogrid was forced to follow the behavior of two pieces, it tried to make the relative displacement as small as possible with the tensile force and then tilted the bottom piece of the wall as a result.

In Case D-gridL, the behavior of the vertically laid geogrid was similar to that of Case D-gridI, while a part of the horizontally laid geogrid was lifted in accordance with pulling out of the vertical geogrid especially at the 20 mm displacement, as shown in **Fig. 4-12**. This result indicates that the geogrid was in tension to resist lifting, which is one of the reasons why the peak resisting force in Case D-gridL was larger than that in Case D-gridI.

4.6 Conclusions

The lateral loading experiments were conducted to investigate the effectiveness of the existing channel walls for the behavior of pipe bends and the effectiveness of geogrid as a reinforcement for existing channels. The conclusions from the experiments are given below.

1 The existing channel wall increased the lateral resistance force acting on pipe bends, and the degree of increase depended on the shapes of the channel walls. This result indicated the possibility of using the channel wall as a thrust countermeasure.

2 When the bottom plate was fixed to the vertical wall, the bottom plate suppressed the rotation of the vertical wall, leading to an increase in the resisting force, whereas when the bottom plate and the vertical wall were not attached, the resisting force was the same as that of only with the vertical wall. This result indicated that the effect of the bottom plate was exerted only when the plate was fixed to the vertical wall.

3 When the vertical wall comprised several pieces, the lateral resistance force was almost the same as that without vertical walls. When geogrids were installed on the divided vertical walls, the lateral resistance increased to the same extent as that of the

undivided vertical walls. This result suggested that geogrids may be used as a reinforcement for vertical walls.

Chapter 5

The contents of this chapter are based on:

Ohta, Y., Sawada, Y., Ono, K., Kawamura, M., and Kawabata, T. (2018), "Effects of shape dimensions of the lightweight thrust restraint method for buried pipe bend on additional lateral resistance", *Geosynth. Eng. J.*, 33, pp. 55–60.

Ohta, Y., Sawada, Y., Kitada, M., and Kawabata, T., "Improved thrust restraint design considering displacement of pipe bend and joint separation", *J. Pipeline Syst. Eng. and Pract.*, in press.

Chapter 5

Thrust restraint mechanism in the method using geogrid and gravel

5.1 General

This chapter examines the effectiveness of the thrust restraint with geogrid and gravel shown in **Fig. 5-1** which geogrids reinforce soil both on the passive and active sides of pipes. Most previous experiments were performed under the plane-strain condition on pipes reinforced with geogrids on the active or passive side only, as summarized in Chapter 2. Therefore, this study focused on the behavior of buried pipes reinforced on both sides with geogrids under three-dimensional conditions, which has not been studied before.

Two types of experiments were conducted in terms of the dimensions and flexibility of the restraint method. One experiment shown in Section 5.2 was conducted on a pipe bend with various dimensions of thrust restraint using geogrids to investigate the mechanism of resistance development. The others shown in Section 5.3 was performed on a model pipe with geogrid and a thrust block model to discuss the influence of the flexibility of the restraint method on the lateral resistance force.

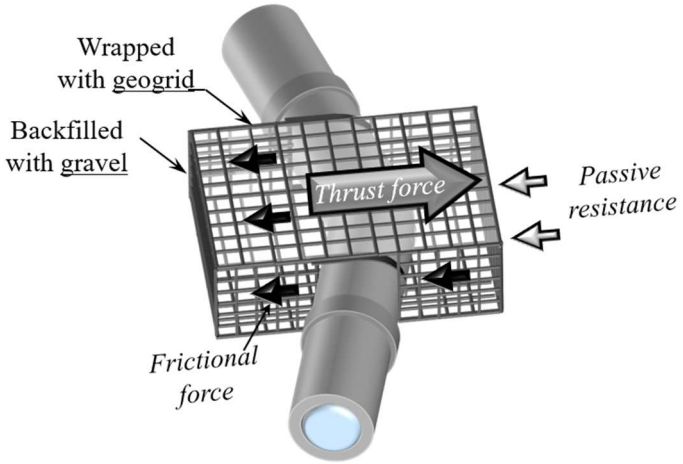

Fig. 5-1 Thrust restraint with geogrid and gravel

5.2 Influence of dimensions of the thrust restraint on the lateral resistance force

This section reports the lateral loading experiments on the pipe bend with geogrid and gravel to investigate the influence of changes in the dimensions of a wrapped area by geogrids on the additional lateral resistance force. A 1/11 scale experimental model was prepared based on the assumption that the prototype pipe has a diameter of 800 mm that is commonly used for irrigation pipelines in Japan based on Yamaguchi (2017), who reported that 41% of the length of irrigation pipelines in Japan are between 500 mm and 1200 mm in diameter.

5.2.1 Outline of the experiments

The model experiments were conducted using the test setup shown in **Fig. 5-2**, which consists of a test container, loading equipment, and a model pipe. The inner dimensions of the rigid test container were 1000 mm, 1100 mm, and 580 mm in width, length, and height, respectively. A hole was created in the wall at the height of 195 mm to allow a loading shaft of a diameter 16 mm to penetrate the container wall. A loading system,

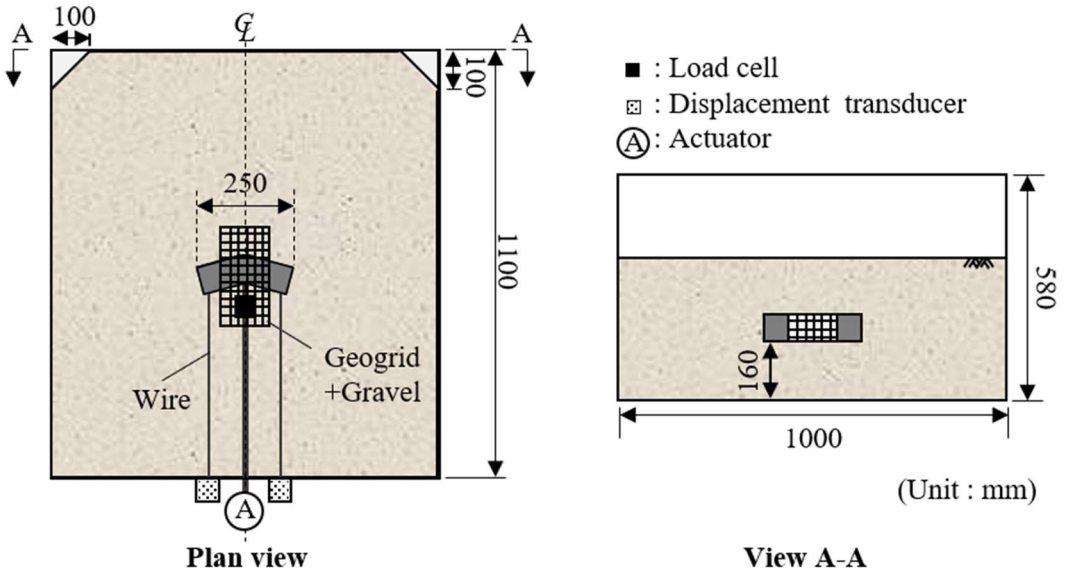

Fig. 5-2 Schematic diagram of test setup for lateral loading experiments on pipe bends with various dimensions of thrust restraint with geogrid

consisting of an electric actuator and a loading shaft, as shown in **Fig. 5-3**, was set outside the test container. The loading shaft was moved at a constant rate controlled by the electric actuator. A spherical seat was set between the shaft and the model pipe; hence, the pipe could move upward and downward. A load cell was placed between the loading shaft and the model pipe to measure the resistance force acting on the model pipes and boxes. The frictional force between the loading shaft and the model ground was ignored in the experiments because the measured frictional force was too small to affect the experimental results. The aluminum model pipe shown in **Fig. 5-3** had an outer diameter of 70 mm, a projected length of 250 mm, and a bending angle of 30º. The displacement measurement system had two displacement transducers, pulleys, and wires which was ϕ0.8. The right and left sides of the pipe were connected to displacement transducers via wires. The wires were passed through an aluminum tube in the model ground to decrease the friction between the wire and the soil. Four earth pressure transducers were installed in the arrangement shown in **Fig. 5-4**.

The dense model ground was prepared using dry silica sand with dry unit weights of 15.0 kN/m^3, corresponding to a relative density of 80%. The particle size distribution is shown in **Fig. 5-5**. The maximum and minimum dry densities of silica sand were 12.5 kN/m^3 and 15.8 kN/m^3, respectively. The internal friction angle of dense sand was 38.5°which was obtained by triaxial compression tests.

Fig. 5-6 shows the procedure for preparing the thrust restraint using the geogrid. The geogrid used in this experiment was the same as that described in Chapter 4. As can be seen in **Fig. 5-6**(a), the geogrid was connected to the model pipe using a jig that consisted of a screw, an L-shaped angle, and a small plate. The enclosed area surrounded by the geogrid was filled with gravel with a dry unit weight of 13.3 kN/m^3. The distribution and properties of the gravel are shown in **Fig. 5-5**. As shown in **Fig. 5-6**(b), the ground on the passive side of the pipe was wrapped with a geogrid. The inside of the geogrid was filled with gravel. The model pipe and passive and active areas were wrapped with the geogrid (**Fig. 5-6**(c)). Non-woven fabrics were placed between the gravel layer and the geogrid to prevent sand from getting into the gravel layer.

A total of 20 tests were conducted, varying the width B and length L_1 of the wrapped area shown in **Fig. 5-7** and the depth of soil cover H. The width B was changed to 100 mm, 125 mm, and 150 mm. The length L_1 was changed into 35 mm, 70 mm, and 105 mm. The depths of soil cover H were 70 mm, and 140 mm, corresponding to the normalized depths

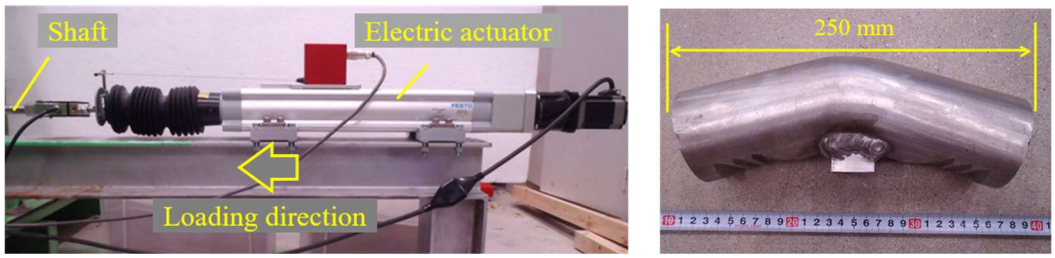

(a) Loading equipment (b) pipe bend

Fig. 5-3 Images of loading equipment and the pipe bend: (a) loading equipment; (b) pipe bend

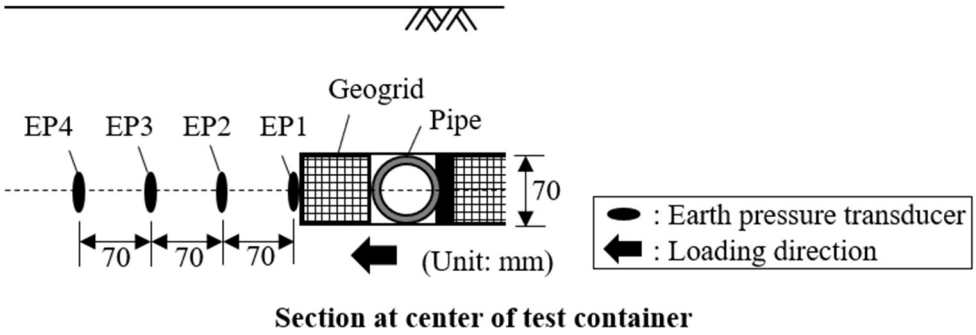

Fig. 5-4 Location of earth pressure transducers in the model ground

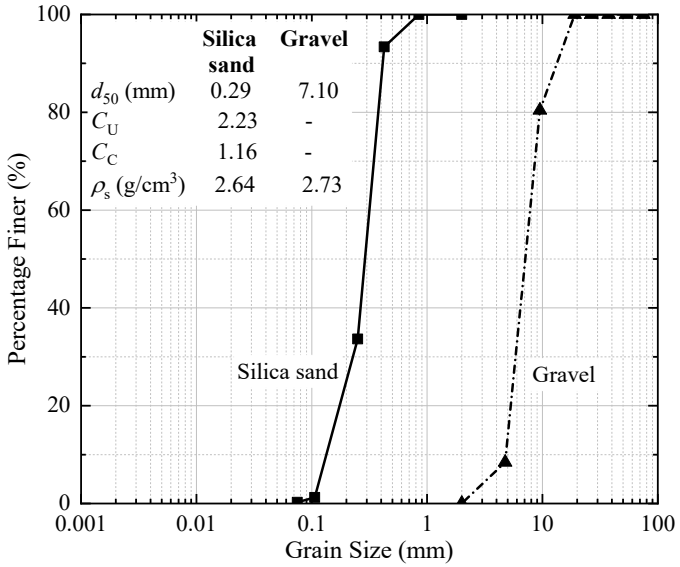

Fig. 5-5 Particle size distribution of silica sand and gravel

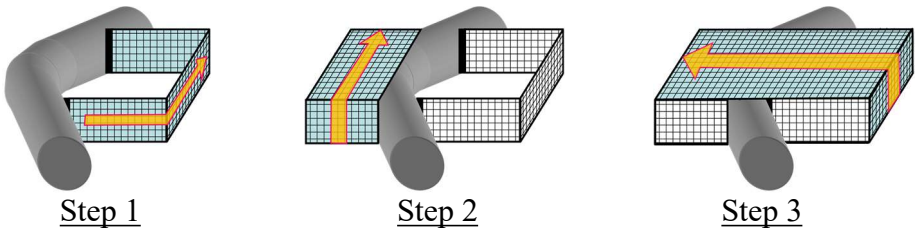

Fig. 5-6 Procedure of geogrid on pipe bends

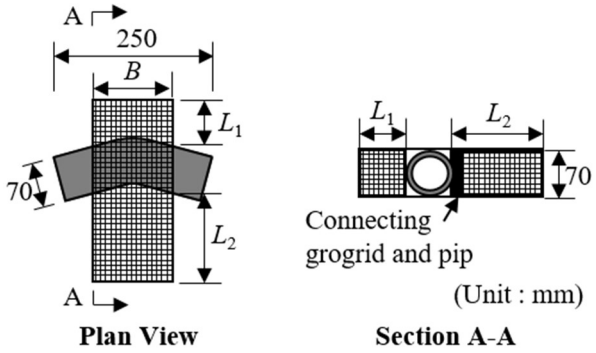

Fig. 5-7 Dimensions of the thrust restraint with geogrid

Table 5-1 Experimental conditions on pipe bend with geogrid-based thrust restraint

Case	***B*** **(mm)**	L_1 **(mm)**	***H*****(mm)**
None	-	-	70 (1.0*D*)
*B*100-*L*35	100	35 (0.5*D*)	
*B*125-*L*35	125		
*B*150-*L*35	150		
*B*100-*L*70	100	70 (1.0*D*)	140 (2.0*D*)
*B*125-*L*70	125		
*B*150-*L*70	150		
*B*100-*L*105	100	105 (1.5*D*)	
*B*125-*L*105	125		
*B*150-*L*105	150		

H /*D* were 1.0 and 2.0, respectively, where *D* (mm) represents the outer diameter of the model pipe. The test conditions were summarized in **Table 5-1**. After preparing the model ground, the model pipe was loaded laterally to the lateral displacement of 50 mm at a rate of 0.1 mm/s. The displacement of the model pipe, the resistance force against the model pipe, and the earth pressure around the pipe were measured during loading. After the tests, the shape of the ground surface was measured by a laser displacement transducer.

5.2.2 Main experimental results

Fig. 5-8 shows the resistance force–displacement relationships during the lateral loading tests. The resistance force in all cases had clear peaks and then settled to residual values in both depths of soil cover, similar to the results of the previous research on the behavior of buried pipelines under plane-strain conditions (e.g., Trautmann and O'Rourke 1985). The resistance force on the pipe with thrust restraint was greater than that on the pipe without any countermeasure, which indicates that the proposed method is effective for increasing the resistance force against the thrust force. In the ultimate lateral displacement that is the displacement at the peak resistance force, the cases with geogrid also had larger values than the cases without geogrid. Since the most important characteristic of the geogrid, tension, is generated by strain, pipe displacement is required for elongating the geogrid and increasing the additional resistance provided by the geogrid.

Fig. 5-9 shows the deformations of the ground surface after the experiments. The vertical and horizontal axes in **Fig. 5-9** represent variations in the height of the ground surface and the distance from the container wall along the center line. The pipe with thrust restraint is illustrated in **Fig. 5-9** at the estimated location of 5 mm displacement which is the average ultimate displacement. The ground surface dropped on the active side and rose on the passive side, similar to previous studies of underground structures.

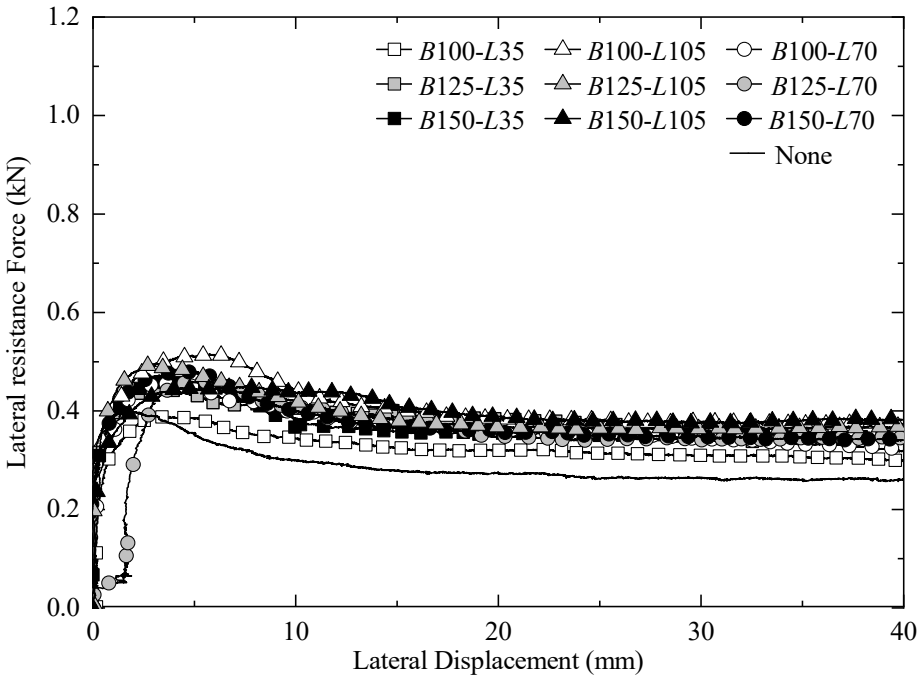

(a) H/D=1.0

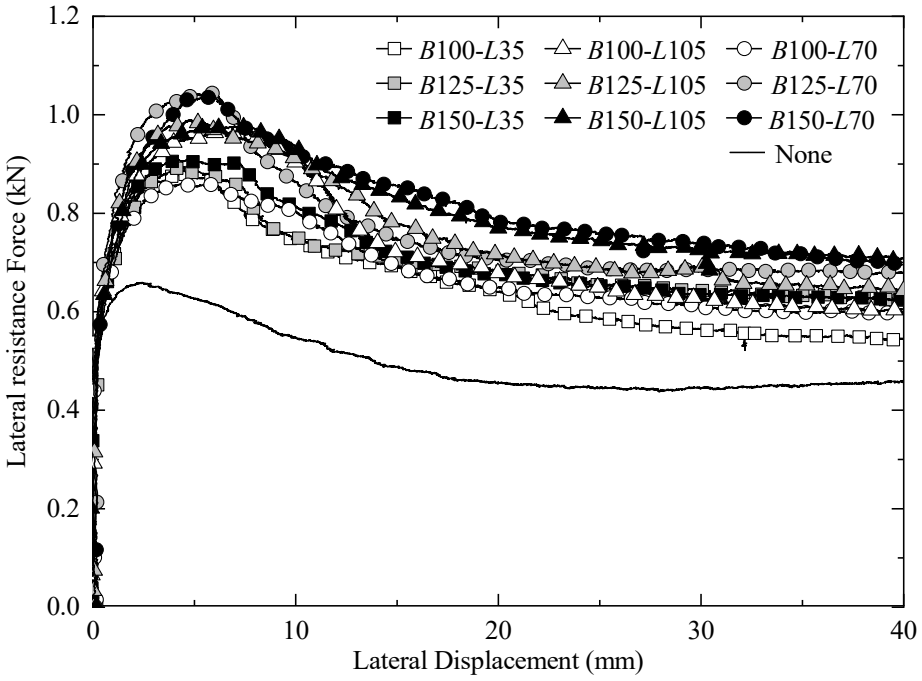

(b) H/D=2.0

Fig. 5-8 Variations of F–D relationships on dimensions of thrust restraint with geogrid

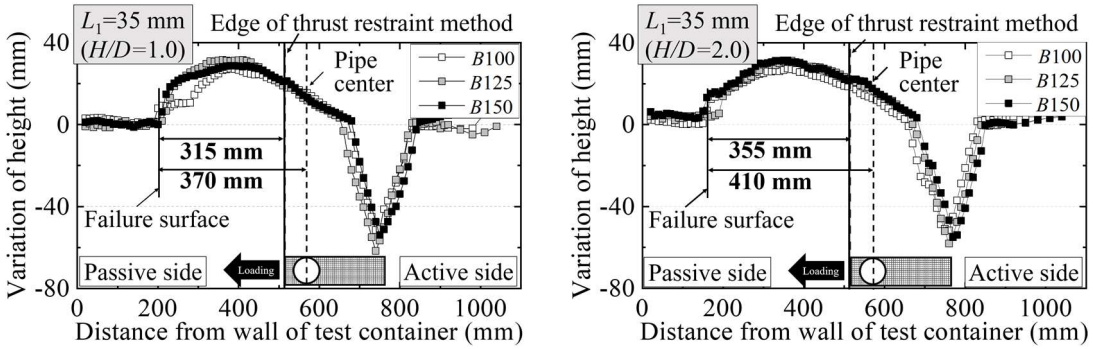

(a) L_1=35 mm

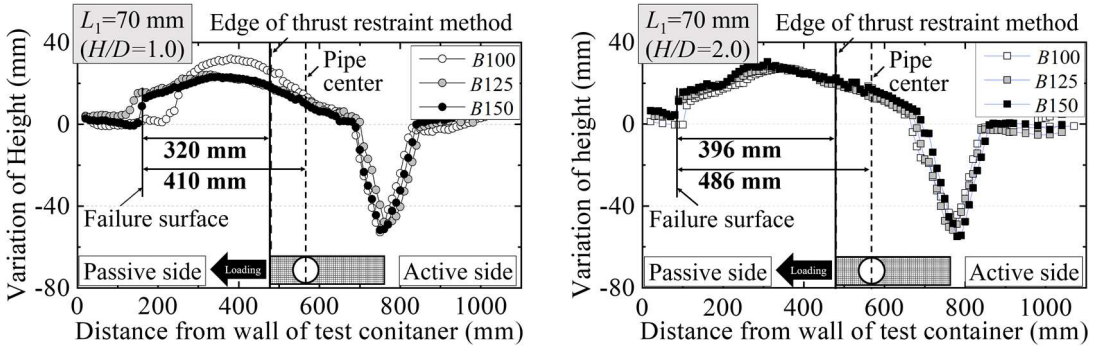

(b) L_1=70 mm

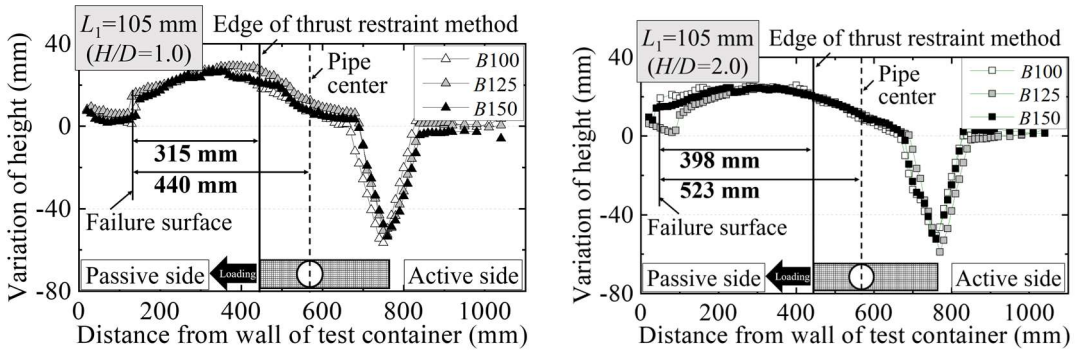

(c) L_1=105 mm

Fig. 5-9 Variations of the ground surface after loading

5.2.3 Difference in the effectiveness of thrust restraint by dimensions

Since it was difficult to find the effect of the dimensions on the resistance force from **Fig. 5-8**, the additional resistance force was calculated based on the results of Case Pipe to clarify the difference in the resistance mechanism with various shape dimensions. **Fig. 5-10** shows the relationships between the additional resistance force and the pipe displacement. The additional resistance–displacement relationships also have a similar shape with a peak value as the relationships shown in **Fig. 5-8**. No clear correlation was found between the magnitude of the peak resistance and the dimensions. In contrast, the additional resistance after the peaks increased following the increase of B, compared under the same L_1, especially in H/D=2.0. The increase in the frictional resistance due to the increase in surface area led to the increase in the additional resistance. In the results under H/D=1.0, little difference in the resistance due to dimensions appeared even after the peak additional force because of the low confining pressure.

There is almost no difference in the depth of subsidence and the height of rising in all cases, while the ranges of the shear region varied from case to case. The arrows in **Fig. 5-9** are the distances between the shear plane and the pipe center or the edge of the thrust restraint to evaluate the size of the shear zone in each case. Note that the location at which the ground surface starts to rise is assumed to be the location of the shear plane on the ground surface. The distances from the pipe center varied between cases, whereas that from the edge of the thrust restraint changed little for the same soil cover: 397 mm in H/D=2.0 and 316 mm in H/D=1.0. The results indicate that the shear zone on the passive side of the ground developed from the end of the thrust restraint rather than from the pipe, which means that the area wrapped by the geogrid behaved as a single unit. As an exception, the distances were 355 mm when L_1=35 mm and H/D=2.0, which is 11% smaller than when L_1= 70 mm and 105 mm. This may be caused by the poor compaction inside the wrapped area due to the narrow interior, which resulted in the insufficient strength of the gravel layer inside the thrust restraint.

5.2.4 Estimation of the location of the shear band on the passive side of the ground

The passive shear region is determined based on the assumption that the wedge-shaped shear zone as shown in **Fig. 5-11** developed during loading. Although the passive shear plane is known to form a logarithmic spiral, it is assumed to be a straight line for simplicity in this study. The angle between the ground surface and the shear plane under

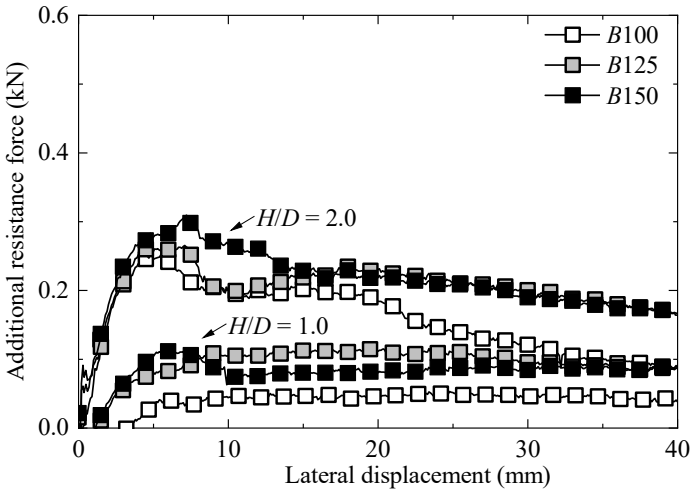

(a) L_1=35 mm

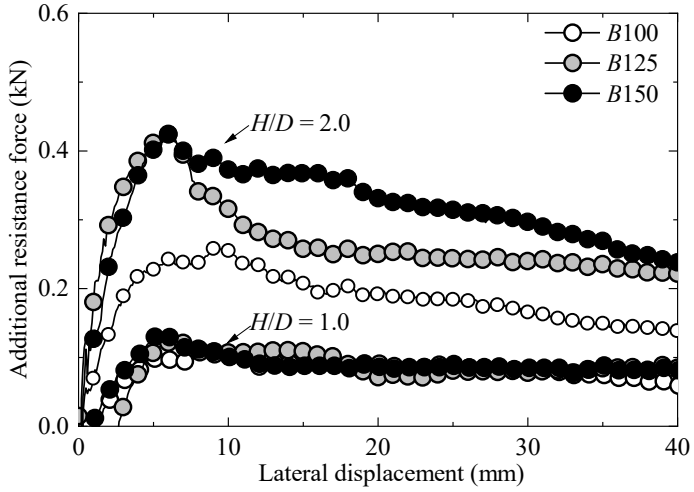

(b) L_1=70 mm

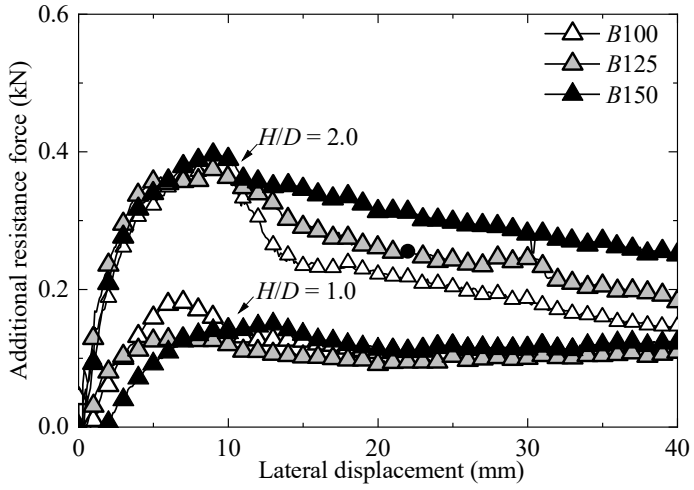

(c) L_1=105 mm

Fig. 5-10 Additional lateral resistance during loading

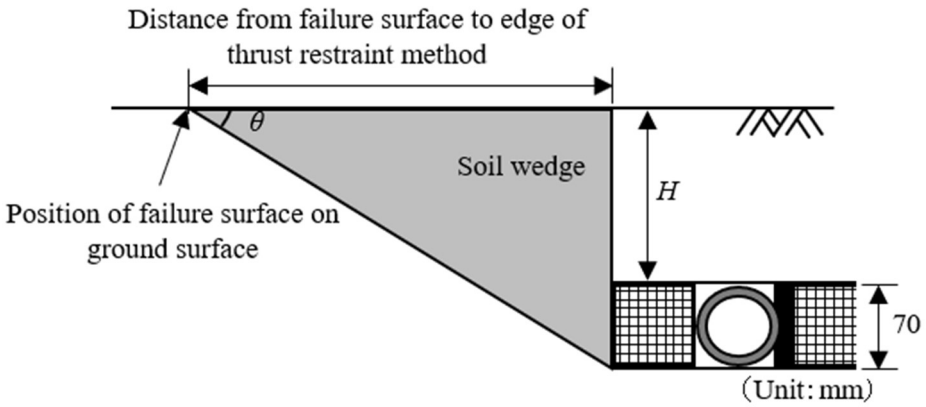

Fig. 5-11 Estimated location of soil wedge

H/D=1.0 and 2.0 are determined as $\theta_{1.0}$ and $\theta_{2.0.}$ The values of $\theta_{1.0}$ and $\theta_{2.0}$ were calculated as follows:

$$\theta_{1.0} = \tan^{-1}\left(140/316\right) \doteq 23.9^{\circ} \tag{3.1}$$

$$\theta_{2.0} = \tan^{-1}\left(210/397\right) \doteq 27.9^{\circ} \tag{3.2}$$

The difference in angle was as small as 4° while the change in soil cover was twice as large. This result indicates that the shear zone can be approximated by the same wedge regardless of the soil cover.

The behavior of pressure gauges in the model ground is examined to investigate the location of shear plane in the ground. **Fig. 5-12** shows variations of earth pressures in Case *B*150-*L*70. The magnitude of pressures was in the order of EP1>EP2>EP3>EP4 at a small lateral displacement. This order is inversely proportional to the distance from the thrust restraint, confirming the validity of the measurements. After the experiment, the position of the pressure gauge was measured and the amount of the uplift was calculated as shown in **Fig. 5-13**. The floatation of EP1 and EP2 were around 17 mm, while that of EP3 and EP4 were -1 mm. The difference in the amount of flotation is visible, which indicates that there was a shear plane between EP2 and EP3, namely between 70 and 140 mm from the thrust restraint. Using the average of $\theta_{1.0}$ and $\theta_{2.0}$, the distance from the thrust restraint was calculated to be 72 mm. Therefore, the passive shear region can be simply approximated by a wedge.

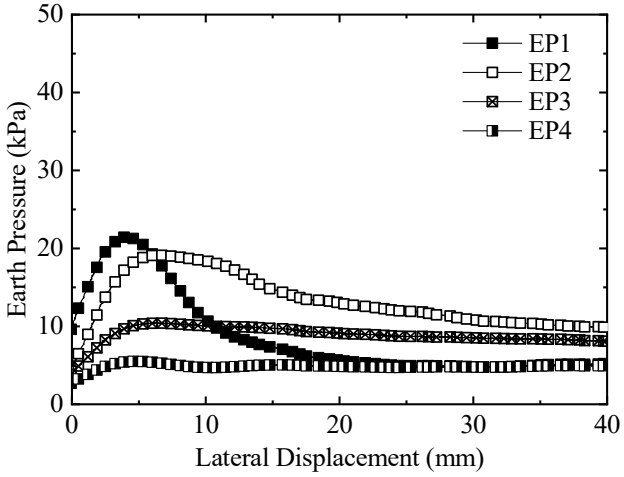

(a) H/D=1.0

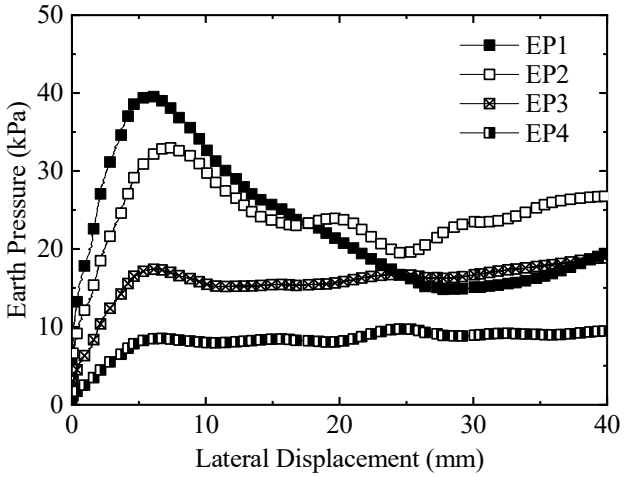

(b) H/D=2.0

Fig. 5-12 Variations of earth pressures during loading

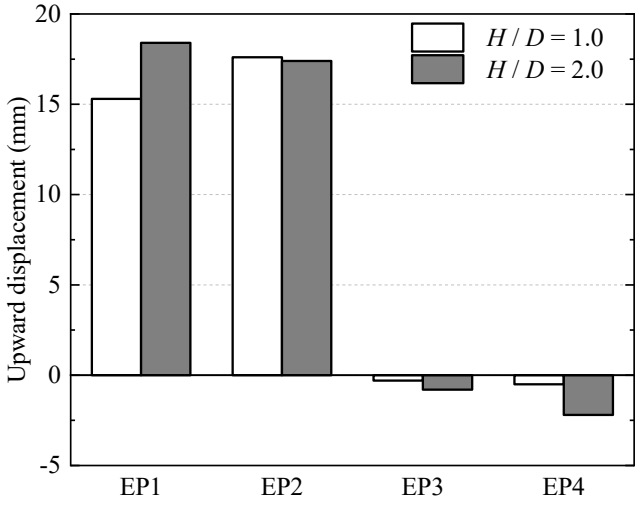

Fig. 5-13 Upward displacements of earth pressure gauges

5.3 Influence of flexibility of the thrust restraint on the lateral resistance force

The aim of the experiments reported in this section is to investigate the difference in lateral behavior of rigid and flexible thrust restraints. From experimental results in Section 5.2, the wrapped area by geogrids might be unified. Assuming the area wrapped by geogrids is completely unified, the wrapped area would behave as a single structure and the passive earth pressure and the frictional force would apply to the wrapped area in the same manner as a thrust block. However, the effectiveness of the method with geogrids is likely to be inferior to that of the thrust block when both methods use structures with same dimensions because the wrapped area with the geogrid is flexible compared to the rigid thrust block. In this study, the lateral loading experiments were conducted to evaluate the effectiveness of thrust restraint with geogrids compared to thrust blocks. The experiments were also prepared at a 1/11 scale, assuming the prototype pipe has a diameter of 800 mm.

5.3.1 Outline of the experiments

The schematic diagram of the test setup is shown in **Fig. 5-14**. The test equipment and ground material were the same as described in Section 5.2.1. Dense and loose model ground was prepared using dry silica sand in the experiments. The dry unit weights of dense and loose silica sand were 13.4 kN/m^3 and 15.0 kN/m^3, respectively, which corresponded to a relative density of 30% and 80%, respectively.

A PVC pipe was used as the model pipe. The outer diameter, thickness, and length of the pipe were 89 mm, 7 mm, and 300 mm, respectively. The boundary effect caused by the side walls of the container was negligible because the test container had sufficient width, more than three times the pipe width. Based on the calculation results, the model pipe was minimally deflected during the experiments. The unit weight of the model pipe was adjusted to 10 kN/m^3, with reference to the unit weight of the fiberglass reinforced plastic mortar (FRPM) pipe filled with water. To simplify the experimental conditions, a straight pipe was chosen even though the thrust force was generated at the pipe bend. Ohta et al. (2018) conducted lateral loading experiments with model pipes with an outer diameter of 70 mm and bending angles of 30°, 60°, and 90°. The experimental results showed that the bending angle had minimal effect on the lateral resistance under the experimental conditions. Because the conditions of the experiments, such as the model scale in the present study, were similar to those of Ohta et al. (2018), the influence of the bending angle on the lateral behavior of buried pipes appears to be insignificant in this experiment.

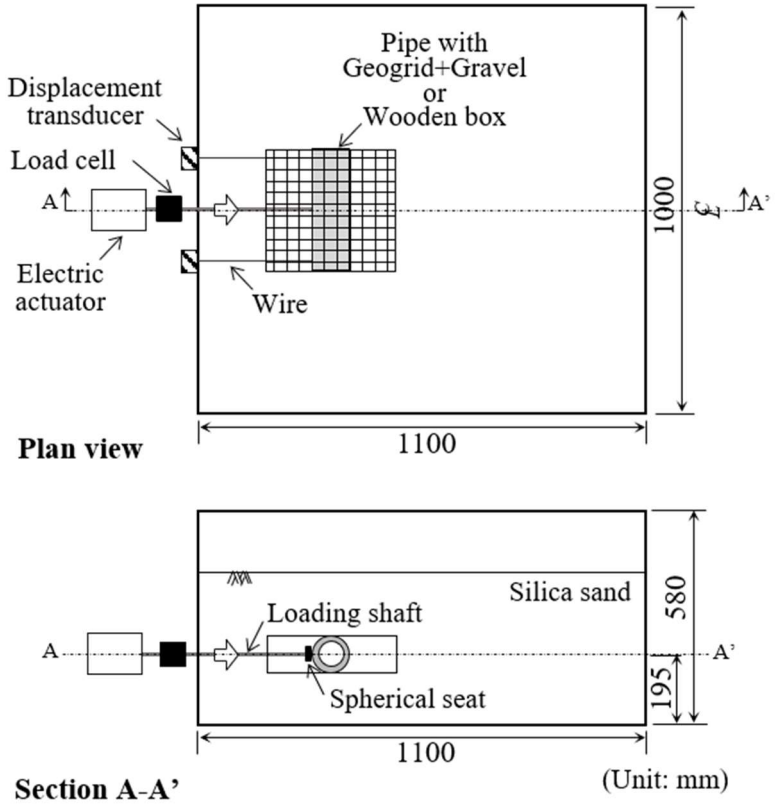

Fig. 5-14 Test equipment with flexible thrust restraint

Fig. 5-15 shows images and dimensions of the flexible and rigid thrust restraint models. The flexible and rigid models had the same dimensions and weights. The value of l' as shown in **Fig. 5-15** was changed into 1.0D (89 mm), 0.75D (67 mm) and 0.5D (45 mm). The width and height of the models were constant at 300 mm and 89 mm, respectively. **Fig. 5-16** shows the procedure for preparing the flexible thrust restraint, essentially the same as the experiments in Section 5.2. Gravel inside of the wrapped area had a dry unit weight of 14.5 kN/m^3. The properties of the geogrid were described in Chapter 4. The stiffness of the geogrid corresponded to approximately 4% of the stiffness of the prototype geogrid used in the field test reported by Kawabata et al. (2010). **Fig. 5-17** shows the comparison between the results of the tensile tests on the prototype and model of the geogrid. The secant modulus at 2% strain obtained from **Fig. 5-17** is regarded as the tensile stiffness in this study. Iai (1989) theoretically derived the similitude for 1g model tests on saturated soil–structure–fluid system. According to the study, the scaling factor for the longitudinal rigidity of buried structures could be represented as the 1.5th power

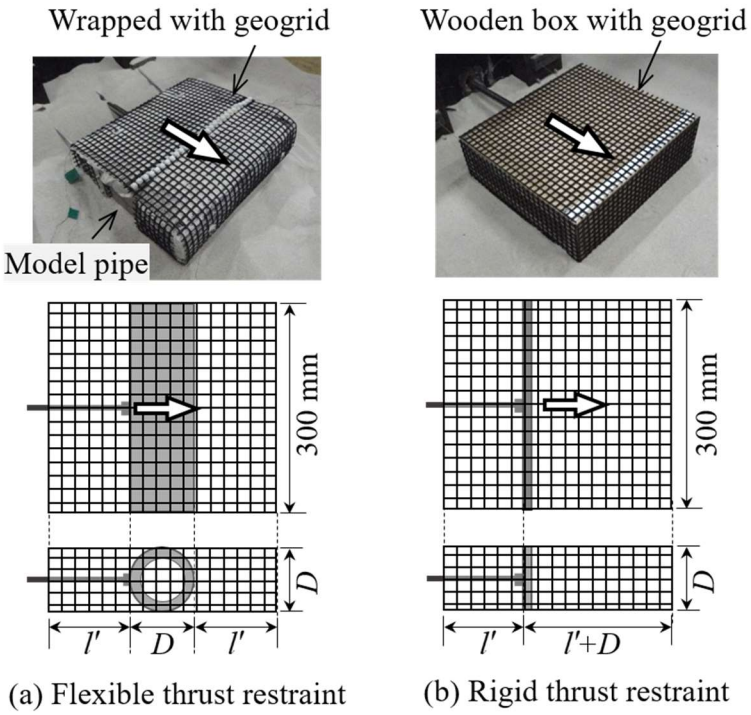

Fig. 5-15 Images and dimensions of flexible and rigid thrust restraint: (a) flexible thrust restraint; (b) rigid thrust restraint

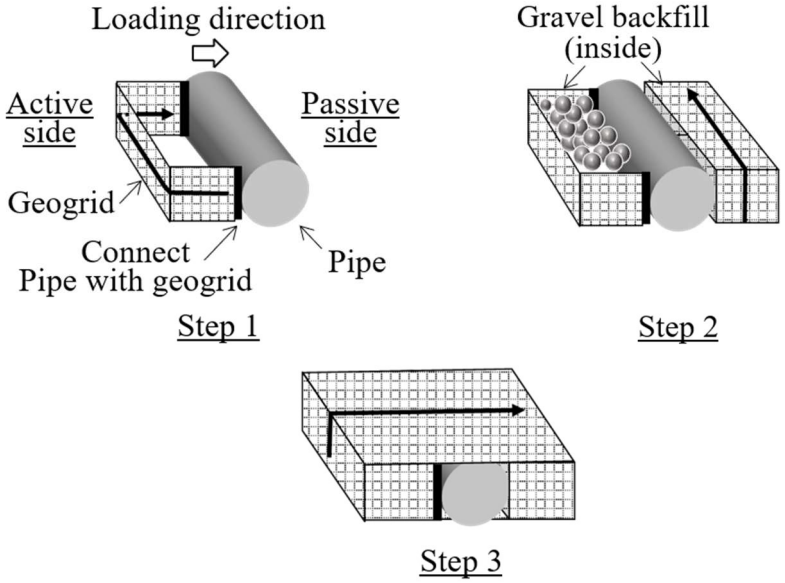

Fig. 5-16 Preparation of flexible thrust restraint

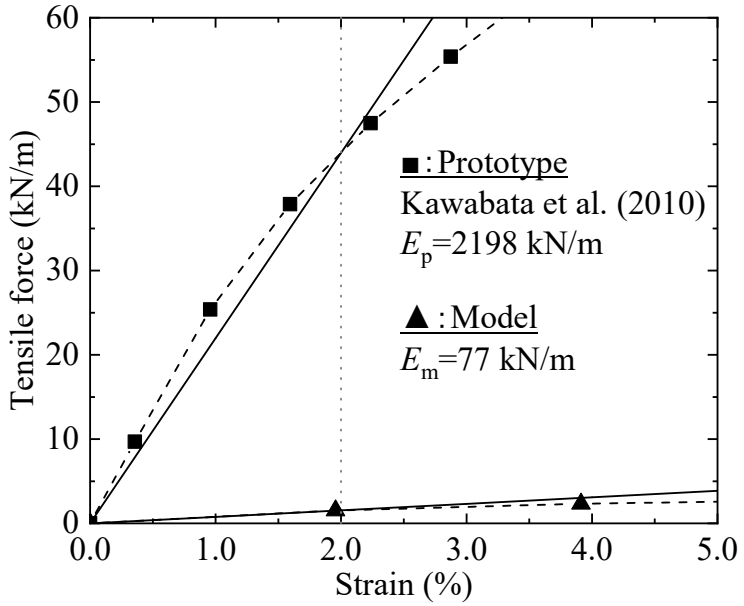

Fig. 5-17 Results of tensile tests on model and prototype geogrid

of the geometrical scale factor. Following Iai's theory, the ideal scaling factor for the tensile stiffness of geogrids in the present study can be obtained as follows:

$$\lambda_{ts} = (\lambda)^{1.5} = (D_m / D_p)^{1.5} = (89/800)^{1.5} = 0.037 \quad (3.3)$$

where λ and λ_{ts} are the scaling factors for the geometry and tensile stiffness, and D_m and D_p are the diameters of the model and prototype pipes, respectively. As described previously, the tensile stiffness of the model geogrid was 0.04 times the prototype. Thus, the model geogrid was suitable for reproducing the behavior of the prototype geogrid.

The rigid thrust restraint was simulated using wooden boxes as shown in **Fig. 5-15**(b). The wood plates had a thickness of 20 mm; this was sufficient to avoid deformation during the experiments. The spherical seat was set inside the box to push the boxes to the same position as the flexible thrust restraint models. The wire connected to the displacement gauge was placed on the active side of the box. The geogrid was fixed on the surface of the rigid thrust restraint models to receive the same frictional resistance as the flexible thrust restraint models.

Table 5-2 Experimental conditions on flexible and rigid thrust restraint

Case	Model type	l' (mm)		Density
F-1.0*D*	Flexible thrust restraint (Pipe with geogrid and gravel)	1.0*D*	(= 89)	Dr = 80%, 30%
F-0.75*D*		0.75*D*	(= 67)	
F-0.5*D*		0.5*D*	(= 45)	
R-1.0*D*	Rigid thrust restraint (Wooden box)	1.0*D*	(= 89)	
R-0.75*D*		0.75*D*	(= 67)	
R-0.5*D*		0.5*D*	(= 45)	
Pipe	Model pipe	-	-	

The experimental procedure is described as follows: The model ground was compacted into six layers. After two compacted layers with a total thickness of 150 mm, thrust restraint models or the model pipe were placed on the second layer. Four soil layers with a total thickness of 178 mm were compacted to fill the test models. After preparing the model ground, the test model was displaced laterally to 50 mm at a rate of 0.1 mm/s. The lateral resistance and displacement of the test models were measured during the experiments. After the experiments, the height of the ground surface was measured using a laser displacement sensor along the center line of the test container to investigate the deformation of the model ground. **Table 5-2** summarizes the test conditions conducted in this study. The model type, dimension of l', and ground density were changed, and a total of 14 tests were conducted.

5.3.2 Main experimental results

Fig. 5-18 shows the variation in the lateral resistance force with the lateral displacement. In dense sand, the F–D curves have peaks at a displacement of approximately 5 mm. In loose sand, the resistance in all cases increases gradually. Similar characteristics of the F–D relationships have been shown in the experimental results of previous research on the behavior of buried pipelines under plane-strain condition (e.g., Trautmann and O'Rourke 1985). In some results of flexible thrust restraint, the development of the lateral resistance force was slightly delayed at the beginning of the lateral displacement. This may be due to voids remaining in the area between the underside of the pipe and the

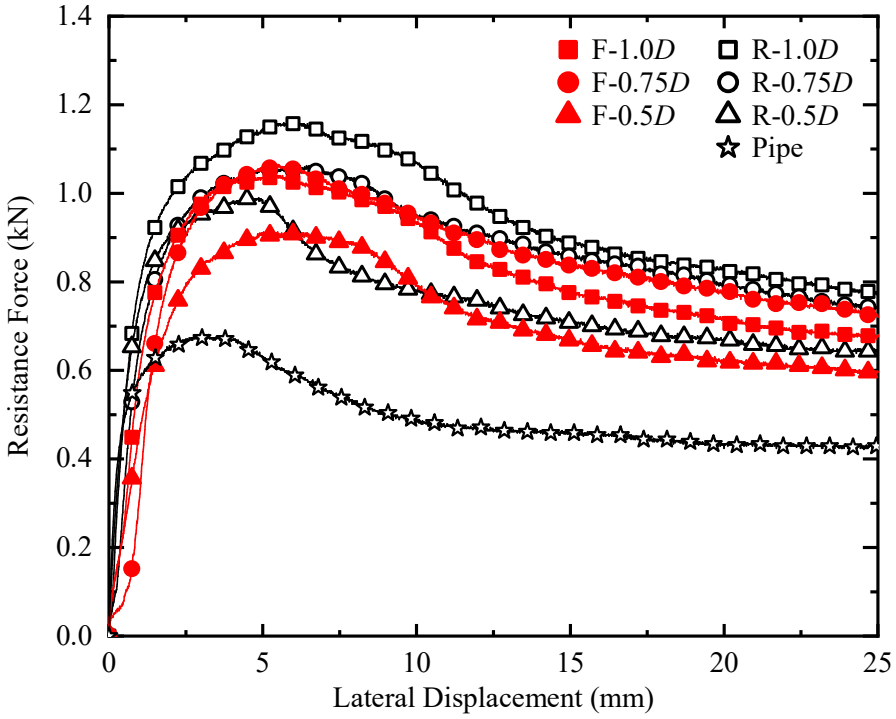

(a) Dense sand

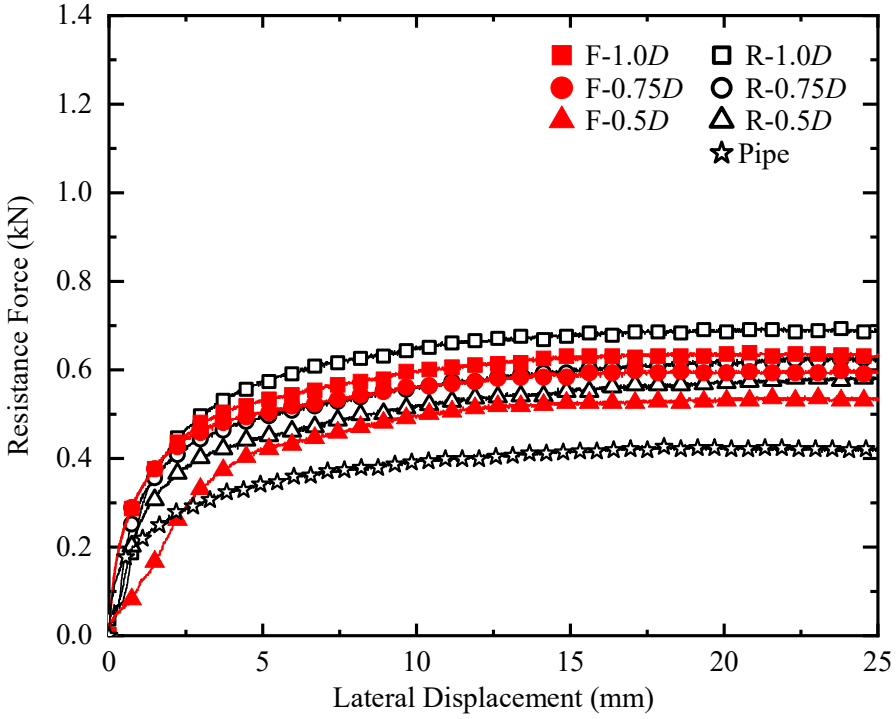

(b) Loose sand

Fig. 5-18 Variation of lateral resistance with lateral displacement

bedding, called the haunch area. Compaction at the haunch area is difficult, as is well known, and even more so for small experimental models. In addition, the gravel used in this experiment was difficult to backfill in a narrow area because it contained no fine particles. Poorly established backfill at the haunch area may reduce the contact area between the pipe and backfill material and thus, decrease the increment of the lateral resistance at the beginning of the pipe displacement.

5.3.3 Comparison between the behavior of the rigid and flexible thrust restraint

Comparing the results of flexible and rigid thrust restraints with the same dimensions, the resistance force of the flexible model is approximately the same as that of the rigid model when $l' = 0.75D$ and $0.5D$. Conversely, when $l' = 1.0D$, the resistance force in the flexible model was smaller than that in the rigid model. The resistance force in the flexible model with $l' = 1.0D$ hardly increased from $l' = 0.75D$ in both ground densities, even though the resistance force in the rigid models increased with an increase of dimensions. **Fig. 5-19** shows the variations in the height of the ground surface at the center line of the test container obtained by the laser displacement sensor and shapes of the shear band appearing at the ground surface judged by sight. Only the results for dense sand are shown in **Fig. 5-19** because the shear band in dense sand was easier to determine than that in loose sand. The failure zone in all cases was extended three-dimensionally. In addition, the failure zones in cases of flexible and rigid thrust restraints were larger than that of Case Pipe. When $l' = 0.75D$ and $0.5D$, there is little difference between the flexible and rigid models. These results correspond to the results that both lateral resistances are almost the same. The deformation of the flexible thrust restraint seems to have little effect on the lateral behavior. Conversely, when $l' = 1.0D$, the failure zone in the flexible model is smaller than that in the rigid model. Therefore, the resistance of the flexible model with $l' = 1.0D$ was smaller than that of the rigid model. Kawabata et al. (2007) conducted full-scale lateral loading experiments on a flexible thrust restraint only on the active side with two different dimensions. The results showed that the resistance force hardly increased with increase in length of the geogrid. They pointed out that there was an optimal dimension for the thrust restraint. A long geogrid is easy to extend owing to the characteristics of the geogrid; however, extending the geogrid seems to hinder unifying the wrapped area surrounded by the geogrid. Based on the experimental results, $l' = 0.75D$ is the optimal dimension under the experimental conditions for the flexible thrust restraint, and the influence of deformation in the wrapped area is minimal if the dimensions are less than $l' = 0.75D$.

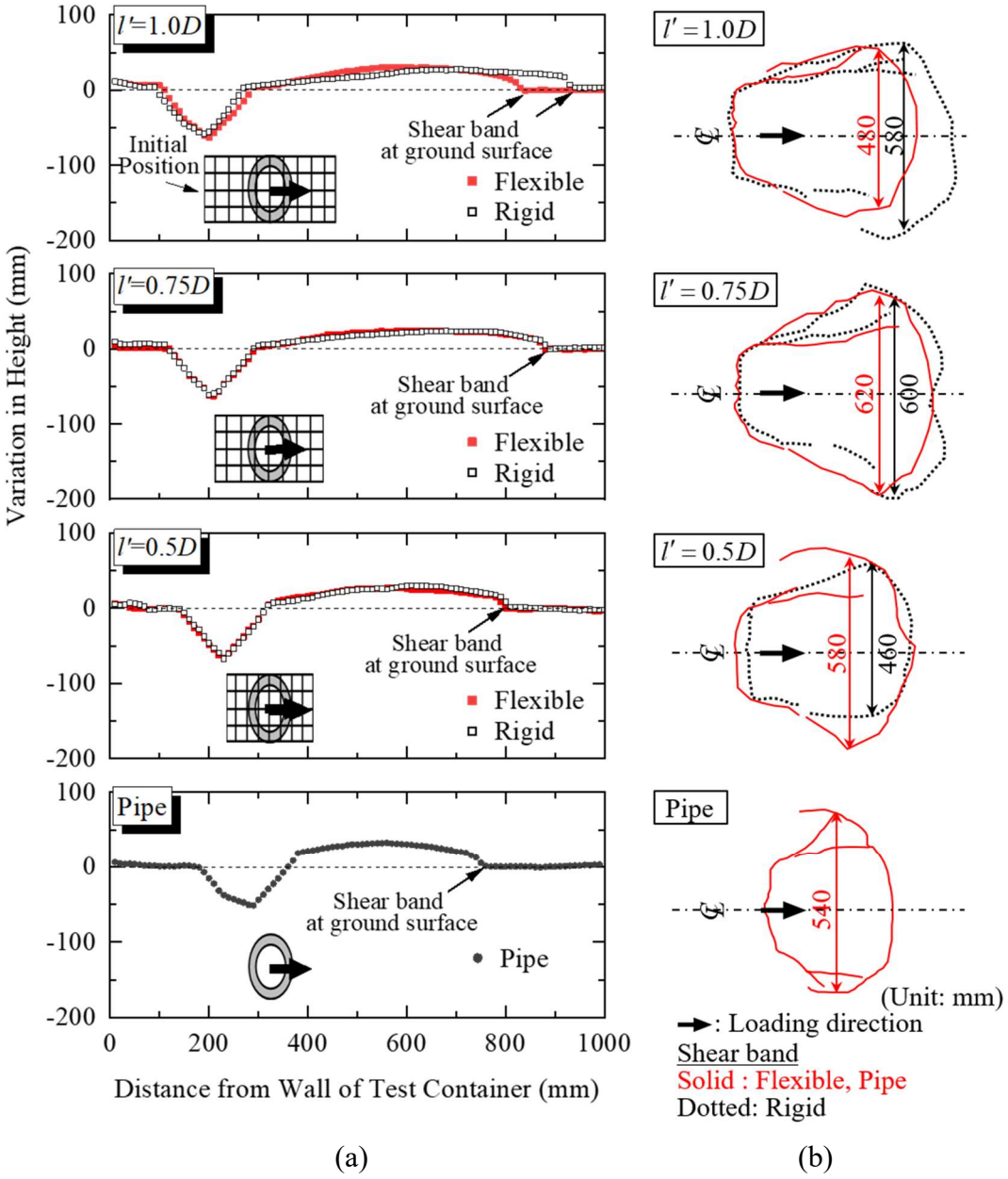

Fig. 5-19 Deformation of ground surface after experiments: (a) variations of height of ground surface at the center of the test container; (b) shear bands appeared at the ground surface

5.4 Conclusions

Two types of experiments were conducted regarding the dimensions and flexibility of the restraint method to investigate the resistance mechanisms and the effectiveness of the geogrid-based thrust restraint method, as shown in **Fig. 5-1**. The following conclusions were obtained from the experiments.

Effect of Dimensions of the wrapped area by geogrid

1 There were few effects of the dimensions of the wrapped area on the peak additional resistance force, whereas additional resistance forces at large displacements increased in accordance with the increased dimensions of the wrapped area.

2 Based on the locations of the shear planes on the ground surface, the shear planes on the passive side of the pipes with thrust restraint were considered to start from the edge of the wrapped area by geogrids, which means that the wrapped area by geogrids was almost completely integrated.

3 The passive shear region, which is important for predicting the resisting force acting on the thrust restraint, was assumed to be wedge-shaped. The estimated wedge-shaped regions roughly fit the experimental results.

The flexibility of the thrust restraint

1 The flexible thrust restrain provides the same level of resistance against pipe displacement as rigid thrust blocks, which means the flexibility of the wrapped area by the geogrid had little effect on the lateral resistance.

2 The lateral resistance did not increase when the dimensions of the wrapped area were larger than a certain dimension probably because the geogrid integration effect was not fully realized. This result implied that there are the optimal dimensions of the wrapped area by geogrid for the thrust restraint.

Chapter 6

The contents of this chapter are based on:

Ohta, Y., Sawada, Y., Kitada, M., and Kawabata, T., “Improved thrust restraint design considering displacement of pipe bend and joint separation”, *J. Pipeline Syst. Eng. and Pract.*, in press.

Chapter 6

Design method for pipe bend considering pipe displacement

6.1 General

As mentioned in Chapeter 1, pipe displacements of pipe bends are needed to predict the amount of joint separation from the thrust force. Although the F–D relationships of buried pipes have been proposed, most previous studies were based on plane-strain conditions and did not consider three-dimensional effects.

This chapter provides the formulation of F–D relationships firstly, using the experimental results presented in Section 5.3, which were conducted under 3D conditions. Then, the design chart considering F–D relationships and the design examples were provided to demonstrate how to consider the pipe displacement in evaluating the stability of pipe bends.

6.2 Formulation of F–D relationships in 3D condition

In this section, the F–D relationship for the thrust restraint method under 3D conditions is formulated based on a hyperbolic approximation to consider the displacement of pipe bends in the design method. Because the experimental results revealed that the lateral behavior in the flexible thrust restraint was almost the same as that in the rigid thrust restraint, except for the results in $l' = 1.0D$, the formulation was conducted without distinguishing between flexible and rigid thrust restraints.

6.2.1 Procedure of formulation of F–D relationships

The F–D relationships in buried structures are often normalized by the ultimate resistance R_u and the ultimate displacement Y_u, where Ru (kN) is determined as the maximum resistance and Yu (mm) is the displacement corresponding to Ru. According to Trautmann and O'Rourke (1985) and Jung et al. (2016), the normalized F–D relationships showed almost the same curve regardless of buried conditions, such as dimensions of structures and depth of soil cover, and were often approximated by a rectangular hyperbola, written

as follows:

$$\frac{R}{R_u} = \frac{Y/Y_u}{k_1 + k_2\left(Y/Y_u\right)} \tag{6.1}$$

$$R' = \frac{Y'}{k_1} + k_2 Y' \tag{6.2}$$

where R' and Y' are the resistance force and displacement normalized by *Ru* and *Yu*, respectively, and k_1 and k_2 are coefficients. An inverse of Eq.(6.2) can be expressed as follows:

$$\frac{1}{R'} = k_1 \frac{1}{Y'} + k_2 \tag{6.3}$$

The experimental results were substituted into Eq.(6.3), and the coefficients *k1* and *k2* are determined by linear approximation with the least squares method. F–D curves can be obtained by substituting the ultimate lateral resistance *Ru* and the ultimate lateral displacement *Yu* into the normalized F–D relationships shown in Eq.(6.1). In other words, not only the normalized F–D relationships but also the ultimate lateral resistance *Ru* and the ultimate lateral displacement *Yu* are required for predicting F–D relationships.

6.2.2 Identification of hyperbolic normalized F–D relationships

Fig. 6-1 shows the normalized F–D curves obtained from the experimental results. The resistance force and displacement were normalized by the ultimate resistance force and ultimate lateral displacement in each experimental result. The results for the rigid thrust restraint and the model pipe, shown in black in **Fig. 6-1**, indicate a general pattern regardless of the soil density, model dimensions, and model type. In contrast, the results of the flexible thrust restraint, shown in red in **Fig. 6-1**, are scattered, especially in case F-1.0*D*, which is a flexible thrust restraint with l'= 1.0*D* buried in dense sand. This is owing to a small increment in the resistance force at the beginning of lateral loading, as described in Subsection 2.2. The broken line in **Fig. 6-1** is the relationship proposed by Trautmann and O'Rourke (1985) based on the 2D experimental results. As can be seen in **Fig. 6-1**, the broken line did not match the experimental results. Thus, a normalized F–D relationship suitable for 3D conditions is proposed with the hyperbolic approximation described in Subsection 6.2.1. The obtained normalized F–D relationship is represented by the following equation:

$$R' = \frac{Y'}{0.096 + 0.903Y'} \tag{6.4}$$

The values of *k1* (= 0.096) and *k2* (= 0.903) in Eq.(6.4) are the average values for each case, except for case F-1.0*D*. The approximated curve is shown as a solid line in **Fig. 6-1**.

6.2.3 Prediction of the ultimate lateral resistance R_u

Duncan and Mokwa (2001), Al-Shayea (2006), Jadid et al. (2018), and Sharma et al. (2021) investigated the lateral resistance against a buried anchor block. In this study, the ultimate resistance is calculated from the equilibrium of the forces acting on a block, as illustrated in **Fig. 6-2**. Force equilibrium in the lateral direction is given by the following equation:

$$R_u = M(P_p - P_a) + P_t + 2P_s + P_b \tag{6.5}$$

where P_p is the passive resistance force (kN), P_a is the active resistance force (kN), P_t is the frictional force at the top of the block (kN), P_s is the frictional force at the side of the block (kN), P_b is the frictional force at the bottom of the block (kN), and M is the 3D effect factor proposed by Hansen (1966) based on the experimental results of Ovesen (1964). M was obtained by the following equation:

$$M = 1 + \left(K_p - K_a\right)^{0.67} \left\{ 1.1k_3^{\,4} + \frac{1.6k_4}{1+5(b/h)} + \frac{0.4\left(K_p - K_a\right)k_3^{\,3}k_4^{\,2}}{1+0.05(b/h)} \right\} \tag{6.6}$$

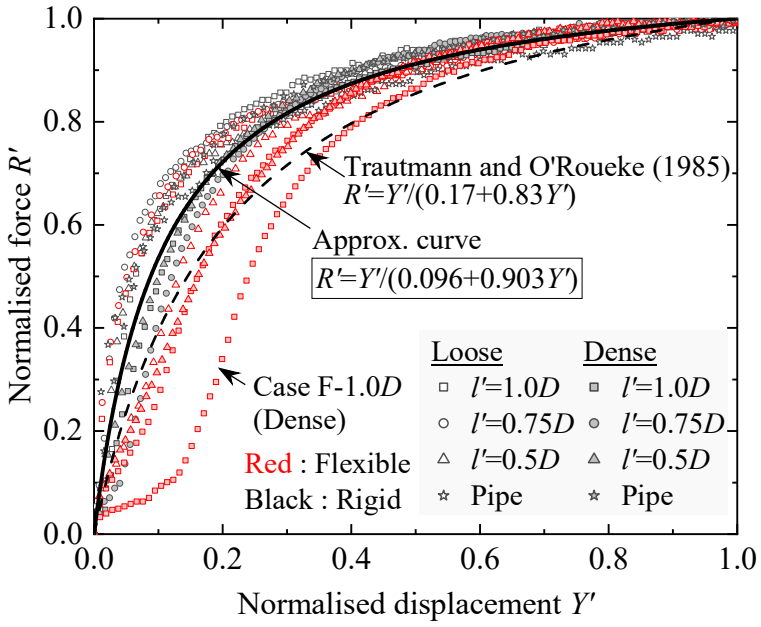

Fig. 6-1 Normalized force–displacement curves

where

$$k_3 = 1 - \frac{h}{h+H} \tag{6.7}$$

$$k_4 = 1 \tag{6.8}$$

Coefficient k_4 enables the effect of the distance between structures to be considered. When a target is a single structure, as in the present study, 1 is substituted for *k4*. Duncan and Mokwa (2001) indicated that the values of the calculated lateral resistance forces were relatively close to the measured values when the coefficient *M* was multiplied by the resistance force calculated from the 2D pressure theories such as Rankine, Coulomb and log spiral theories. Each force in Eq.(6.5) is calculated as follows:

$$P_{\mathrm{p}} = N_{\mathrm{h}} hbH' \gamma_{\mathrm{soil}} \tag{6.9}$$

$$P_{\mathrm{a}} = K_{\mathrm{a}} hbH' \gamma_{\mathrm{soil}} \tag{6.10}$$

$$P_{\mathrm{t}} = W_{\mathrm{soil}} \tan \phi_{\mathrm{g\text{-}s}} = blH \gamma_{\mathrm{soil}} \tan \phi_{\mathrm{g\text{-}s}} \tag{6.11}$$

$$P_{\mathrm{s}} = hlH' \gamma_{\mathrm{soil}} K_0 \tan \phi_{\mathrm{g\text{-}s}} \tag{6.12}$$

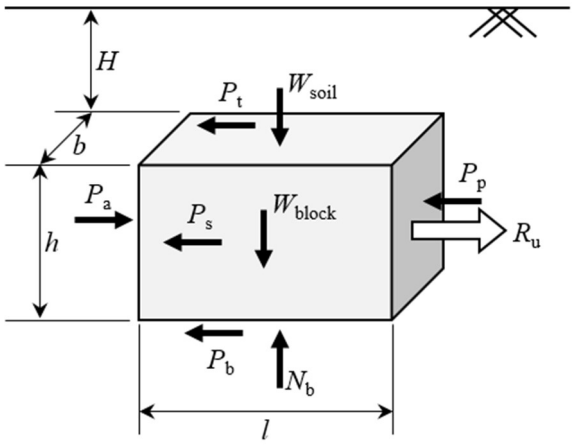

Fig. 6-2 External forces acting on buried block

$$P_{\mathrm{b}} = \left[W_{\mathrm{block}} + W_{\mathrm{soil}} \right] \cdot \tan \phi_{\mathrm{g\text{-}s}} \tag{6.13}$$

where N_{h} is the bearing capacity factor, h is the height of the block, b is the width of the block (m), l is the length of the block (m), H is the depth to the top of the block (m), H' is the depth to the center of the block (m), γ_{soil} is the unit weight of the surrounding soil (kN/m^3), $\phi_{\mathrm{g\text{-}s}}$ is the friction angle between the soil and the geogrid (º), K_{a} is the coefficient of active earth pressure, K_0 is the coefficient of earth pressure at rest, W_{soil} is the weight of the soil above the block (kN), and W_{block} is the weight of block including the weights of the pipe bend, water in the pipe, and gravel or concrete (kN). The bearing capacity factor Nh is determined by a chart, as shown in **Fig. 6-3** which was based on Ovesen's theory (Ovesen, 1964) and illustrated by Trautmann and O'Rourke (1985).

In the buried pipe without thrust restraint, the ultimate resistance force Ru was calculated using Eq.(6.14), which is based on the equation proposed by Trautmann and O'Rourke (1985).

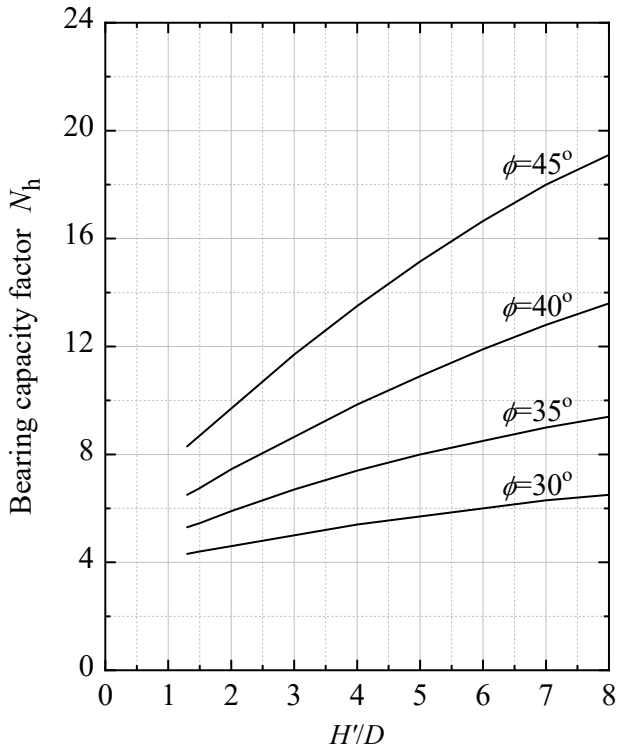

Fig. 6-3 Bearing capacity factors obtained by Ovesen's theory (Trautmann and O'Rourke, 1985; modified by author)

$$R_u = MN_h DB_{bend} H' \gamma_{soil} \tag{6.14}$$

where D is the pipe diameter (m) and B_{bend} is the projected width of the pipe bend (m). When determining the values of M and Nh for a buried pipe, b and h are replaced by $Bbend$ and D, respectively. To confirm the validity of the calculated values of Ru obtained from Eqs.(6.5) and (6.14), a comparison between the calculated values and the experimental results is shown in **Fig. 6-4**. The internal frictional angle of soil was substituted for the friction angle between the geogrid and the surrounding soil, following the guidelines of the Committee for Promotion of Geotextile Reinforced Soil Method (2013). The values of Nh in dense and loose sand were 6.75 and 5.45, respectively, as shown in **Fig. 6-3**. All the plots in **Fig. 6-4** are near the straight line which is the diagonal line in **Fig. 6-4**. The calculated values obtained using Eqs.(6.5) and (6.14) were 83–106% of the experimental results. Thus, the ultimate resistance force of the thrust restraint and buried pipe can be predicted using the proposed equations.

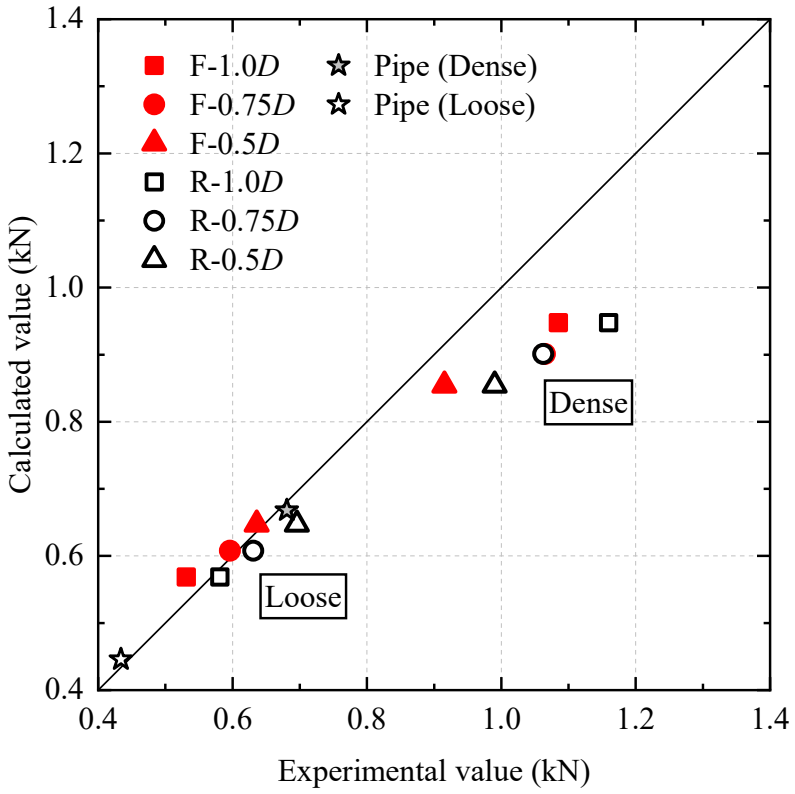

Fig. 6-4 Comparison between the calculated and experimental value of lateral resistance

6.2.4 Prediction of the ultimate lateral displacement Y_u

For buried pipes, Audibert and Nymann (1977) and Trautmann and O'Rourke (1985) presented equations for calculating the ultimate displacement according to soil cover, soil density, and pipe diameter. These equations were based on 2D experimental results and did not support the 3D condition. Therefore, new equations that consider 3D conditions are proposed in this study. In addition to the date set obtained in this study, the results of the experiments described in Subsection 5.2 are also used for formulation. **Fig. 6-5** shows the relationships between the ultimate displacement *Yu*, the dimensions of blocks *b*, *l*, and *h*, and the depth to the center of block *H′*. The results of the pipe without thrust restraint are also plotted in **Fig. 6-5** with b = 300 mm, $l = D$ = 89 mm, and $h = D$ = 89 mm. For each soil density, the relationships between *Yu/l/(H′/h)* and *b/l* were almost linear. *Yu* is represented by the following two equations, which are obtained from the linear approximation for each soil density.

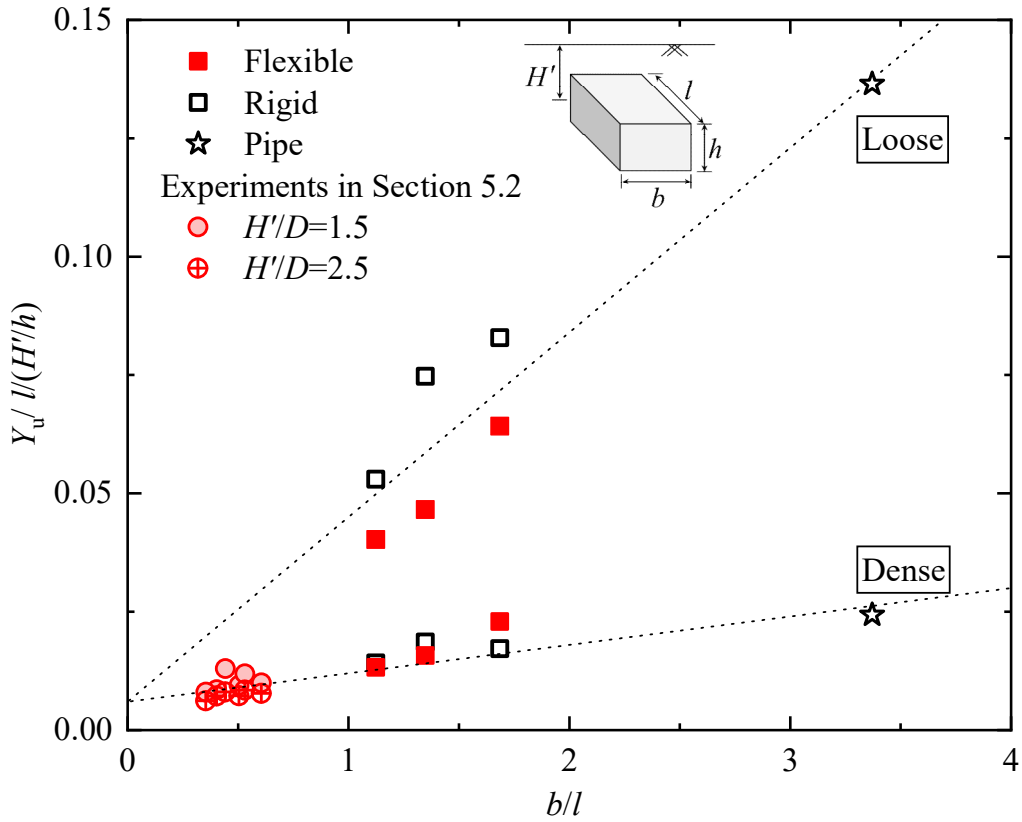

Fig. 6-5 Relationships between ultimate lateral displacement and buried conditions

$$Y_u = \left(0.006b + 0.006l\right)\frac{H'}{h} \quad \text{(for dense sand)} \tag{6.15}$$

$$Y_u = \left(0.039b + 0.006l\right)\frac{H'}{h} \quad \text{(for loose sand)} \tag{6.16}$$

6.2.5 Comparison between predicted and experimental F–D relationships

The validity of the predicted F–D curves obtained from the proposed equations is verified in this section. **Fig. 6-6** shows the predicted and measured F–D relationships. In loose sand, the calculated curves almost fit the experimental results. In dense sand, the calculated value is close to the actual value at small displacements; however, at large displacements, it is significantly different from the measured value. This is because the calculated curves based on the hyperbolic approximation cannot predict the softening behavior of the resistance force. Although the proposed equations cannot reproduce the F–D relationship perfectly, this manually-calculated method is useful in predicting the resistance force at small displacements, which is important for the stability of the pipe bend. Thus, the proposed equations can help predict the resistance of a pipe bend with or without thrust restraint considering the lateral displacement.

6.3 Proposal of a design method based on F–D relationships

The design procedure using the proposed equations is shown in this section. A specific method for considering pipe displacement in the design of thrust restraint is illustrated. An example of calculations using the proposed design procedure is provided in the latter half of this section.

6.3.1 Design chart for pipe bend

The proposed design procedure is illustrated in **Fig. 6-7**. The thrust force was calculated using the following well-known equation:

$$T = 2pA\sin\frac{\theta}{2} \tag{6.17}$$

where T is the thrust force (kN), p is the internal water pressure (kPa), A is the cross-sectional area of the pipe (m^2), and θ is the bending angle of the pipe bend (º). To investigate the necessity of the thrust restraint, the F–D relationship of the pipe bend without thrust restraint is calculated first. The ultimate resistance R_{u1} was calculated using

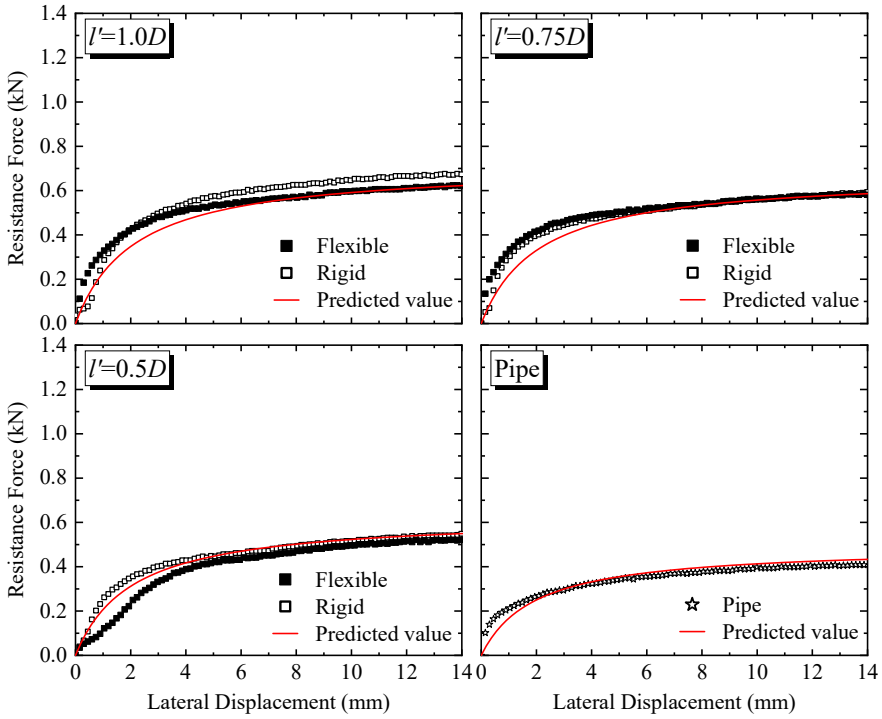

(a) Loose sand

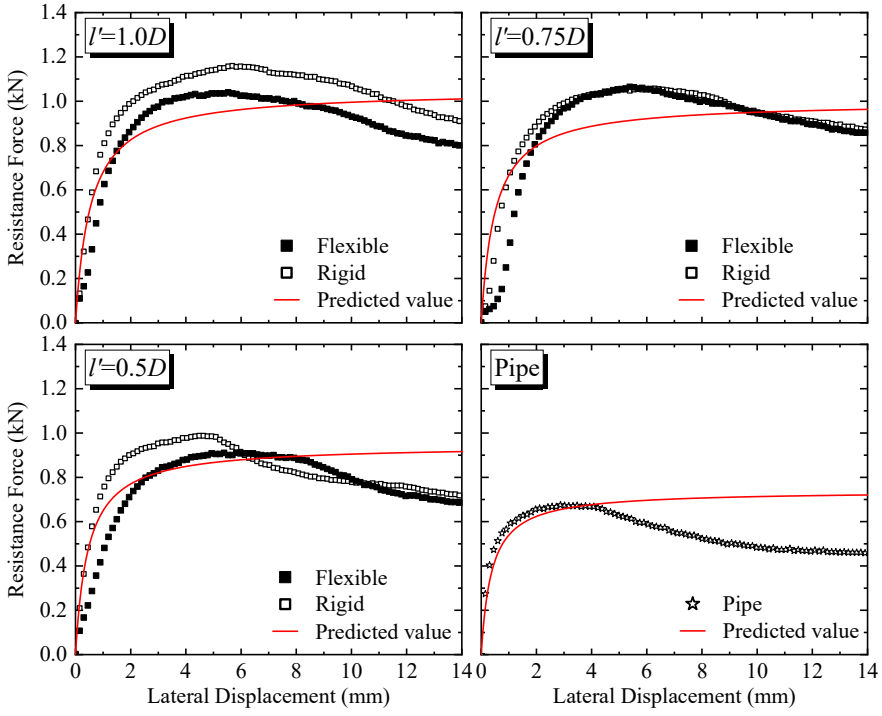

(b) Dense sand

Fig. 6-6 Predicted and measured F–D curves of flexible and rigid thrust restraint and buried pipe: (a) results in loose sand; (b) results in dense sand

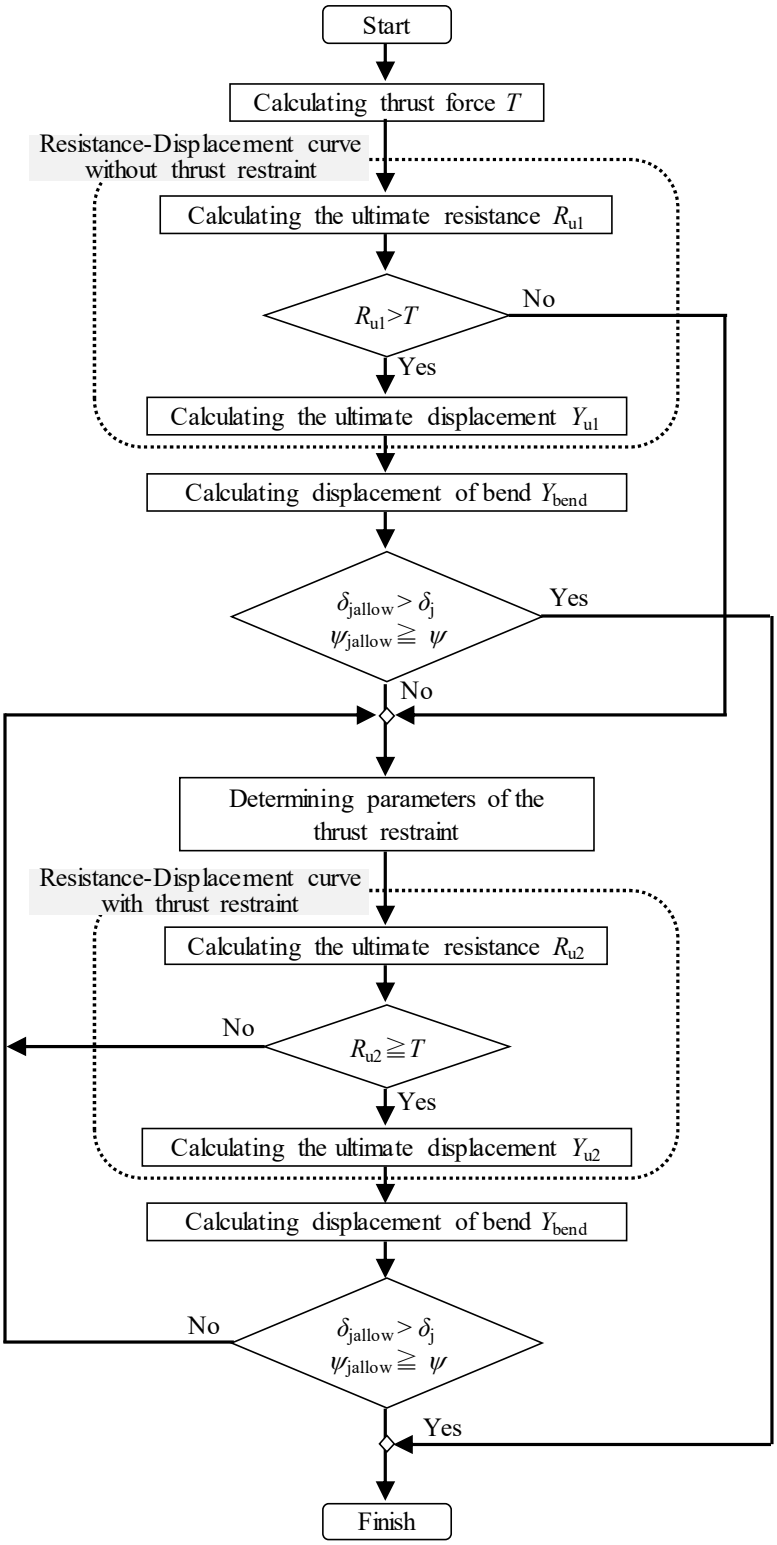

Fig. 6-7 Proposed design procedure considering pipe displacement

Eq.(6.14) and compared to the thrust force *T*. If *Ru1* ≤ *T*, the pipe bend needs thrust restraint, and the thrust restraint is designed without calculating the ultimate lateral displacement Y_{u1}. If *Ru1* >*T*, the ultimate displacement, *Yu1*, is calculated using Eqs.(6.15) or (6.16), and the calculated values of *Ru1* and *Yu1* are substituted into Eq.(6.4) to obtain the F–D relationship: Y_{bend}, which is the pipe displacement when the value of the resistance force becomes equal to that of the thrust force *T*, is calculated by substituting *T* for *R* in the obtained F–D relationships. In this method, the stability of the pressure pipe bend is examined based on the allowable joint separation δ_{jallow}, and the allowable angular deflection ψ_{allow} for consideration of the behavior of the pipe bend. There are particular values of *δjallow* and *ψallow* for each product. The separation and deflection angle of a pipe joint can be obtained geometrically using the displacement of a pipe bend, *Ybend*. Itani et al. (2016) and Shumaker et al. (2017) provided equations for calculating the joint separation from the displacement of a pipe bend, based on the assumption of geometry, as shown in **Fig. 6-8**(a). The adjacent straight pipe in **Fig. 6-8** was inserted fully in a straight alignment at the initial position. The separation δ_j and the angular deflection *ψ*are caused by the displacement of the pipe bend *Ybend* and are calculated by the following equations:

$$\alpha = \sqrt{\left(L_{straight} + Y_{bend}\sin\frac{\theta}{2}\right)^2 + \left(Y_{bend}\cos\frac{\theta}{2}\right)^2} - L_{straight} \tag{6.18}$$

$$\psi = \tan^{-1}\left[\frac{Y_{bend}\cos(\theta/2)}{L_{straight} + Y_{bend}\sin(\theta/2)}\right] \tag{6.19}$$

$$\delta_{jb} = D_{out}\sin\psi \tag{6.20}$$

$$\delta_{ja} = \frac{\alpha}{2} - \frac{D_{out}}{2}\sin\psi \tag{6.21}$$

$$\delta_j = \delta_{ja} + \delta_{jb} \tag{6.22}$$

where α is the joint separation at the pipe center (m), $L_{straight}$ is the length of the straight pipe (m), ψ is the angular deflection (º), *δj* is the total joint separation (m), δ_{ja} is the axial separation (m) and, δ_{jb} is the separation with angular movement (m). The value of separation *δj* can be negative depending on the combination of the values of D_{out}, *Lstraight*, and *ψ*. When *δj* <0, there is no axial separation *δja*, as shown in **Fig. 6-8**(b),

and the separation δj needs to be recalculated using the following equation to avoid a negative value of δj.

$$\delta_{\mathrm{j}} = \delta_{\mathrm{jb}} = \frac{\alpha}{2} + \frac{D_{\mathrm{our}}}{2}\sin\psi \tag{6.23}$$

Predicted δj and ψ need to satisfy the following equations.

$$\delta_{\mathrm{jallow}} \geq \delta_{\mathrm{j}} \tag{6.24}$$

$$\psi_{\mathrm{allow}} \geq \psi \tag{6.25}$$

If δj or ψ exceeds the allowable value, thrust restraint is required for the pipe bend. After determining the dimensions of the thrust restraint, the ultimate resistance R_{u2} was calculated using Eq.(6.5), and compared to the thrust force T. If $Ru2 \leq T$, the dimensions

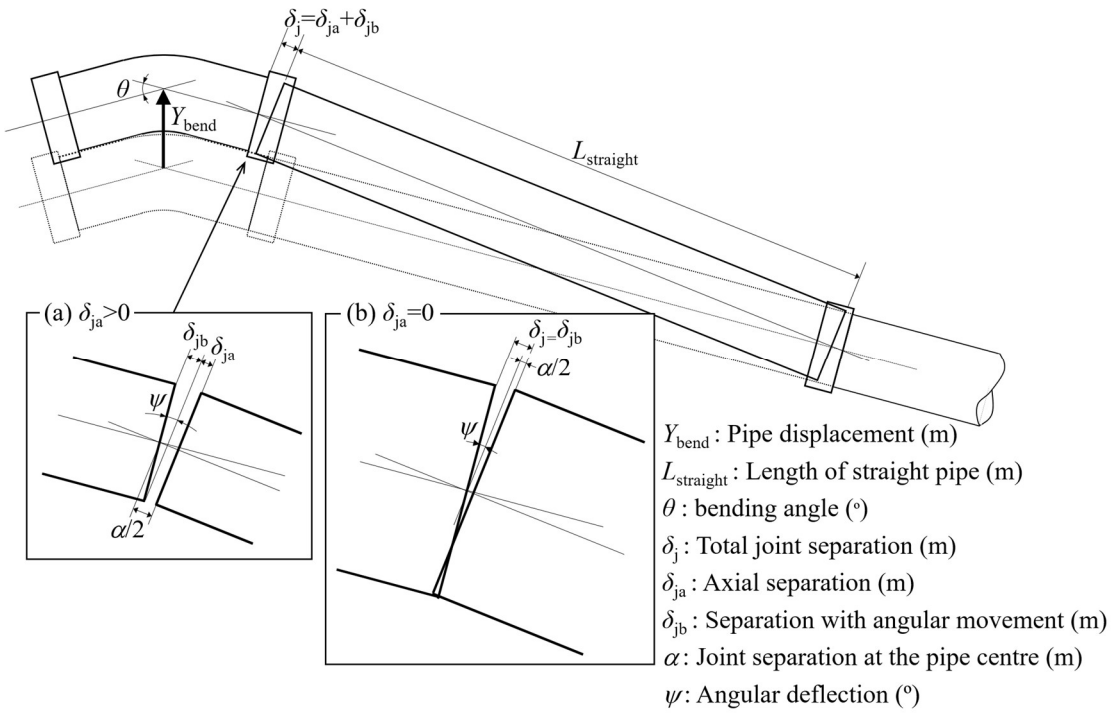

Fig. 6-8 Geometric relationships between pipe displacement Y_{bend} and joint separation δ_{j} as proposed by Itani et al. (2016) and Shumaker et al. (2017)

of the thrust restraint are reconsidered. If *Ru2* > *T*, the F–D relationship with thrust restraint is predicted using Eqs.(6.4), (6.5), (6.15) and (6.16). *Ybend* is recalculated by substituting *T* into *R* for the F–D curve, and then δj and ψ are obtained using Eqs.(6.18)–(6.22). If the relationships shown in Eqs.(6.24) and (6.25) are not satisfied, the dimensions of the thrust restraint are reconsidered.

6.3.2 Calculation example using the proposed design method

A calculation example is presented to demonstrate the aforementioned procedure.

Table 6-1 and **Fig. 6-9** summarize the calculation conditions. The conditions for the pipe bends and joints were determined based on the actual values of an FRPM pipe with a diameter of 800 mm. The thrust force acting on the pipe bend is

$$T = 2 \cdot p \cdot A \cdot \sin\left(\frac{\theta}{2}\right) = 2 \times 1.0 \times 10^3 \times \frac{800^2}{4} \times \pi \times \sin\frac{30^\circ}{2} \doteq 260.2\,(\mathrm{kN}) \tag{6.26}$$

The ultimate resistance against pipe bend *Ru1* is calculated as follows: *Nh* is determined as 5.45, as shown in **Fig. 6-3**.

$$K_\mathrm{a} = \frac{1-\sin\phi_\mathrm{soil}}{1+\sin\phi_\mathrm{soil}} = \frac{1-\sin 35^\circ}{1+\sin 35^\circ} \doteq 0.27 \tag{6.27}$$

$$K_\mathrm{p} = \frac{1+\sin\phi_\mathrm{soil}}{1-\sin\phi_\mathrm{soil}} = \frac{1+\sin 35^\circ}{1-\sin 35^\circ} \doteq 3.69 \tag{6.28}$$

$$M = 1+\left(K_\mathrm{p}-K_\mathrm{a}\right)^{0.67}\left\{1.1k_3{}^4 + \frac{1.6k_4}{1+5\left(B_\mathrm{pipe}/D_\mathrm{out}\right)} + \frac{0.4\left(K_\mathrm{p}-K_\mathrm{a}\right)k_3{}^3k_4{}^2}{1+0.05\left(B_\mathrm{pipe}/D_\mathrm{out}\right)}\right\}$$

$$= 1+\left(3.69-0.27\right)^{0.67}\left[1.1\times 0.5^4 + \frac{1.6\times 1}{1+5\times\left(1000/832\right)} + \frac{0.4\times\left(3.69-0.27\right)\times 0.5^3\times 1^2}{1+0.05\left(1000/832\right)}\right]$$

$$= 2.04 \tag{6.29}$$

$$R_\mathrm{u1} = MN_\mathrm{h}D_\mathrm{out}B_\mathrm{pipe}H'\gamma_\mathrm{soil} = 2.04\times 5.45\times 832\times 1000\times 1248\times 18.0\times 10^{-9} \doteq 208.2 \tag{6.30}$$

The predicted ultimate resistance *Ru1* is smaller than the thrust force *T*. Thus, the pipe bend requires thrust restraint.

The dimensions of the thrust restraint are determined, as shown in

Table 6-1 and **Fig. 6-9**. A flexible thrust restraint was selected in this example. The ultimate resistance against the pipe bend with thrust restraint R_{u2} was calculated as follows:

$$M = 1+\left(K_{\mathrm{p}}-K_{\mathrm{a}}\right)^{0.67}\left\{1.1k_3{}^4+\frac{1.6k_4}{1+5\left(b/h\right)}+\frac{0.4\left(K_{\mathrm{p}}\text{-}K_{\mathrm{a}}\right)k_3{}^3k_4{}^2}{1+0.05\left(b/h\right)}\right\}$$

$$=1+\left(3.69-0.27\right)^{0.67}\left[1.1\times0.5^4+\frac{1.6\times1}{1+5\times\left(1200/832\right)}+\frac{0.4\times\left(3.69-0.27\right)\times0.5^3\times1^2}{1+0.05\left(1200/832\right)}\right]$$

$$=1.96 \tag{6.31}$$

$$K_0=1-\sin\phi_{\mathrm{soil}}=1-\sin35^\circ=0.43 \tag{6.32}$$

$$P_{\mathrm{p}}=N_{\mathrm{h}}hbH'\gamma_{\mathrm{soil}}=5.45\times832\times1200\times1248\times18.0\times10^{-9}=122.2\,(\mathrm{kN}) \tag{6.33}$$

$$P_{\mathrm{a}}=K_{\mathrm{a}}h_{\mathrm{g}}b_{\mathrm{g}}H'\gamma_{\mathrm{soil}}=0.27\times832\times1200\times1248\times18.0\times10^{-9}=6.1\,(\mathrm{kN}) \tag{6.34}$$

$$P_{\mathrm{t}}=W_{\mathrm{soil}}\tan\phi_{\mathrm{g\text{-}s}}=blH\gamma_{\mathrm{soil}}\tan\phi_{\mathrm{g\text{-}s}}=1200\times1200\times832\times18.0\times10^{-9}\times\tan35^\circ=15.1\,(\mathrm{kN}) \tag{6.35}$$

$$P_{\mathrm{s}}=hlH'\gamma_{\mathrm{soil}}K_0\tan\phi_{\mathrm{g\text{-}s}}=832\times1200\times1248\times18.0\times10^{-9}\times0.43\times\tan35^\circ=6.7\ (\mathrm{kN}) \tag{6.36}$$

$$W_{\mathrm{water}}=\frac{D^2\pi}{4}\cdot\frac{B_{\mathrm{bend}}}{\cos\left(\phi_{\mathrm{soil}}/2\right)}\cdot\gamma_{\mathrm{water}}=\frac{800^2\pi}{4}\times\frac{1000}{\cos\left(35^\circ/2\right)}\times9.8\times10^{-9}=5.1\,(\mathrm{kN}) \tag{6.37}$$

$$W_{\mathrm{gravel}}=\left(hbl-\frac{D_{out}{}^2\pi}{4}\cdot\frac{b}{\cos\left(\phi_{\mathrm{soil}}/2\right)}\right)\cdot\gamma_{\mathrm{gravel}}$$

$$=\left\{832\times1200\times1200-\frac{832^2\pi}{4}\cdot\frac{1200}{\cos\left(35^\circ/2\right)}\right\}\times10^{-9}\times20.0=10.5\,(\mathrm{kN}) \tag{6.38}$$

Table 6-1 Design parameters

Inner diameter of pipe	D	800 (mm)
Outer diameter of pipe	D_{out}	832 (mm)
Bending angle	θ	30.0 (°)
Width of pipe bend	B_{bend}	1000 (mm)
Length of straight pipe	$L_{straight}$	4000 (mm)
Allowable angular deflection	ψ_{allow}	2.0 (°)
Allowable total axial displacement	δ_{jallow}	128 (mm)
Weight of pipe bend	W_{bend}	1.2 (kN)
Depth to pipe center	H'	1248 (mm)
Width of thrust restraint	b	1200 (mm)
Height of thrust restraint	h	832 (mm)
Length of thrust restraint	l	1200 (mm)
Unit weight of soil	γ_{soil}	18.0 (kN/m^3)
Unit weight of gravel	γ_{gravel}	20.0 (kN/m^3)
Unit weight of water	γ_{water}	9.8 (kN/m^3)
Water pressure	p	1.0 (MPa)
Internal friction angle	ϕ_{soil}	35.0 (°)
Friction angle between geogrid and soil	$\phi_{g\text{-}s}$	35.0 (°)

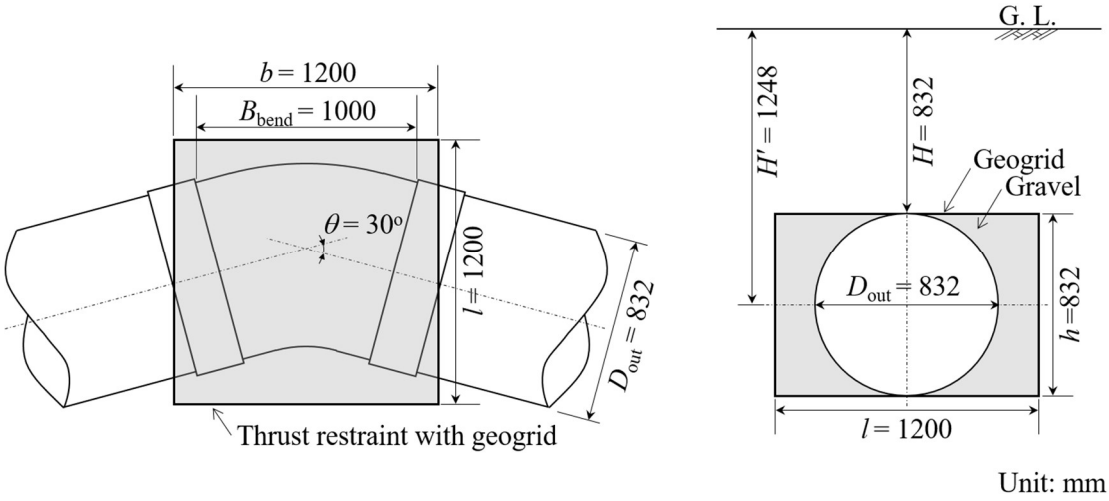

Fig. 6-9 Installation condition for target pipe bend

$$P_{\mathrm{b}} = N_{\mathrm{b}} \tan \phi_{\mathrm{g\text{-}s}} = \left(W_{\mathrm{bend}} + W_{\mathrm{water}} + W_{\mathrm{gravel}} + blH\gamma_{\mathrm{soil}} \right) \cdot \tan \phi_{\mathrm{g\text{-}s}}$$

$$= \left(1.2 + 5.1 + 10.5 + 1200 \times 1200 \times 832 \times 10^{-9} \times 18.0 \right) \times \tan 35^{\circ} = 26.8\,(\mathrm{kN}) \tag{6.39}$$

$$R_{\mathrm{u2}} = M(P_{\mathrm{p}} - P_{\mathrm{a}}) + P_{\mathrm{t}} + 2P_{\mathrm{s}} + P_{\mathrm{b}} = 1.96 \times (122.2 - 6.1) + 15.1 + 2 \times 6.7 + 26.8$$

$$= 283.5 \quad (\mathrm{kN}) \tag{6.40}$$

The thrust restraint was confirmed to have the capacity to resist thrust force. Next, the ultimate lateral displacement Y_{u2} is calculated to obtain the F–D relationships.

$$Y_{\mathrm{u2}} = (0.006b + 0.006l)\frac{H'}{h} = (0.006 \times 1200 + 0.006 \times 1200) \times \frac{1248}{832} = 23.0\,(\mathrm{mm}) \tag{6.41}$$

The F–D relationship can be expressed by substituting the calculated *Ru2* and *Yu2* into Eq.(6.4).

$$R = \frac{R_{\mathrm{u2}} Y}{0.096 Y_{\mathrm{u}} + 0.903 Y} = \frac{283.5 Y}{2.212 + 0.903 Y} \tag{6.42}$$

The pipe displacement *Ybend* was calculated by substituting the thrust force *T* for *R* in Eq.(6.42).

$$T = \frac{283.5 Y_{\mathrm{bend}}}{2.212 + 0.903 Y_{\mathrm{bend}}} \tag{6.43}$$

$$Y_{\mathrm{bend}} = \frac{2.212T}{283.5 - 0.903T} = \frac{2.212 \times 260.2}{283.5 - 0.903 \times 260.2} = 11.9\,(\mathrm{mm}) \tag{6.44}$$

The separation δj and angular deflection ψ are calculated using Eqs.(6.18)–(6.23).

$$\alpha = \sqrt{\left(L_{\mathrm{straight}} + Y_{\mathrm{bend}} \sin \frac{\theta}{2} \right)^2 + \left(Y_{\mathrm{bend}} \cos \frac{\theta}{2} \right)^2} - L_{\mathrm{straight}}$$

$$= \sqrt{\left(4000 + 11.9 \times \sin \frac{30^{\circ}}{2} \right)^2 + \left(11.9 \times \cos \frac{30^{\circ}}{2} \right)^2} - 4000 = 3.1\,(\mathrm{mm}) \tag{6.45}$$

$$\psi = \cos^{-1}\frac{L_{\text{straight}} + Y_{\text{bend}}\sin(\theta/2)}{L_{\text{straight}} + \alpha} = \cos^{-1}\frac{4000 + 11.9 \times \sin(30^{\circ}/2)}{4000 + 3.1} = 0.17\,(^{\circ}) \tag{6.46}$$

$$\delta_{j2} = D_{\text{out}}\sin\psi = 832 \times \sin(0.17^{\circ}) = 2.7\,(\text{mm}) \tag{6.47}$$

$$\delta_{j1} = \frac{\alpha}{2} - \frac{D_{\text{out}}}{2}\sin\psi = \frac{3.6}{2} - \frac{832}{2}\sin(0.17^{\circ}) = 0.3\,(\text{mm}) \tag{6.48}$$

$$\delta_{j} = \delta_{j1} + \delta_{j2} = 0.3 + 2.7 = 3.0\,(\text{mm}) \tag{6.49}$$

The calculated joint separation δj (=3.0 mm) and deflection angle ψ (=0.17º) were within the allowable values of $\delta jallow$ (=128.0 mm) and $\psi allow$ (=2.0º), respectively. This result indicates that the thrust restraint is sufficient to maintain the stability of the pipe bend.

6.4 Conclusions

The F–D relationship of a pipe with thrust restraint was formulated under 3D conditions based on the experimental results. At the end of the study, a design procedure considering pipe displacement was proposed using the formulated equations. The main conclusions are summarized as follows.

1 The normalized F–D relationships showed almost the same curve regardless of the dimensions of the buried structure and soil densities. In addition, the normalized relationships based on the results of the 3D condition could be approximated by a hyperbola, as with those of previous studies of the 2D condition.

2 The ultimate lateral resistance force could be predicted by the proposed equations that were obtained from the equilibrium of forces considering the 3D effects.

3 The relationship between the ultimate lateral displacement and burial conditions was found to be linear.

4 By comparing the calculated values with the experimental results, the proposed equations were found to be able to predict the resistance force at a small lateral displacement. By combining the proposed equations with the joint separation model proposed in previous studies, the pipe displacement and performance of joints can be considered in the design of thrust restraints.

Chapter 7

Chapter 7

Conclusions and future works

7.1 Conclusions

In this study, several model experiments were conducted to solve the challenges of irrigation pipe bends, hoping to make the design procedure of pipe bends more practical and rational. The conclusions obtained for each topic are as follows:

Seismic performance of gravel layer as thrust restraint: Chapter 3 describes the centrifugal shaking table experiments conducted on pipes buried with gravel layers. The results indicated that gravel layers, especially on the passive side from the bottom to the top of the pipe, work effectively as a thrust restraint against typical thrust force generated on pipes during earthquakes.

The effect of existing open channels to support pipe bends from thrust forces: Chapter 4 reports lateral loading experiments conducted on pipes buried with various shapes of channel walls. In the experiments, the existing channel wall increased the lateral resistance force acting on pipe bends, whereas the degree of increase depends on the shape and deterioration of the walls. Especially when the vertical wall comprises several separated pieces, the lateral resistance force hardly increases. For such separated walls, geogrids are helpful as a reinforcement of the walls.

Effectiveness of thrust restraint method with geogrids and gravel: Based on the results of lateral loading experiments explained in Chapter 5, the resistance mechanisms and the effectiveness of the thrust restraint method with geogrids were discussed, especially regarding the dimensions and flexibility of the restraint method. The experimental results indicated that the geogrid-based thrust restrain provides the same resistance level against pipe displacement as thrust blocks when wrapped areas by geogrids are fully unified. In other words, the flexibility of thrust restraint is hardly influenced. However, when the wrapped area by geogrids is larger than a particular dimension, the effectiveness of thrust restraint with the geogrid becomes inferior to that of the thrust blocks. These results implied the geogrid's optimal dimensions of

the wrapped area for the thrust restraint.

Design procedures considering pipe displacement: Chapter 6 provides the proposed design procedure for pipe bends considering pipe displacement. First, equations for estimating F–D relationships of pipe bends with thrust restraint were developed based on the results of experiments reported in Chapter 5. Although the proposed equations cannot perfectly reproduce the F–D relationship, this manually-calculated method helps predict the resistance force at small displacements. Subsequently, the design chart with F–D relationships and the design examples were provided to demonstrate how to consider the pipe displacement in evaluating the stability of pipe bends.

7.2 Future works

The most significant limitation of this study is that most experiments were conducted entirely on small models, and scale effects were not considered. As the behavior of soils depends on the confining pressure, the behavior of underground pipes may also change significantly. In addition, the type of model ground was mainly limited to dry silica sand, which does not consider the various characteristics of soils. Although additional experiments are needed to solve the above problem, it is unrealistic to conduct exhaustive experiments using all sizes and types of soils present worldwide. Therefore, it is necessary to conduct experiments under appropriate experimental conditions to clarify the effects of size and soil types on pipe behaviors and to propose a quantitative method to evaluate these effects.

In addition to experiments, numerical studies should be conducted in the future. Numerical analyses that reproduce model experiments offer results that cannot be obtained from model experiments, such as the propagation of forces in the soil, and thus provide a more detailed understanding of the behavior of buried pipelines. The numerical results are also expected to compensate for the limitations of model experiments, such as the limited size of pipes in laboratory experiments, regarding the effects of scale and ground properties described above.

Future directions for each research topic are as follows:

Seismic performance of gravel layer as thrust restraint: Although the experimental results concluded that gravel layers on the passive side of the pipe

mitigate pipe displacement during earthquakes, there may be an overestimation of the gravel layer's effectiveness owing to the large size of the gravel, as explained in Chapter 3. Further investigations are required to carefully consider the effect of gravel properties on the effectiveness of the gravel layer as a thrust restraint.

The effect of existing open channels to support pipe bends from thrust forces: Since the experiments were in the beginning stage, a simple plate was used as a model of channel walls to simplify the experimental conditions in these experiments. However, a cross-section of actual channel walls cannot be represented by a simple rectangle, and the behavior of existing walls may differ from the model walls in the experiments. In addition, characteristics of aging walls, such as wear and cracks, were not considered correctly in the model walls, although the target of this study was existing old open channels. Furthermore, to address the above challenges, three-dimensional experiments are necessary to get closer to the actual conditions.

Effectiveness of thrust restraint method with geogrids and gravel: The optimum dimensions of the wrapped area with geogrids pointed out in Section 5.3 may vary depending on the properties of the geogrids, especially their tensile properties. In future experiments, comparative experiments using several types of geogrids should be conducted to quantitatively evaluate the effect of the tensile properties of geogrids on the degree of integration of the wrapped area by geogrids.

Design procedures considering pipe displacement: As the prediction equation of the F–D relationship was developed based on experimental results under limited conditions, the equation needs to be modified using experimental and numerical results under different conditions, such as various ground materials and scales. Future work should be conducted to formulate the F–D relationship for other countermeasure methods than thrust restraint with geogrids based on the results of additional experiments and previous research, thus proposing a more comprehensive design method.

References

Al-Shayea, N. (2006), "Pullout capacity of block anchor in unsaturated sand", *Proc. 4th Int. Conf. Unsaturated Soils*, pp. 403-414.

Ansari, Y., Kouretzis, G., and Sloan, S. W. (2021), "Physical modelling of lateral sand–pipe interaction", *Géotechnique*, 71(1), pp. 60-75.

Audibert, J. M. E., and Nyman, K. J. (1977), "Soil restraint against horizontal motion of pipes", *J. Geotech. Eng. Div.* 103(10), pp. 1119–1142.

Chaloulos, Y. K., Bouckovalas, G. D., and Karamitros, D. K. (2017), "Trench effects on lateral p-y relations for pipelines embedded in stiff soils and rocks", *Comput. Geotech.*, 83, pp. 52-63.

Committee for Popularization of Geotextile Reinforced Soil [translated by author] (2013), *Design and Construction Manual for Reinforced Soil using Geotextiles* [translated by author], 2nd ed. Tokyo: Public Works Research Center. [in Japanese]

Das, B. M., and Seely, G. R. (1975), "Load-displacement relationship for vertical anchor plates", *J. Geotech. Eng. Div*. 101(7), pp. 711–715.

Duncan, J. M., and Mokwa, R. L. (2001), "Passive earth pressures: theories and tests", *J. Geotech. Geoenv. Eng.* 127(3), pp. 248–257.

Fujita, N., Mohri, Y. and Suzuki, H. (2007a), "Performance of flexible joints formed underground pipeline for seismic motion", *Trans. JSIDRE*, 75(3), pp. 63-73. [in Japanese with English summary]

Fujita, N., Mohri, Y. and Kishida, T. (2007b), "Behavior of Curved Pipeline Formed with Flexible Joints Subjected to Internal Pressure", *Trans. JSIDRE*, 75 (2), pp. 27-34. [in Japanese with English summary]

Guo, P. J. and Stoll, D. F., (2005), "Lateral pipe–soil interaction in sand with reference to scale effect", *J. Geotech. Geoenv. Eng*., 131(3), pp. 338-349.

Hansen, J. B. (1966), "Resistance of a rectangular anchor slab", *Bull. Danish Geotechnical Institute*, 21, pp. 12–13.

Harada, K. (1998), "Shallow bury of pipe in the open channel", *J. Agri. Eng. Society, Japan*, 66(5), pp. 493-496. [in Japanese]

Harima, M., Aiba, C., Chihara, M., and Kakita, K. (2015), "Regarding characteristic maintenance on completion of "RYOSO" irrigation project", *Water, Land and Environ. Eng.*, 83(3), pp. 203-208. [in Japanese]

Harumoto, T., Miyata, T., Ariyoshi M., Mohri, Y., Itani, Y., and Kawabata, T. (2015), "Pipe behavior in liquefied ground – seismic damage to the main agricultural pipeline

in the Kumado river region", *Proc. 72th Regional Conference of JSIDRE Kyoto Branch*, pp. 210–211. [in Japanese]

Hokuriku Regional Agricultural Administration Office (2012), "Supplementary material 1-2 (2) Cost Reduction Achievements in the fiscal year of 2011 [translated by author]", https://www.maff.go.jp/hokuriku/nnjigyou/kuzu/pdf/20_h240214.pdf (Accessed April 7, 2021) [in Japanese]

Hsu, T. W. (1993), "Rate effect on lateral soil restraint of pipelines", *Soils and Foundations*, 33(4), pp. 159-169.

Iai, S. (1989), "Similitude for shaking table tests on soil-structure-fluid model in 1g gravitational field", *Soils Found*., 29 (1), pp. 105–118.

Itani, Y., Fujita, N, Ariyoshi, M., Mohri, Y., and Kawabata, T. (2016), "Dynamic behavior of flexibly jointed pipeline with a bend in liquefied ground", *Trans. JSIDRE*, 84(1), pp. I_1-I_8. [in Japanese with English summary]

Itani, Y., Fujita, N., Yokota, Y., Ariyoshi, M., Mohri, Y., and Kawabata, T. (2015), "Mechanical Behavior of Flexibly Jointed Pipeline with a Bend on Lateral Loading Tests", *Trans. JSIDRE*, 83(6), pp. 177-183. [in Japanese with English summary]

Jadid, R., Abedin, M. Z., Shahriar, A. R., and Arif, M. Z. U. (2018), "Analytical model for pullout capacity of a vertical concrete anchor block embedded at shallow depth in cohesionless soil", *Int. J. Geomech*. 18(7), 06018017.

Jung, K. J., O'Rourke, D. T., and Argyrou, C. (2016), "Multi-directional force–displacement response of underground pipe in sand", *Canadian Geotech. J.*, 53(11), pp. 1763-1781.

Kawabata, T., Mohri, Y., and Ling, H. I. (2002), "Earth pressure distribution for buried pipe bend subjected to internal pressure", *Proc. Pipeline Div. Specialty Conf. 2002*, CD-ROM.

Kawabata, T., Sawada, Y., Izumi, A., Kashiwagi, A., Hanazawa, T., Okuno, S., and Suzuki, M. (2010), "Field verification test for buried bend with lightweight thrust restraint using geogrid", *Proc., 9th Int. Conf. Geosynth. Soc*., pp. 1327–1332.

Kawabata, T., Sawada, Y., Kashiwagi, A., Mohri, Y. and Uchida, K. (2008), "Reinforcement of Passive Area against Thrust Force for Buried Bend using Geosynthetics", *Geosynth. Engi. J.*, 23, pp.127-132. [in Japanese with English summary]

Kawabata, T., Sawada, Y., Ogushi, K., and Uchida, K., (2007), "Large scale tests of buried bend with lightweight thrust restraint method", *Proc. 17th Int. Soc. Offshore and Polar Eng. Conf.,* pp. 908-913.

Kawabata, T., Uchida, K., Tanaka, Y., Hirai, T., Saito, K., Sawada, Y., Nakase, H.,

Hirayama, T. and Imai, M. (2003), "Thrust protecting method for buried bend using the geosynthetics", *Geosynth. Eng. J.*, 18, pp. 215-220. [in Japanese with English summary]

Klinkvort, R. T., Black, J. A., Bayton, S. M., Haigh, S. K., Madabhushi, G. S. P., Blanc, M., Thorel, L., Zania, V., Bienen, B., and Gaudin, C. (2018), "A review of modelling effects in centrifuge monopile testing in sand", *Proc. 9th Int. Conf. Physical Model. in Geotech.*, pp. 719–724.

Kouretzis, G. P., Sheng, D., and Sloan, S. W. (2013), "Sand–pipeline–trench lateral interaction effects for shallow buried", *Comput. Geotech.*, 54, pp. 53-59.

Ling, H. I., Mohri, Y., Kawabata, T., Liu, H., Burke, C., and Sun, L. (2003), "Centrifugal modeling of seismic behavior of large-diameter pipe in liquefiable soil", *J. Geotech. Geoenv. Eng.*, 129(12), pp. 1092–1101.

MAFF (Ministry of Agriculture, Forestry and Fisheries of Japan) (2021), *Planning and design criteria of land improvement project (Pipeline)* [translated by author], The Japanese Society of Irrigation, Drainage and Rural Engineering. [in Japanese]

MAFF (Ministry of Agriculture, Forestry and Fisheries of Japan) (2019), *Basic survey report on agricultural infrastructure information in the fiscal year of 2019*, MAFF. [in Japanese]

Mohri, Y., Masukawa, S., Hori, T., and Ariyoshi, M. (2014), "Damage to agricultural facilities." *Soils Found.*, 54 (4), pp.588–607.

Mohri., Y., Yasunaka, M., and Tani, S. (1995), "Damage to buried pipeline due to liquefaction induced performance at the ground by the Hokkaido-Nansei Oki Earthquake in 1993", *Proc. 1st Int. Conf. Earthquake Geotech. Eng.*, pp. 31–36.

Nozu, A. and Iai, S. (2001), "Indicator of earthquake motion for immediate damage estimation for a quay wall", *Proc. 28th Regional Conf. of JSCE Kanto Branch*, pp. 18–19. [in Japanese]

Ohta, Y., Sawada, Y., Ono, K., Ling, H. I., and Kawabata, T. (2018), "Model experiments on influence of the bending angles on lateral resistance acting on buried pipe bends", *Proc. 28th (2018) Int. Ocean and Polar Eng. Conf.*, pp. 589–593.

Ono, K., Minaka, U. S., and Okamura, M. (2019), "Dynamic centrifuge tests on dissipation effects of excess pore water pressure by gravel drains", *J. Japan Assoc. Earthquake Eng.*, 19(6), pp.6_68–6_75. [in Japanese]

Ono, K., Yokota, Y., Sawada, Y., and Kawabata, T. (2016), "Lateral loading test for buried pipe under different hydraulic gradient", *Proc. 26th (2016) Int. Ocean and Polar Eng. Conf.*, pp. 664-669.

Ono, K., Yokota, Y., Sawada, Y., and Kawabata, T. (2018), "Lateral force-displacement

prediction for buried effective stress condition", *Int. J. Geotech. Eng.*, 12(4), pp. 420-428.

Ono, K., and Okamura, M. (2022), "Dynamic behavior of pipe bend subjected to thrust force buried in liquefiable sand", *Proc. 4th Int. Conf. Perform. Based Design in Earthquake Geotech. Eng.*, pp. 1647-1655.

Ovesen, N. K. (1964), "Anchor Slabs, Calculation Methods, and Model Tests." *Bull. Danish Geotech. Inst.*, 16, pp. 5-39.

Palmer, M. C., O'Rourke, T. D., Olson, N. A., Abdoun, T., Ha, D., and O'Rourke, M. J. (2009), "Tactile pressure sensors for soil-structure interaction assessment", *J. Geotech. Geoenviron. Eng.*, 135(11), pp. 1638–1645.

Robert, D. J., Soga, K., O'Rourke, T. D., and Sakanoue, T. (2016), "Lateral load-displacement behavior of pipelines in unsaturated sands", *J. Geotech. Geoenviron. Eng.*, 142(11), 04016060.

Roy, K., Hawlader, B., Kenny, S., and Moore, I. (2018), "Lateral resistance of pipes and strip anchors buried in dense", *Canadian Geotech. J.*, 55, pp. 1812-1823.

Sawada, Y., Kawabata, T., Mohri, Y., and Uchida, K. (2009), "Evaluation for additional resistance by lightweight thrust resistant on pressure pipe bend", *Trans. of JSIDRE*, 77(1), pp. 43-51. [in Japanese with English summary]

Sawwaf, I. M., and Nazir, A. (2006), "The effect of soil reinforcement on pullout resistance of an existing vertical anchor plate in sand", *Comput. Geotech.*, 33, pp. 167-176.

Sharma, A., Alzaylaie, M., Vandanapu, R., and Khalaf, K. (2021), "Numerical and analytical studies of 3D effects on pullout capacity of anchor blocks in granular compacted fill", *Int. J. Geosynth. Ground Eng.*, 7(13), pp. 1–8.

Shiraeda, T., Miyato, K., and Shimose. K. (2008), "Design and construction method of Flume in pipe for Kitano M siphon of the Kitano main channel [translated by author]", *Water and soils* [translated by author], 156, pp. 39-46. [in Japanese]

Shumaker, S., Cashon, G., Cox, A., Conner, R., and Rajar, S. (2017), "Update to the improved approach for the design of thrust blocks in buried pipelines", *Proc. Pipelines 2017*, pp. 586-596.

The Hokkaido branch of JSIDRE (2019), "Seismic damage of agricultural farmland and facilities due to the 2018 Hokkaido Earstern Iburi Earthquake", Water, Land and Environ. Eng., 87(5), opening page.

Trautmann, C. H., and O'Rourke, T. D. (1985), "Lateral force-displacement response of buried pipe", *J. Geotech. Eng.*, 111 (9), pp. 1077–1092.

Wham, B. P., and O'Rourke, T. D. (2016), "Jointed pipeline response to large ground

deformation", *J. Pipeline Syst. Eng. Pract*., 7(1), 04015009.

Yamaguchi, Y. (2017), "A study on maintenance situation and risk management of irrigation pipeline", *Water, Land and Environ. Eng*., 85(10), pp. 945–948. [in Japanese]

Yimsiri, S., Soga, K., Yoshizaki, K., Dasari, G. R., and O'Rourke, T. D. (2004), "Lateral and upward soil-pipeline interactions in sand for deep embedment conditions", *J. Geotech. Geoenv. Eng.*, 130(8), pp. 830–842.

Zaitsu, T., Otsuka, N., Nishioka, S., and Hiraiwa, M. (2016), "Design and construction of large-diameter pipeline: national project for agricultural water supply in lower basin area of the kuzuryugawa river", *Water, Land and Environ. Eng.*, 84(12), pp. 1069-1073.